

Gating-induced Structural and Functional Dynamics of Magnesium Channels in Membranes

By

Satyaki Chatterjee

LIFE05201604001

Saha Institute of Nuclear Physics, Kolkata

A thesis submitted to the

Board of Studies in Life Sciences

In partial fulfillment of requirements

for the Degree of

DOCTOR OF PHILOSOPHY

of

HOMI BHABHA NATIONAL INSTITUTE



July 2021

Homi Bhabha National Institute

Recommendations of the Viva Voce Committee

As members of the Viva Voce Committee, we certify that we have read the dissertation prepared by **Satyaki Chatterjee (LIFE05201604001)** entitled "**Gating-induced structural and functional dynamics of magnesium channels in membranes**" and recommend that it may be accepted as fulfilling the thesis requirement for the award of Degree of Doctor of Philosophy.

Chairman - Prof. Rahul Banerjee

R Banerjee 30/6/2021

Guide / Convener - Prof. H. Raghuraman

H. Raghuraman 30/6/2021

Examiner - Prof. Nitin Chaudhary, IIT-Guwahati

N Chaudhary 30/06/2021

Member 1- Prof. Kaushik Sengupta

Kaushik Sengupta 30/06/2021

Member 2- Prof. Padmaja P. Mishra

P. Mishra 30/06/2021

Member 3- Prof. Soumen Kanti Manna

Soumen Kanti Manna 30/6/21

Final approval and acceptance of this thesis is contingent upon the candidate's submission of the final copies of the thesis to HBNI.

I hereby certify that I have read this thesis prepared under my direction and recommend that it may be accepted as fulfilling the thesis requirement.

Date: July 6, 2021

Place: Kolkata

Signature

Guide

Dr. H. Raghuraman

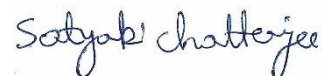
Associate Professor

Crystallography & Molecular Biology Division
Saha Institute of Nuclear Physics
1/AF, Bidhannagar, Kolkata 700 064

STATEMENT BY AUTHOR

This dissertation has been submitted in partial fulfillment of requirements for an advanced degree at Homi Bhabha National Institute (HBNI) and is deposited in the Library to be made available to borrowers under rules of the HBNI.

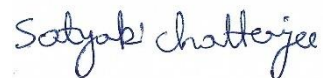
Brief quotations from this dissertation are allowable without special permission, provided that accurate acknowledgement of source is made. Requests for permission for extended quotation from or reproduction of this manuscript in whole or in part may be granted by the Competent Authority of HBNI when in his or her judgment the proposed use of the material is in the interests of scholarship. In all other instances, however, permission must be obtained from the author.



Satyaki Chatterjee

DECLARATION

I, hereby declare that the investigation presented in the thesis has been carried out by me. The work is original and has not been submitted earlier as a whole or in part for a degree / diploma at this or any other Institution / University.

A handwritten signature in black ink that reads "Satyaki Chatterjee". The signature is written in a cursive style with a clear, legible font.

Satyaki Chatterjee

CERTIFICATE

This is to certify that the work incorporated in the thesis titled “**Gating-induced Structural and Functional Dynamics of Magnesium Channels in Membranes**” submitted by Mr. Satyaki Chatterjee for the award of the degree of Doctor of Philosophy is an authentic record of the research work carried out under my guidance in the Crystallography and Molecular Biology division, Saha Institute of Nuclear Physics, Kolkata. The work is original and has not been submitted in part or full for any other degree of any other University/Institute.



Dr. H. Raghuraman
Associate Professor
Crystallography & Molecular Biology Division
Saha Institute of Nuclear Physics
1/AF, Bichannagar, Kolkata 700 064

Signature of the supervisor

(Dr. H. Raghuraman)

Date: 09-04-2021

List of Publications

Journal:

In thesis:

1. **Chatterjee, S.**, Das, A., and Raghuraman, H. (2019) Biochemical and biophysical characterization of a prokaryotic Mg^{2+} ion channel: implications for cost-effective purification of membrane proteins. *Protein Expr. Purif.* 161: 8-16.
2. **Chatterjee, S.**, Brahma, R., and Raghuraman, H. (2020) Gating-related structural dynamics of the MgtE magnesium channel in membrane-mimetics utilizing site-directed tryptophan fluorescence. *J. Mol. Biol.* [In press]
3. **Chatterjee, S.**, and Raghuraman, H. Gating-related structural dynamics of the Mg^{2+} sensing N-domain of the MgtE magnesium channel in membrane-mimetics. (Manuscript in preparation)

Not in thesis:

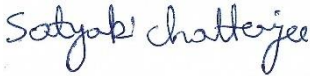
1. Raghuraman, H., **Chatterjee, S.**, and Das, A. (2019) Site-directed fluorescence approaches for dynamic structural biology of membrane peptides and proteins. *Front. Mol. Biosci.* 6: 96.
2. Das, A., **Chatterjee, S.**, and Raghuraman, H. (2020) Structural dynamics of the paddle motif loop in the activated conformation of KvAP voltage sensor. *Biophys. J.* 118: 873-884.

Satyaki Chatterjee

Satyaki Chatterjee

Conferences attended

1. **Chatterjee, S.**, and Raghuraman, H. (2016) Gating-induced Structural and Functional Dynamics of Magnesium Channels in Membranes, Workshop on practical aspects of Membrane Protein Crystallization held at Indian Institute of Science, Bangalore, India, December 15-16, 2016. *Poster presentation.*
2. **Chatterjee, S.**, and Raghuraman, H. (2018) A Cost-effective Approach to the Purification of Mg²⁺ channel MgtE from *Thermus thermophilus*, 42nd Annual Meeting of the Indian Biophysical Society held at Indian Institutes of Science Education and Research, Pune, India, March 9-11, 2018. *Poster presentation.*
3. **Chatterjee, S.**, and Raghuraman, H. (2019) Purification and Biophysical Characterization of a Prokaryotic Mg²⁺ Ion Channel in membrane mimetic-systems: A cost-effective approach, 43rd Annual Meeting of the Indian Biophysical Society held at Indian Institutes of Science Education and Research, Kolkata, India, March 15-17, 2019. *Poster presentation.*


Satyaki Chatterjee

Dedicated to my parents

Acknowledgement

I would like to take this rare opportunity to thank Prof. H. Raghuraman for his excellent guidance throughout my thesis work. He has nurtured my understanding of biological membrane and membrane proteins. His excellent scientific criticisms have helped me immensely to rectify my faults and help me grow professionally from day one in the lab. Most importantly his constant motivations in the face of difficulties have helped me overcome many problems and achieve heights which I would have otherwise failed to reach. He has always strived to maintain an amicable environment in the lab, giving immense freedom to independently work and design experiments without compromising the quality of research. Not only did he supervise my thesis work, but also taught me the intricacies of writing and reviewing research articles. It would be remiss of me to not mention that his teachings went far beyond science, which has not only helped me to grow as a scholar but as a human being. It is a great privilege to work with him, and throughout the course of my journey, it was an educative and enlightening experience for me.

I would like to thank the HOD, faculties and members of the crystallography and molecular biology division (C&MB) for their constant support and cooperation during my thesis work. I sincerely thank the HOD and faculties of the chemical sciences division (CSD) for giving me unhindered access to the steady-state and time-resolved fluorimeters. Additionally, my thanks go to all the members of biophysics & structural genomics division (BSG) as well.

I sincerely thank all my beloved lab members for their help and critical suggestion. In particular, I would like to thank Anindita who has always been by my side through thick and thin during the course of my work.

Finally, this acknowledgement would not be complete without expressing my heartiest gratitude and love to my parents without whose unrelenting support and compassion I would not be here today.

CONTENTS

	Page No.
Abbreviations	xv
Summary	xvii
List of figures	xix
List of tables	xxii
Chapter 1: Introduction	1
1.1. Structure and function of membrane proteins	2
1.2. Organization of Trp residues in membrane proteins	4
1.3. Transport across membranes	7
1.4. Movement through ion channels	10
1.4.1. Ion channels vs ion pumps	10
1.4.2. Gating in ion channels	11
1.4.3. Ion channel selectivity	12
1.5. Magnesium transport across membranes	13
1.5.1. Biochemistry, distribution and pathophysiology of magnesium dysregulation	14
1.5.2. Diversity of Mg ²⁺ transporters in the vertebrate cell	15
1.5.3. Implication of Magnesium and its transporters in cancer	18
1.5.4. Magnesium transport in bacteria	19
1.6. Structure, function, and regulation of prokaryotic Mg ²⁺ channels	20
1.6.1. Diversity and regulation of the CorA Mg ²⁺ channel	22
1.6.2. The MgtE Mg ²⁺ channel	24

1.6.2.1. Diversity and distribution of the MgtE Mg ²⁺ transporter system	24
1.6.2.2. Structure of the MgtE Mg ²⁺ ion channel	28
1.6.2.3. Cytosolic metal binding sites of MgtE	31
1.6.2.4. MgtE is a Mg ²⁺ selective ion channel	32
1.6.2.5. Mg ²⁺ -induced cytoplasmic domain movement	33
1.6.2.6. Negative feedback regulation of MgtE by Mg ²⁺	34
1.6.2.7. Cytoplasmic domain of MgtE as a divalent cation sensor	35
1.6.2.8. MgtE ion pore	36
1.6.2.9. Regulation of MgtE gating at the periplasmic site	37
1.6.2.10. Modulation of MgtE gating by ATP	39
1.6.2.11. Dual role of MgtE	40
1.7. Objectives	42
Chapter 2: Materials and methods	44
2.1. Materials	45
2.2. Cloning and expression test of MgtE	45
2.3. Detergent-mediated solubilization of MgtE	46
2.4. Large scale expression and purification of MgtE	47
2.5. Mutagenesis, channel expression and purification	47
2.6. Site-directed fluorescence labelling of MgtE single-cysteine mutants	48
2.7. Membrane reconstitution of MgtE and its mutants	49
2.8. Circular dichroism (CD) measurements	49
2.9. Limited protease protection assay	50
2.10. Mg ²⁺ transport assay	50

2.11. Steady-state fluorescence measurements	51
2.12. Time-resolved fluorescence measurements	53
2.13. Maximum Entropy Method (MEM) analysis of fluorescence intensity decay	54
2.14. Fluorescence quenching measurements	55
Chapter 3: Biochemical and biophysical characterization of a prokaryotic	57
Mg²⁺ ion channel: implications for cost-effective purification of membrane	
proteins	
3.1. Introduction	58
3.2. Results	61
3.2.1. Temperature-dependent expression of MgtE	61
3.2.2. Extraction of MgtE from membranes by detergents	63
3.2.3. MgtE extracted by alternative detergents is stably folded and α -helical	67
3.2.4. Mg ²⁺ -induced protease protection of MgtE	69
3.2.5. Organization and dynamics of MgtE	72
3.2.6. Acrylamide quenching of MgtE tryptophan fluorescence	77
3.3. Discussion	80
Chapter 4: Gating-related structural dynamics of the MgtE magnesium	85
channel in membrane-mimetics utilizing site-directed tryptophan	
fluorescence	
4.1. Introduction	86
4.2. Results	89
4.2.1. Structural integrity of single-Trp MgtE mutants is preserved	89
4.2.2. Transport activity and ligand-induced conformational changes of Trp-less	92

mutant of MgtE	
4.2.3. Microenvironment of single-Trp residues of MgtE in micelles and membranes	97
4.2.4. Gating-related rotational dynamics of MgtE-Trp residues in micelles and membranes	106
4.2.5. Extent of water penetration for single-Trp mutants of MgtE	110
4.2.6. Hydration dynamics and conformational substates of MgtE-Trps as probed by REES	113
4.2.7. Conformational heterogeneity of MgtE-Trp by Maximum Entropy Method (MEM)	118
4.3. Discussion	123
Chapter 5: Gating-related structural dynamics of the Mg²⁺ sensing N-domain of the MgtE magnesium channel in membrane-mimetics	130
5.1. Introduction	131
5.2. Results	133
5.2.1. NBD labeling does not perturb the structural integrity of MgtE	133
5.2.2. Microenvironment of interfacial N-domain residues upon gating	135
5.2.3. Extent of water penetration for the interfacial N-domain residues	141
5.2.4. Rotational dynamics of NBD-labeled interfacial N-domain residues upon gating	143
5.2.5. Hydration dynamics of the NBD-labeled interfacial residues of the N-domain	147
5.2.6. Gating-induced alteration of conformational heterogeneity of N-domain	148

residues	
5.2.7. Probing small-scale conformational changes in N-domain residues using Tryptophan-induced quenching (TrIQ)	151
5.3. Discussion	154
Chapter 6: Conclusion and future perspectives	158
6.1. Conclusion	159
6.2. Future perspectives	164
References	168

List of Figures:

	Page. No.
1.1. Schematic representations of functionally relevant structural changes in membrane proteins	4
1.2. “Aromatic ring” formed by Trp and Tyr residues of membrane proteins at the membrane interface	6
1.3. Schematic representation of two major classes of membrane transport proteins	9
1.4. Magnesium transport in cellular physiology	18
1.5. Differences in architecture/ sub-unit arrangement in Mg ²⁺ channels	21
1.6. Closed-state crystal structure of MgtE	29
1.7. TM-domain of MgtE	31
3.1. Expression of MgtE at different temperature	62
3.2. Molecular structure of detergents used to extract MgtE	64
3.3. Effect of salt and glycerol on detergent solubilization of MgtE	66
3.4. Stability of MgtE extracted using various detergents	69
3.5. Protease protection assay of MgtE in DDM micelles	71
3.6. Steady-state tryptophan fluorescence of MgtE	75
3.7. Acrylamide quenching of MgtE tryptophan fluorescence	79
4.1. Single-Trp mutants of MgtE	91
4.2. Schematic of fluorescence transport assay	93
4.3. Fluorescence transport assay and ligand-induced conformational changes	96
4.4. Steady-state fluorescence of MgtE-Trp mutants	99
4.5. Amino acids surrounding MgtE-Trp residues	100

4.6. Tryptophan fluorescence emission maximum of the MgtE single-Trp mutants in membrane-mimetic systems	102
4.7. Fluorescence lifetimes of MgtE single-Trp residues in micelles and membranes	105
4.8. Rotational mobility of MgtE single-Trp mutants upon gating in micelles and membranes	107
4.9. Apparent rotational correlation times of MgtE single-Trp mutants in membranes	109
4.10. Apparent rotational correlation times of MgtE single-Trp mutants in micelles	110
4.11. Water accessibility probed by acrylamide quenching of Trp fluorescence in membranes	112
4.12. Water accessibility probed by acrylamide quenching of Trp fluorescence in micelles	113
4.13. REES of single-Trp mutants of MgtE	117
4.14. Conformational heterogeneity of MgtE single-Trp mutants during gating in membranes	121
4.15. Comparison of fluorescence lifetime distribution of MgtE single-Trp mutants in micelles and membranes	122
4.16. Gating-related conformational dynamics of MgtE in micelles and membranes	126
4.17. Comparison of MgtE TM-domain structures in Mg ²⁺ -free and -bound forms	128
5.1. Residues at the interface of N- and CBS-domain	134
5.2. Fluorescence emission maximum of the NBD-labeled N-domain residues in membrane-mimetic systems	136
5.3. Fluorescence lifetimes of NBD-labeled N-domain residues in micelles and membranes	138

5.4. Water accessibility probed by iodide quenching of fluorescence for NBD-labeled N-domain residues in membrane-mimetics	142
5.5. Rotational mobility of MgtE N-domain residues upon gating in micelles and membranes	144
5.6. Apparent rotational correlation times of NBD-labeled N-domain residues of MgtE in membrane-mimetics	146
5.7. REES of NBD-labeled N-domain residues of MgtE	148
5.8. Conformational heterogeneity of interfacial N-domain residues of MgtE during gating in micelles and membranes	150
5.9. Tryptophan-induced quenching of MgtE N-domain residues	153

List of Tables:

	Page. No.
1.1. Solved structures of MgtE in various conditions	27
3.1. Fluorescence emission characteristics of MgtE	74
3.2. Fluorescence lifetimes of MgtE in open state	77
4.1. Fluorescence lifetimes of Single-Trp mutants of MgtE in different functional states	104
5.1. Fluorescence lifetimes of NBD-labeled N-domain mutants of MgtE in different functional states	139

Chapter 6

Conclusion and Future Perspectives

6. 1. Conclusion

Biomembranes are dynamic in nature and form the site for various cellular functions like signal transduction, muscle contraction, cell-to-cell contact, and recognition and ion transport due to the interplay between lipid-lipid and lipid-protein interactions (Shai, 2001). However, the lack of high-resolution three-dimensional structures of membrane-bound proteins has hampered the detailed understanding of the function and dynamics of membranes. Moreover, less than 2% of structures deposited in the Protein Data Bank (PDB) account for membrane proteins since structural studies of membrane proteins is challenging. Interestingly, about 60% of known drugs target membrane proteins like G-protein coupled receptors (GPCRs) and ion channels (Terstepanni and Reggiani, 2001; Yildirim et al., 2007; Bakheet and Doig, 2009; Bull and Doig, 2015). Therefore, it is important to understand the mechanistic and functional details of membrane proteins. Among them, ion channels are specialized membrane proteins that transport charged ions through an otherwise hydrophobic membrane (Hille, 2001). Although relatively new, the structural studies of ion channels gained tremendous momentum after the first crystallographic snapshot of the prokaryotic potassium channel KcsA from *Streptomyces lividans* (Doyle et al., 1998). From then to now, Na⁺ and K⁺ channels from various kingdoms of life have been extensively characterized and studied. In this regard, however, studies on Mg²⁺ channels have been relatively rare, although Mg²⁺ is the most abundant divalent cation in cells (Maguire and Cowan, 2002). Among Mg²⁺ channels, considerable effort has been given to understand the structure, function, and gating mechanisms of the CorA family of Mg²⁺ channels (Payandeh et al., 2013). However, the other major family of Mg²⁺ channels, MgtE, has been studied relatively less. Therefore, this thesis focuses on understanding the gating-related structural dynamics of

MgtE in an attempt to understand the regulation and permeation mechanisms of MgtE in a physiologically relevant membrane environment.

MgtE is a homodimeric Mg^{2+} ion channel having 450 amino acids (~ 50 KDa monomer molecular weight) and negatively regulated by its permeating ion. While it is ubiquitously present and is responsible for Mg^{2+} transport in ~50 % of prokaryotic species, most of the structural and functional knowledge comes from *T. thermophilus* MgtE (Chapter 1, Section 1.6.2). MgtE is a distant ortholog of the SLC41A1 transporter in humans which has been implicated in Parkinson's (Kolisek et al., 2013) and cancer (Wolf and Trapanni, 2012). Importantly, although both CorA and MgtE are Mg^{2+} channels have no distinct sequence similarity, they have similar gating and permeation mechanisms. Further, the architecture and subunit organization of CorA and MgtE is very different. Therefore, it is quite intriguing how two evolutionary distinct Mg^{2+} transporters have similar gating and Mg^{2+} -dependent regulation mechanisms. Interestingly, while all other ion channels like Na^+ and K^+ channels recognize their cognate ions without their hydration shells, MgtE and CorA recognize a fully-hydrated ion and therefore the pore-residues of these channels have to accommodate the large fully-hydrated Mg^{2+} (Chapter 1, Section 1.6). Most importantly, while Na^+ and K^+ channels contain a selectivity filter which is highly conserved throughout all domains of life, Mg^{2+} channels, particular MgtE, has no such conserved selectivity filter. Therefore, Mg^{2+} channels are quite unique in nature and the lesser-studied MgtE is a prime candidate to understand the gating and permeation mechanisms of Mg^{2+} channels in general, MgtE in particular.

In general, structural studies of proteins require the protein to be extracted from its native environment. For soluble proteins, the process is rather straightforward in most cases, as in to lyse the expressing cells and separate the soluble fraction from the debris. However, an extra step

is necessary for membrane proteins, that is, extraction of the protein from its native membrane environment (Arachea et al., 2012). This is usually achieved with the help of detergents, which are soluble amphipathic molecules having the property to self-assemble into organized molecular aggregates called micelles in solutions above a threshold concentration, called the critical micellar concentration (CMC) (Seddon et al., 2004). Unfortunately, there is no ‘magic bullet’ detergent that can universally extract all membrane proteins, and therefore before proceeding with structural studies of any membrane protein, an extensive screen of detergents that can extract the membrane protein in question in a stable and pure form is crucial. Therefore, detergent solubilization of membrane proteins forms a ‘rate-limiting step and the bulk of the purification cost lies in the choice of suitable detergents for the extraction, purification, and crystallization of membrane proteins.

The most commonly used detergents for membrane purification and crystallization include alkyl maltosides (DDM) and glycosides (n-octyl-β-d-glucopyranoside, OG) (Stetsenko and Guskov, 2017). However, these nonionic detergents are very expensive, and therefore less expensive alternatives are required to optimize the cost of purification. Triton X-100 is one of the oldest non-ionic detergents which has been used to extract several membrane proteins in the functional state (Banerjee, 1999) and only recently Triton X-100 mediated extraction of stable and functional ion channels have been demonstrated (Tilegenova et al., 2016; Elberson et al., 2017). Further, Triton X-100 is several folds less expensive than the commonly used non-ionic detergents. However, despite its usefulness, the use of Triton X-100 is about 20 times less than that of DDM due to few technical limitations which include low probability of forming well-ordered crystals due to its chemical heterogeneity and its interference with protein quantitation due to its strong absorption in the UV region of the electromagnetic spectrum. We have therefore

devised a ‘dual-detergent strategy’ for the extraction of MgtE where the Triton X-100 is used only in the extraction step and is substituted with DDM in the subsequent washing and steps (Chapter 3). We have demonstrated that using the relatively inexpensive Triton X-100, large amounts of pure, stably folded, and functional MgtE can be extracted which can be suitable for sophisticated biophysical studies. We believe that our study will have potential implications for the cost-effective extraction of membrane proteins in general, and the MgtE family of magnesium channels, in particular.

As mentioned earlier, membrane proteins are extracted from their source membranes into membrane-mimetic detergent micelles to stabilize them in solution form. Further, due to the inherent heterogeneity and complexity of model membranes, most structural studies like X-ray crystallography and Nuclear magnetic resonance (NMR) of membrane proteins is carried out in detergent micelles. Importantly, micelles have been shown to drastically affect the function, dynamics and structural integrity of several membrane proteins (Encinar et al., 2005; Kofuku et al., 2014; Ge et al., 2016; Frey et al., 2017). Recently, our group has shown that the organization and conformational heterogeneity of the paddle motif loop in the KvAP voltage sensor is altered in membranes compared to micelles (Das et al., 2020). Therefore, it is important to understand differences in organization and dynamics of membrane proteins in membrane-mimetics.

Most of the structural information of MgtE is obtained from the crystal structures of the closed state of full-length MgtE in micelles, open and closed forms of isolated cytoplasmic domain in solution, divalent cation bound forms of MgtE transmembrane domain and solution NMR studies of full-length MgtE in micelles (see Chapter 1, Section 1.6.2 for details and references). Recently, the cryo-EM structure of MgtE in amphipols indicate a ‘partially-open’ form of MgtE in absence of Mg^{2+} (Jin et al., 2020). Despite, the plethora of structural

information available for MgtE, the structural-dynamics of full-length MgtE upon gating, especially in physiologically relevant membrane environment is not well understood. Therefore, to properly understand the structure-function relationship of MgtE, the knowledge of changes in the structural organization and dynamics of MgtE in membrane-mimetics as well as monitoring the gating-related structural dynamic changes in membranes is crucial. Considering this, we have engineered single-Trp mutants of MgtE to obtain site-specific structural and dynamics information exploiting the fluorescence properties of the native Trps of MgtE (Chapter 4). Overall, our results indicate that the organization and dynamics of MgtE is altered in micelles compared to membranes and that MgtE undergoes a ligand-induced ‘conformational wave’ from the Mg^{2+} -sensing N-domain to the TM-domain upon gating.

MgtE is unique in the fact that it is gated by the ion that it conducts. In this light, the cytoplasmic domain which approximately forms ~50 % of the channel is considered to be the gating modulator which negatively regulates MgtE in presence of excess Mg^{2+} (Hattori et al., 2009). The cytoplasmic domain can be sub-divided into the N- and the CBS-domains (Chapter 1, Section 1.6.2). Repulsion between the negatively charged residues present in the cytoplasmic domain keeps the channel open, while in presence of high intracellular Mg^{2+} , these charges get neutralized and therefore the closed state of the channel gets stabilized. The high-resolution crystallographic snapshot of the Mg^{2+} bound form of full-length MgtE in detergent micelles shows the presence of six binding sites in the cytosolic domain out of which three binding sites reside at the interface of the N- and CBS-domain. Consequently, the N-domain is believed to lock and stabilize the closed state of MgtE in presence of concentrations >10 mM of Mg^{2+} (Hattori et al., 2009). Therefore, the cytoplasmic domain, particularly the N-domain, acts as a Mg^{2+} -sensor.

While simulation studies and crystal structures of the isolated cytoplasmic domain indicates that the N-domain swings away from the CBS-domain in absence of Mg^{2+} , the exact structural and conformational change of the protein backbone at the interface of the N- and CBS-domain of full-length MgtE in a membrane environment is not very clear. Therefore, we have selected representative residues at the interface of the N- and CBS-domain and labeled them with the environment-sensitive probe (NBD) using site-directed mutagenesis to investigate the gating-related changes in structural dynamics of these sites utilizing site-directed fluorescence approaches (Chapter 5). Overall, our results indicate a restricted mobility and reduced conformational heterogeneity upon gating which is in excellent agreement with the fact that the N-domain of MgtE senses Mg^{2+} and stabilizes the closed state of MgtE.

6.2. Future perspectives

Although MgtE from *Thermus thermophilus* has been characterized extensively both functionally and structurally (including the work presented in this thesis) to understand Mg^{2+} channels and their gating and permeation mechanisms, particularly for the MgtE family of ion channels, the mechanism of pore-opening is not completely understood. Further questions can be asked to understand the stability, gating and pore-opening mechanism of MgtE in physiologically relevant membranes. How many open states of MgtE are possible? What is the structural dynamics associated with the pore residues? How does the gating mechanism vary with different lipid-composition? What is the stability associated with MgtE and its single-Trp and Trp-less mutants? What is the gating and permeation mechanism of the MgtE ortholog from *P. aeruginosa*, which is not only implicated for Mg^{2+} transport but also has been implicated for virulence? Future studies can be aimed at the following approaches to answer some, if not all, of

these questions. These studies will not only help understand the gating and permeation mechanism of MgtE and its various orthologs but also will be relevant in understanding the structure, function and evolution of Mg^{2+} channels as whole, and MgtE family in particular.

Significant functional characterization of MgtE in *E. coli* spheroplasts (Hattori et al., 2009) and simulation studies of the isolated cytoplasmic domain (Imai et al., 2012) indicates that the open and closed state of the channel is in equilibrium. The equilibrium is favored towards the closed state in presence of high intracellular Mg^{2+} . Interestingly, HS-AFM studies indicate a jagged-topography of the cytoplasmic domain which is difficult to resolve in absence of Mg^{2+} suggesting multiple conformations possible for the cytoplasmic domain (Haruyama et al., 2019). Due to the absence of crystal structure of full-length MgtE in absence of Mg^{2+} and the limited resolution of techniques like HS-AFM, the structural dynamics and conformation of the pore-residues in the different functional states is not understood. A recent Cryo-EM structure of MgtE TM-domain in amphipols shows a partial pore-opening in absence of Mg^{2+} (Jin et al., 2020) further supporting the observation that more than one open state is possible for MgtE. High resolution cryo-EM structures of CorA in nanodisc have provided useful insights into the pore-opening mechanisms of the CorA Mg^{2+} channel (Matthies et al., 2016). Therefore, cryo-EM structures with various defined lipid compositions using nanodiscs (Timothy and Sligar, 2010) to trap other possible open states of MgtE will provide rather useful information about the conformational change of full-length MgtE upon transition from the closed to the open state.

While the recent cryo-EM structure of MgtE in the absence of Mg^{2+} suggest a partial opening of MgtE towards the cytoplasmic end of the TM-domain, the gating-related structural dynamics of the residues lining the ion pore of MgtE is not yet understood. Therefore, a cysteine scanning mutagenesis of the residues lining the ion pore of MgtE can be performed and the

resulting single-cysteine mutants labeled with the thiol-reactive probe, NBD. Utilizing sophisticated steady-state and time-resolved fluorescence techniques, gating-related structural dynamics associated with NBD-labeled residues lining the ion pore of MgtE can be studied. It is a widely known fact that membrane protein function and stability is affected by membrane lipid composition (Valiyaveetil et al., 2002; Lee, 2003; Hunte, 2005, Ramu et al., 2006; Xu et al., 2008; Jiang and Gonen, 2012). Utilizing site-directed fluorescence approaches, lipid-protein interactions between MgtE and physiologically relevant membrane lipids can be studied (Raghuraman et al., 2019). Understanding the gating-related structural dynamics and function of MgtE in various membrane lipids can shed light into the lipid-protein interaction of Mg^{2+} channels in general, and MgtE in particular.

As discussed earlier (Chapter 1, Section 1.2), while Trp residues are placed randomly and to a lesser extent (~1 mol%) in soluble proteins, in membrane proteins Trp residues are not only more in number (~3-7 mol%) but also preferentially localize at the membrane interface (Killian and von Heijne, 2001). Importantly, considering the high cost of Trp synthesis in cells, especially in lower organisms (Akashi and Gojobori, 2002), Trp is judiciously incorporated in proteins of lower organisms. Therefore, Trps are believed to play an important role in stabilizing membrane proteins. Although, several Trp-less variants of membrane proteins including MgtE (shown in this thesis) is shown to be functional, most of the studies of these Trp-less variants have been done in room temperature (Weitzman et al., 1995; Rasmussen et al., 2007, Kozackov and Padan, 2011; Swartz et al., 2020). It will be interesting to understand the role of each Trp residue in temperature-induced stability of MgtE utilizing calorimetric techniques like Differential Scanning Calorimetry (DSC) and circular dichroism.

Although the MgtE ortholog from *P. aeruginosa* possesses some sequence similarity, it contains extra 37 residues in addition to the N-domain. Interestingly, truncating the first 37 residues of MgtE ortholog from *P. aeruginosa* showed a loss of Mg²⁺ transport activity but retained cytotoxicity (Coffey et al., 2014). Therefore, this particular truncated variant of MgtE showed a separation of transport activity from cytotoxicity. So far, this ortholog has not been purified yet and it would be interesting to perform biochemical, biophysical and structural characterization of *P. aeruginosa* MgtE ortholog to shed light on the importance of the dual functionality of MgtE Mg²⁺ channel.

SUMMARY

Magnesium is the most abundant divalent cation present in the cell, and abnormal Mg^{2+} homeostasis is associated with several diseases in humans. However, among ion channels, the mechanisms of intracellular regulation and transport of Mg^{2+} are poorly understood. MgtE is a homodimeric Mg^{2+} -selective channel and is negatively regulated by high intracellular Mg^{2+} concentration where the cytoplasmic domain of MgtE acts as a Mg^{2+} sensor. To date, the purification and structure determination of MgtE from *Thermus thermophilus* has been carried out using the widely used nonionic detergent, n-dodecyl- β -D-maltopyranoside (DDM). However, DDM is an expensive detergent and alternative methods to produce high-quality proteins in a stable and functional form will be practically advantageous to carry out structural studies in a cost-effective manner. We have developed a ‘dual-detergent strategy’ to successfully purify MgtE channel in a stable and functional form by employing relatively inexpensive detergents (Triton X-100 and Anzergent 3–14) for membrane solubilization and subsequently changed to DDM during purification. Our results show that Triton X-100 and Anzergent 3-14 extract MgtE well and the quality of purified protein is comparable to DDM-extracted MgtE. Interestingly, the addition of a high concentration of salt and glycerol during solubilization does not significantly affect the quantity and quality of MgtE. Importantly, limited proteolysis assay, circular dichroism spectroscopy, and ensemble tryptophan fluorescence strongly support the use of Triton X-100, in particular, as an inexpensive, alternative detergent for the purification of MgtE without compromising the structural integrity of the channel and Mg^{2+} -induced gating-related conformational dynamics. Further, we monitored the changes in gating-related structural dynamics, hydration dynamics, and conformational heterogeneity of MgtE in micelles and membranes using site-directed intrinsic Trp fluorescence. For this purpose, we have engineered six single-Trp mutants in the functional Trp-less background of MgtE to obtain site-specific

information on the gating-related structural dynamics of MgtE in membrane-mimetic systems. Our results indicate that Mg^{2+} -induced gating might involve the possibility of a ‘conformational wave’ from the cytosolic N-domain to the transmembrane domain of MgtE. Although MgtE is responsive to Mg^{2+} -induced gating in both micelles and membranes, the structural dynamics of MgtE is substantially altered in physiologically important phospholipid membranes compared to micelles. This is accompanied by significant changes in hydration dynamics and conformational heterogeneity. Importantly, the cytoplasmic domain of MgtE, particularly the N-domain, is known to function as a ‘ Mg^{2+} -sensor’ and a gating-modulator. However, the structural-dynamics changes of the N-domain residues in response to Mg^{2+} -dependent gating is not well understood. For this purpose, we have constructed single-cysteine mutants in the N-domain in such a way that it is possible to probe around the Mg^{2+} binding sites between the N- and CBS-domains without perturbing the residues responsible for coordinating Mg^{2+} to MgtE and labeled them with the environment-sensitive probes, 7-nitrobenz-2-oxa-1,3-diazol-4-yl (NBD) and bimane. Utilizing site-directed fluorescence approaches we have studied the gating-induced changes in mobility, hydration dynamics, and conformational heterogeneity of these N-domain residues. Our results suggest an overall decrease in the mobility and variation in hydration dynamics of the N-domain residues upon gating in membrane mimetics. In addition, maximum entropy method (MEM) analysis of lifetime distribution indicates a decrease in the conformational heterogeneity of the N-domain residues upon gating. Further, using a novel tryptophan-induced quenching (TrIQ) analysis and lifetime distribution analysis we demonstrate that the structural integrity of the N-domain is preserved upon gating. Overall, the work presented in this thesis highlights the importance of membrane environment and lipid-protein interactions in the gating mechanisms of ion channels in general, and the MgtE Mg^{2+} channel in particular.

Chapter 1

Introduction

1.1. Structure and function of membrane proteins

Biological membranes are made up of amphipathic lipid molecules with a polar headgroup and two non-polar acyl chains which can be saturated or unsaturated depending on the lipid composition. This amphiphilic nature causes lipid molecules to spontaneously aggregate and form a bilayer which is sealed end-to-end when placed in a polar environment like water, due to the hydrophobic effect (Luckey, 2008). Biological membranes define cells and organisms by compartmentalizing them from the external milieu. Early membranes played a crucial role in the origin of life by determining what was inside them and what was excluded from defined boundaries, and in a process aiding in controlled chemical reactions occurring within a given space. Over time as cells evolved, membranes became the site of complex processes like energy generation derived from chemical and charge gradients, regulation of enzyme activities, relaying of signals or stimulus from the external to the internal environment, maintain osmotic pressure across the cell, etc. Some membranes even developed specialized functions; for instance, the rod cell membranes capture light, ciliated epithelial membranes in the respiratory tract trap foreign materials and ensure efficient flow of mucus, and membranes of electrically excitable cells generate membrane potential to receive and/or relay electrical impulses. While prokaryotes have either one cell membrane (Gram-positive) or inner and outer membranes (Gram-negative) without a well-defined nucleus, eukaryotic cells have many membrane-bound organelles (like endoplasmic reticulum, mitochondria, Golgi apparatus) with a well-defined double membraned nucleus to serve the various metabolic needs essential for the cell's survival (Luckey, 2008).

The most widely accepted structure of cellular membranes was depicted by Singer and Nicholson in 1972 and is often depicted as a sea of lipid with icebergs of integral membrane proteins floating over it (Singer and Nicholson, 1972). Generally, the structure and function of

membrane proteins are influenced by their membrane environment and the interactions within the structure (protein-protein interactions) and between lipids and proteins (lipid-protein interactions). Therefore, knowledge of how membranes shape protein structure with respect to its partitioning, change in orientation of α -helices, oligomerization, structural transition etc. is of vital importance to decipher the mechanism(s) of membrane protein function (Fig. 1.1). Further, there exist significant differences between soluble and membrane proteins (Eilers et al., 2002; Zhou and Cross, 2013). For instance, the intrahelical hydrogen bonds are shorter in membrane proteins (Kim and Cross, 2002) and the backbone atoms of transmembrane helices experience less competition from water and hydrophilic side chains. In addition, the transmembrane helices of membrane proteins have significantly reduced highly polar (Asn and Gln) and charged (Arg and Lys) residues by a factor of ~ 3 (Eilers et al., 2002). A notable exception is the S4 helix of the voltage-sensing domains of voltage-gated ion channels and voltage-sensitive phosphatases (Jiang et al., 2003; Murata et al., 2005), in which there are several charged residues- mainly Arg and are called gating charges- present that help to generate electrical signaling in biology (Jiang et al., 2003; Catterall, 2010). Even the amino acids Gly and Pro, which are known as helix breakers, are present in high content throughout the transmembrane helices compared to helices from soluble proteins. Particularly, Gly plays an important role in facilitating interhelical interactions and the folding stability of α -helical proteins.

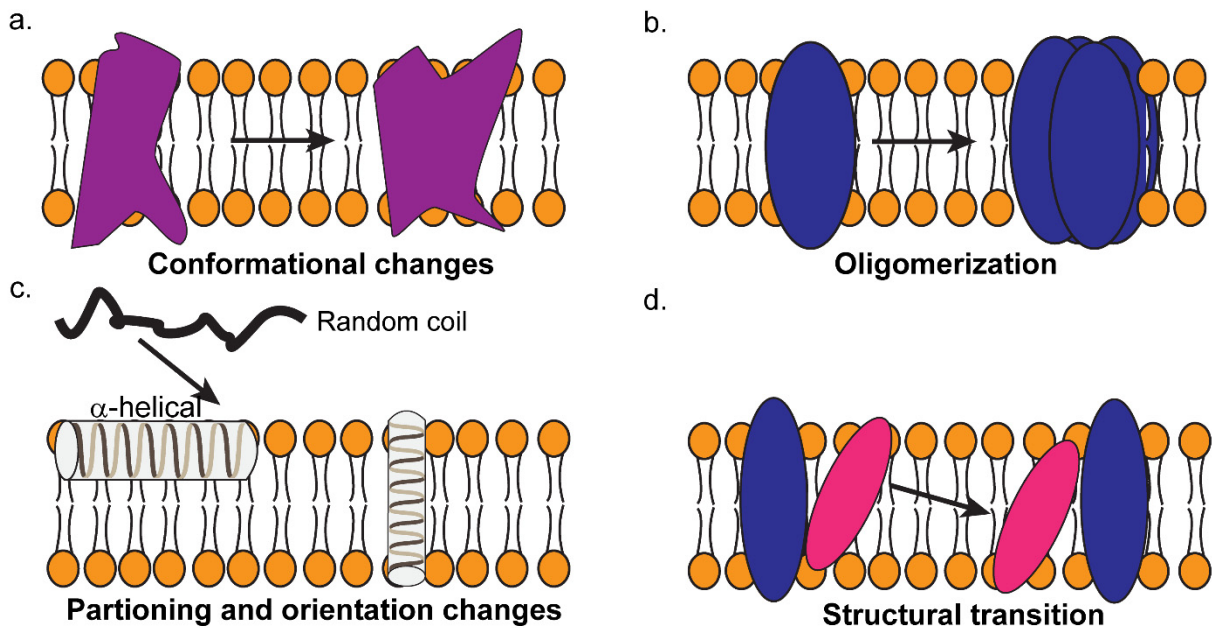


Fig. 1.1. Schematic representations of functionally relevant structural changes in membrane proteins. (a) Conformational changes in response to a physiological signal such as voltage, ligand, pH, membrane tension, etc. (b) Oligomerization involving protein-protein interactions, (c) Partitioning, folding, and insertion of membrane proteins such as pore-forming proteins (d) Lipid-protein interactions resulting in structural transition. Adapted and modified from Raghuraman et al., 2019.

1.2. Organization of Trp residues in membrane proteins

Interestingly, transmembrane proteins have a significantly higher content of Trp amino acids compared to water-soluble proteins (Schiffer et al., 1992; Eilers et al., 2002). Generally, Trp residues comprise ~ 1 mol% in soluble proteins, whereas the relative abundance of Trp is much higher (~ 3 – 7 mol%) in most membrane proteins (Wallace and Janes, 1999). For instance, membrane proteins like bacteriorhodopsin, cytochrome oxidase, α -hemolysin, and KcsA

potassium channel have ~3% of Trp residues; photosynthetic reaction center and maltoporin have ~4.5%; and light-harvesting complex has as high as 7% Trp residues. Of course, there are exceptions to this high abundance of Trp residues in membrane proteins-MgtE magnesium channel has 1.3% of Trp residues that is comparable to soluble proteins, and OmpF, a beta-barrel porin, has only 0.6% of Trp residues. Another important difference is the distribution of Trp residues in soluble and membrane proteins. While Trp residues are distributed throughout the soluble protein structures (Chothia, 1976), it is well known that Trp (and Tyr) amino acids in many transmembrane proteins and peptides are not uniformly distributed and that they prefer to localize at the membrane interface, which accounts for almost half of the bilayer's thermal thickness (White and Wimley, 1994; Raghuraman et al., 2005). For example, crystal structures of membrane proteins like potassium channels, KcsA (Zhou et al., 2001) and KirBac1.1 (Kuo et al., 2003), MgtE magnesium channel (Hattori et al., 2009; Tomita et al., 2017), maltoporin (Schirmer et al., 1995), glycerol conducting channel (Fu et al., 2000), and others have shown that Trp and Tyr residues seem to have an anchoring role by forming an "aromatic ring" around them at the membrane interface (Fig. 1.2) and defines the hydrophobic length of transmembrane helices (Yau et al., 1998; Killian and von Heijne, 2000; Demmers et al., 2001; de Jesus and Allen, 2013). It is also worth noting that the distribution of aromatic residues in the membrane bilayer for β -barrel membrane proteins is different from those of α -helical membrane proteins. Although "aromatic ring" is formed in different families of both α -helical and β -barrel membrane proteins (see Fig. 1.2), the "aromatic rings" from both sides of the membrane are closer together in β -barrel proteins (spacing of ~20 Å) compared to ~30 Å spacing in α -helical membrane proteins (Ulmschneider and Sansom, 2001). Contrary to the preferential localization of Trp residues at the membrane interface of membrane proteins, the Trp is also localized at the

hydrophobic core of the membrane in a few cases, e.g., KvAP voltage-sensing domain (Krepkiy et al., 2009) and transmembrane domain of human inositol requiring enzyme, IRE1 α (Cho et al., 2019).

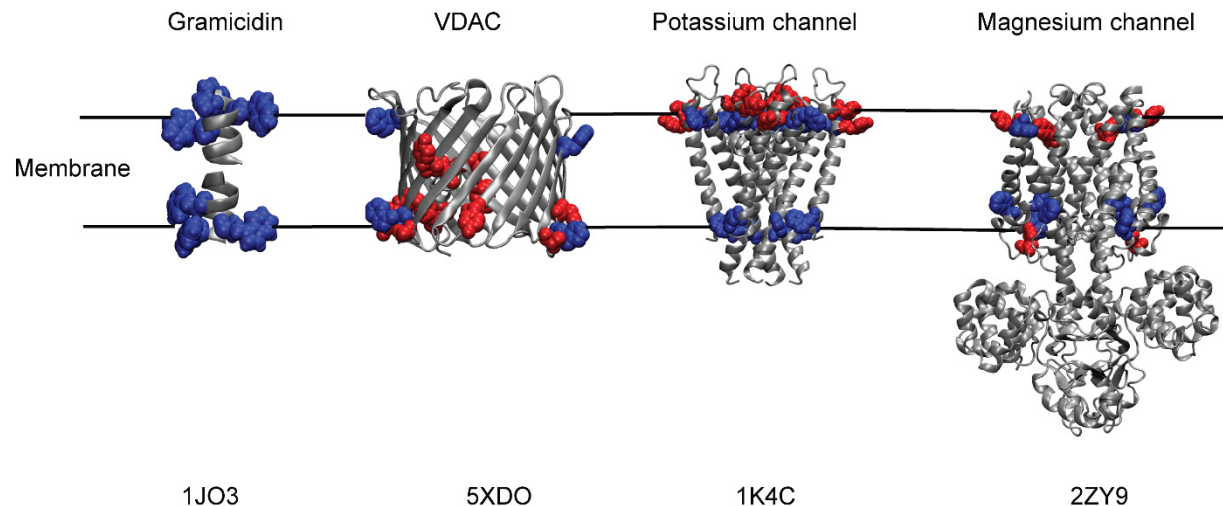


Fig. 1.2. “Aromatic ring” formed by Trp and Tyr residues of membrane proteins at the membrane interface. Cartoon representations of Gramicidin A; human voltage-dependent anion channel, VDAC; potassium channel, KcsA and magnesium channel, MgtE with their respective tryptophan (blue) and tyrosine (red) residues depicting the membrane interfacial localization of the aromatic ring. Only the transmembrane Tyr and Trp residues are shown for MgtE. PDB IDs of the respective protein are indicated below each representation. See text for details. From Raghuraman et al., 2019.

1.3. Transport across membranes

One of the very early observations supporting the presence of a hydrophilic pore or carrier to ferry charged molecules across the membrane was proposed by Adrian Parsegian (Parsegian, 1969). In his pioneering work where he calculated the energy of charging to transport a charged molecule across a hydrophobic “slab” of membrane, it was shown that the presence of a “carrier” or “pore” would significantly reduce the energy needed to transport a charged molecule across the membrane (Parsegian, 1969). This led to the basic framework for the conceptualization of membrane transporters and channels which provide a hydrophilic passage to polar molecules through the otherwise hydrophobic membrane.

Membrane proteins at the bilayer can exist either as loosely bound extrinsic (peripheral) membrane proteins or as integral membrane proteins embedded in the bilayer. Some important extrinsic membrane proteins include cytochrome c of the electron transport chain, ankyrin that mediates linkage of the cytoskeleton to the plasma membrane, phospholipases, etc. (Luckey, 2008). Membrane transport proteins which form a part of the integral membrane protein class of proteins, facilitate the movement of specific polar molecules by selectively permeating them over others (Alberts et al., 2008). Some polar molecules in biological systems include ions, sugars, amino acids, and water. Transport proteins are known for their amphipathic nature, having a hydrophobic region that can interact with the lipid bilayer and anchor them while hydrophilic portions are positioned away from the bilayer, forming a hydrophilic core traversing the hydrophobic bilayer. Polar molecules interact with the hydrophilic region of transporters and thus overcome the otherwise high energy barrier needed to translocate through the membrane.

Membrane transport proteins can be broadly classified into two types; transporters and channels (Fig. 1.3). While transporters bind to its cognate polar molecule(s) on one side and undergo a number of conformational changes to release the molecule(s) to the other side, channels select for the cognate polar molecule(s) and facilitate its movement through an aqueous pore through the membrane (Hille, 2001). The movement of molecules along its electrochemical gradient utilizes the stored energy in the gradient to spontaneously translocate molecules across the membrane. This process is defined as passive transport or facilitated diffusion as it requires no energy. In contrast, the movement of molecules against their concentration gradient involves the expenditure of energy (in the form of ATP hydrolysis or co-transportation of a second polar molecule down its concentration gradient). While transporters can mediate both active and passive transport, channels only perform passive transport which mostly includes transport of small, inorganic ions (Alberts, 2008).

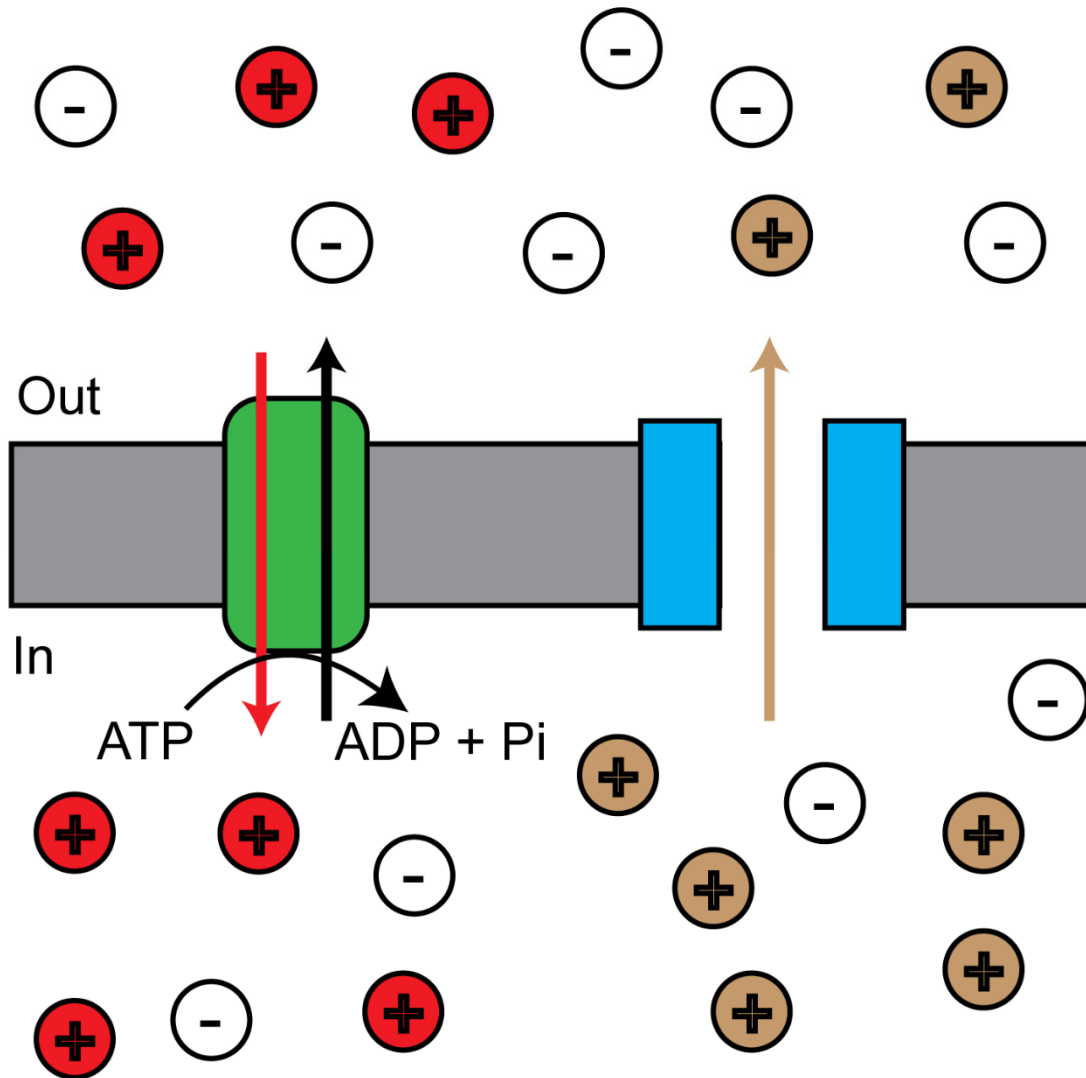


Fig. 1.3. Schematic representation of two major classes of membrane transport proteins. Channels (blue) facilitate the movement of a polar molecule or molecules (brown cations) across the bilayer through an aqueous pore. Transporters (green) shuttle molecules from one side of the membrane to the other by undergoing a series of conformational changes. Channels are only capable of performing passive transport, which requires a concentration gradient of the molecule, but no energy consumption. Transporters, on the other hand, are capable of

performing both active and passive transport and obtain energy for active transport through ATP hydrolysis or by co-transportation of a second polar molecule down its chemical gradient.

1.4. Movement through ion channels

The controlled movement of ions in and out of the cell and organelles is essential for life. While ion flux in single cells mediates processes like signaling, pH balance, volume regulation, cell cycle, and in higher organisms, ion movement controls fertilization, immune responses, secretion, muscle contraction, and all electrical impulses in nerves, all of which are essential for the survival and efficient functioning of organisms (Luckey, 2008). The flow of ions through channels generates transmembrane electric currents. While changes in membrane potential caused by currents of sodium and potassium ions act as physical signals, calcium ions themselves form a chemical signal (Catterall, 2000). Since ion flow through channels dissipates gradients that drive them, ion flow through channels is regulated through gating mechanisms inherent to their respective channels.

1.4.1. Ion channel vs ion pumps

While ion channels permit the flux of ions to flow along their concentration gradient without the expulsion of energy, pumps use a secondary energy source to actively transport ions against their concentration gradients. Depending on the type of energy used, pumps can be classified into primary pumps, that are ATPases and use energy from ATP hydrolysis to transport ions actively; secondary pumps on the other hand exploit energy stored in electrochemical gradients of ions by coupling thermodynamically downhill movements to transport ions and other solutes against their gradients (Gadsby, 2009). Thus, secondary pumps

are sometimes called co-transporters or counter-transporters, according to the relative directions of the coupled downhill and uphill ion flows. Ion flow through channels or pumps is regulated by gates that prevent a random flow of ions that would otherwise be catastrophic for cells. Ion channels and pumps are different from each other by the fact that while ion channels have a single gate, ion pumps have two gates to regulate ion flow through them (Gadsby, 2009). Since the net flow of ions through a channel is always down the electrochemical gradient, the rate of ion flow is extremely high (as high as $\sim 10^7$ ions flow per second for some channels) which is almost close to the diffusion limit ($\sim 10^8$ ions per second) for most channels. Ion pumps involve an 'ion occlusion' gating mechanism where ions are allowed to enter through one side of the membrane while the other gate remains closed. Following internalization, the ion is then let out the other side by the opening of the second gate while the former gate remains closed. Thus, the speed of ion flow is determined by the gating reactions which is several orders of magnitude (~ 100 to $10,000$ ions per second) lower than ion channels (Volkov, 2015).

1.4.2. Gating in ion channels

The movement of ions through ion channels is tightly regulated by gating mechanisms. Ion channels can be broadly categorized into three types based on their mechanism of gating: Type I, Type II, and Type III (Goldschen-Ohm and Chanda, 2017). Type I channels include ligand-gated channels which recognize chemical stimuli in the form of small molecules (like ions, neurotransmitters) or proteins. They are characterized by having a conserved structural domain for the recognition of small molecules. For instance, ionotropic glutamate neurotransmitter receptors (Plested, 2016), nucleotide-gated channels like Kir channels (Craven and Zagotta, 2006), protein-gated channels like Orai/STIM, and channels gated by the cognate

ions they transport like CorA and MgtE (Payandeh et al., 2013). Type II channels include proton-gated channels, which responds to change in the pH of the environment by protonation of titratable groups in the channel. Some examples include the prokaryotic KcsA channel (Cuello et al., 2010), Acid-sensing ion channels (ASICs) (Boscardin et al., 2016). The third category of ion channels, Type III channels, includes ion channels that sense changes in physical stimuli like voltage, temperature, or mechanical stress. Voltage-gated channels are characterized by having a conserved voltage-sensing domain (VSD) which utilizes gating charges present in the S4 helix to open or close a channel in response to change in membrane potential (Catterall, 2010). Some examples include the large family of voltage-gated potassium channels like KvAP, BK channel, Kv channel (Yellen, 2002; Kim and Nimigean, 2016).

1.4.3. Ion channel selectivity

One of the most interesting features of ion channels is the selective translocation of ions across the membrane bilayer. In general, ion channels contain a selectivity filter in their conduction pore which selects for ions based on their physico-chemical properties. For a selectivity filter to recognize an ion, an ion must shed its hydration shell in the bound state. Hence, the free energy cost of dehydration must be compensated by the interaction of the ion with the hydrophilic residues of the selectivity filter (usually carbonyl groups) (Roux, 2017). Selectivity for a particular ion over the other comes from the difference in free energy for the ion to be transported than the bulk ions in solution which makes the transport of the cognate ion thermodynamically favorable. One of the well-studied selectivity filters is that of K^+ ion channels which are characterized by having the conserved 'TTVGYGD' sequence in the narrow ion pore known to select K^+ ions (Heginbotham et al., 1994). Recent studies have shown the conduction

of K^+ ions follow a ‘knock-on’ model where a single-file translocation of 2-3 K^+ ions interspersed by water molecules resulting in the net translocation of one K^+ ion and one water molecule across the membrane. (Zhou et al., 2001; Berneche and Roux, 2003; Kratochvil et al., 2016). Conceptually, the high selectivity of K^+ ions over Na^+ ions has been explained as the carbonyl ligands having a perfect fit to accommodate K^+ ions but Na^+ are too small to fit (Doyle et al., 1998; Zhou et al., 2001). However, in reality, channels are flexible molecules and may be able to deform and adapt around ions, thus not merely size constraints of ions but the number and physico-chemical properties of ion-coordinating ligands play an important role (Roux, 2017).

1.5. Magnesium transport across membranes

Magnesium is the second most abundant cation in the cell and forms an important co-factor for the replication, transcription, and translation machineries of the cell (Fig 1.4.) (Hartwig, 2001; Klein et al., 2004; Yang et al., 2006; Selmer et al., 2006, de Baaij et al., 2015). The total intracellular Mg^{2+} concentration in cells is tightly maintained at ~ 20 mM while ~ 0.5 to 1.0 mM Mg^{2+} occurs free having a considerable amount bound as Mg-ATP (Maguire and Cowan, 2002; Romani and Scarpa, 1992). Despite the importance of Mg^{2+} transport regulation in the cell and the identification of cellular Mg^{2+} transport systems almost 40 years ago, the study of Mg^{2+} transport and regulation is underrepresented due to the lack of sufficient structural information. While many Mg^{2+} transporters are conserved from bacteria to man (Quamme, 2010), the sequence identity across evolutionarily related Mg^{2+} transporters tends to be low. Interestingly, while K^+ channels are known to share a single pore architecture (Doyle et al., 1998), Mg^{2+} transporters have widely varied structural folds and architecture ranging from having 2 transmembrane helices to 6 transmembrane helices per monomer (Payandeh et al.,

2013). Further, while K^+ channels have a conserved selectivity filter throughout the tree of life (MacKinnon, 2003), Mg^{2+} channels lack a conserved selectivity filter (discussed in below).

1.5.1. Biochemistry, distribution and pathophysiology of magnesium dysregulation

Although, Mg^{2+} is one of the most important macronutrients required for the proper functioning of the cell, chemically it is a unique element compared to the other essential minerals like K^+ , Na^+ , and Ca^{2+} . The ionic radius of Mg^{2+} is substantially smaller than its hydrated radius (~7.3 times) whereas the ionic radii of K^+ , Na^+ , and Ca^{2+} are ~1.7-3.0 times smaller than their hydrated radii (Maguire and Cowan, 2002). Consequently, the hydrated volume is ~400 times larger than the ionic volume of Mg^{2+} , whereas for K^+ , Na^+ , and Ca^{2+} the hydrated volume is ~24 times larger than their ion volumes due to volume dependency on the third power of the radius. Such marked differences in physico-chemical characters compared to other ions coupled with the slow rate of water exchange pose challenging problems in Mg^{2+} transport. While binding Mg^{2+} to proteins require the presence of a hydration shell on Mg^{2+} , classically, transport of ions requires them to be stripped off of their hydration shell. This especially poses a challenging issue for the transport of Mg^{2+} since removing the hydration shell would render it ~7.3 times smaller, in effect reducing the strength of interactions between the amino acid backbones of the transport proteins and Mg^{2+} . All these properties of Mg^{2+} make magnesium transport proteins unique (Moomaw and Maguire, 2008).

Sixty percent of the available Mg^{2+} is present in the bone, of which one-third is exchangeable and functions as a reservoir to stabilize the serum concentrations. Only 0.3% of total body Mg^{2+} is present in the serum of which 20% is protein-bound, 65% is ionized and the remaining is complexed with various anions like phosphate and citrate (Swaminathan, 2003).

Importantly, the distribution of Mg^{2+} within the cell is heterogenous with perinuclear regions having more than the peripheral region of cytoplasm (de Rouffignac and Quamme, 1994). Although the uptake and regulation of Mg^{2+} is not well understood, the loss of Mg^{2+} regulation has severe implications ranging from cardiac arrhythmia to asthma (Swaminathan, 2003; Houston, 2011). A deficiency of magnesium (hypomagnesemia) can affect cardiac electrical activity, myocardial contractility, and vascular tone and may also cause digoxin toxicity (Swaminathan, 2003). Since Mg^{2+} is involved in many enzyme systems, its deficiency can disrupt glucose homeostasis. Further, magnesium deficiency is known to inhibit insulin release in response to a glucose challenge and may cause insulin resistance (Nadler and Rude, 1995). Magnesium deficiency may also contribute to the progression of atherosclerosis by affecting lipid metabolism, platelet aggregation, and blood pressure (Nadler and Rude, 1995). Interestingly, low Mg^{2+} has been observed in the cortex, basal ganglia, white matter, and brain stem of patients suffering from Parkinson's disease (de Baaij et al., 2015). Moreover, a mutation in the gene encoding for the SLC41A1 Mg^{2+} transporter (see below) has been associated with Parkinson's disease (Kolisek et al., 2013). Hypermagnesaemia or excess magnesium is implicated in neuromuscular problems, hypotension, smooth muscle paralysis (Swaminathan, 2003). Additionally, the role of Mg^{2+} and its transporters in cancer has recently attracted a lot of attention (see below). Hence, it is evident from the havoc that dysregulation of Mg^{2+} can cause, that the regulation and uptake of Mg^{2+} must be tightly controlled in the cell.

1.5.2. Diversity of Mg^{2+} transporters in the vertebrate cell

Based on their occurrence in the mammalian cell, Mg^{2+} transporters can be classified into two major types: ubiquitously expressed transporters/channels like transient receptor potential

melastatin type 7 (TRPM7) channel, Mg²⁺ transporter 1 (MagT1), and solute carrier 41 family member 1 (SLC41A1) and tissue-specific Mg²⁺ transporters/channels like transient receptor potential melastatin type 6 (TRPM6) channel, cyclin M2 (CNNM2) and cyclin M4 (CNNM4) transporters (de Baaij et al., 2015). Fig. 1.4 shows the ubiquitously expressed Mg²⁺ transporters and their proposed mechanism of Mg²⁺ transport. While TRPM6 is responsible for regulating Mg²⁺ levels in specific tissues like the kidney and colon, TRPM7 is responsible for most of the Mg²⁺ uptake in cells and is considered to be important for cell viability (Nadler et al., 2001; Schmitz et al., 2003). The tetrameric TRPM7 channel contains a carboxy-terminal kinase domain which regulates autophosphorylation but has not been linked to channel function (Takezawa et al., 2004). Recently, it has been reported that the TRPM7 selectivity filter recognized a partially hydrated Mg²⁺ (Duan et al., 2018). While the ubiquitously expressed MagT1 can partially rescue TRPM7 deficient cells, it failed to show Mg²⁺ dependent currents in mammalian cells (de Baaij et al., 2015). Further, mutations in the *magT1* gene have been implicated in congenital glycosylation disorder (Blommaert et al., 2019). Therefore, the cellular function of MagT1 is not yet fully understood.

The SLC41A1 transporter is proposed to exist primarily in intracellular compartments and on the plasma membrane (Kolisek et al., 2008, Mandt et al., 2011). SLC41A1 is a distant ortholog of the prokaryotic Mg²⁺ channel MgtE (Wabakken et al., 2003; Hattori et al., 2009). Interestingly, while the MgtE has a large N-terminal domain which has been implicated in Mg²⁺ transport (Hattori et al., 2009), SLC41A1 has been predicted to have a short N-terminal domain which has been implicated in its regulation by Mg²⁺-dependent endosomal recycling (Mandt et al., 2011). The regulation and mechanism of action of SLC41A1 is described below (see Section 1.6.2.1).

While most members of the CNNM family of transporters show tissue-specific expression like CNNM1, mainly expressed in the brain, CNNM2 mostly found in the kidney, and CNNM4 primarily expressed in the intestine (de Baaij et al., 2013), CNNM3 is ubiquitously expressed and is a key player in maintaining cellular Mg^{2+} homeostasis and also has been implicated in tumor growth (Hardy et al., 2014). Although most of the information on MRS2 (mitochondrial RNA splicing 2) comes from yeast, MRS2 is considered to be important for regulating mitochondrial Mg^{2+} homeostasis. Interestingly, it has been observed that knockdown of MRS2 results in reduced Mg^{2+} uptake in mitochondria and subsequent cell death (Piskacek et al., 2009). Considering the importance of Mg^{2+} in ATP binding, it is speculated that MRS2 can regulate the mitochondrial citric acid cycle by modulating intramitochondrial Mg^{2+} .

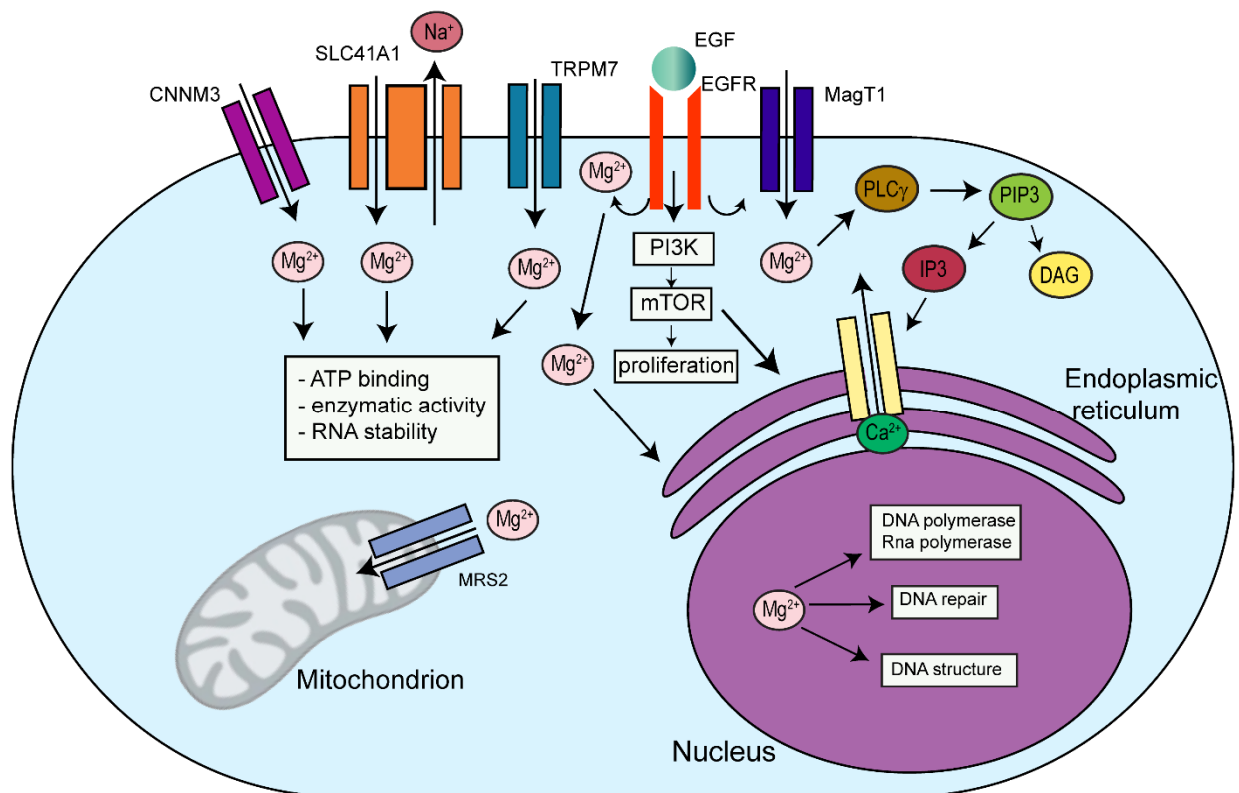


Fig. 1.4. Magnesium transport in cellular physiology. A schematic representation of the importance and predicted transport mechanisms of Mg^{2+} along with the proposed Mg^{2+} transporters/channels in the vertebrate cell is shown. Adapted and modified from de Baaij et al., 2015.

1.5.3. Implication of Magnesium and its transporters in cancer

Since, magnesium is known to play important biochemical roles in cellular processes like proliferation, differentiation, apoptosis, and migration (Wolf and Trapani, 2012), it has been postulated that magnesium may play a central role in the regulation of protein synthesis and cell proliferation during neoplastic transformation (Rubin, 2005). The effect of Mg^{2+} on cancer

progression involves a complex interplay between neoplastic growth and tumor cell metastasis. While Mg^{2+} deficiency inhibits proliferation, neo-angiogenesis, and DNA repair, it can also elevate the metastatic potential of the cell (Wolf and Trapani, 2012). Therefore, the pros and cons of altering Mg^{2+} availability to the cell should be evaluated before proceeding to therapeutic measures.

Downregulation of the ubiquitously expressed TRPM7 has been implicated to low-magnesium-induced cellular growth inhibition (Wolf and Trapani, 2012). TRPM7 is required for the proliferation of several types of tumor cells like leukemia, retinoblastoma, carcinoma etc. (Wolf and Trapani, 2012). Interestingly, TRPM7-mediated Mg^{2+} influx has been found to influence the signaling along the phosphoinositide 3-kinase (PI3K)/Akt/mTOR pathway which is involved in the metabolic reprogramming of cancer cells. Therefore, TRPM7 channels, which are versatile channels modulating cancer cell plasticity and proliferation, can be potential therapeutic targets. Interestingly, overexpression of the SLC41A1 gene has been observed in head and neck cancer patients (Lin et al., 2015). Further, the expression of the SLC41A1 gene was downregulated after chemotherapy (Lin et al., 2015). Moreover, it was observed that overexpression of SLC41A1 reduces the internal cellular Mg^{2+} concentration and modulates the pro-survival (anti-apoptotic) signal of cells (Sponder et al., 2018). Therefore, the complex interplay between cellular proliferation and SLC41A1 expression is an interesting avenue for future studies and can prove to be a beneficial therapeutic target during cancer treatment.

1.5.4. Magnesium transport in bacteria

In general bacteria have three distinct classes of Mg^{2+} transporters: CorA, MgtE, and MgtA (Hmiel et al., 1989; Smith et al., 1995). Further, most of the bacterial genome encodes

multiple magnesium transporters belonging to either class. While both CorA and MgtE are predominantly Mg^{2+} channels (discussed below), the MgtA family of Mg^{2+} transporters are P-type ATPases (Groisman et al., 2013). Conversely, MgtA classes of proteins have been reported to transport Mg^{2+} along the electrochemical gradient (Tao et al., 1998), therefore the process of coupling ATP hydrolysis to transport is unclear. Importantly, it was seen that in low Mg^{2+} conditions the PhoP/PhoQ system in *Salmonella* modulates the expression of *mgtA* and *mgtB* genes for proper growth of the bacteria (Groisman et al., 2013). In addition to regulation at the protein level, bacterial Mg^{2+} transporter genes are also regulated at a transcription level and thereby having a tight regulation of Mg^{2+} homeostasis (Cromie et al., 2006; Dann et al., 2007). The PhoP/PhoQ system is essential for virulence in many pathogens and since *mgtB* expression is linked to this system it is hypothesized that *mgtE* and *mgtC*, which is an absolute requirement for the survival of *Salmonella* in macrophages, act as virulence modulators (Groisman et al., 2013). It was also shown that CorA is required for the virulence of *Salmonella* (Papp-Wallace et al., 2008). In addition, MgtE is important for adherence to surfaces and biofilm formation in *Aeromonas hydrophila* (Merino et al., 2001) and the expression of the type III secretion system in *Pseudomonas aeruginosa* (Anderson et al., 2010). Despite the plethora of genetic and biochemical studies performed on various Mg^{2+} transporters, most of our current knowledge on molecular basis of Mg^{2+} transport comes from the functional and structural studies on CorA and MgtE Mg^{2+} channels (discussed in details below).

1.6. Structure, function, and regulation of prokaryotic Mg^{2+} channels

It is now known that MgtE, like CorA, is the primary Mg^{2+} transport system in ~50% of all prokaryotic species. In addition, unlike K^+ and Na^+ channels, the architecture of the Mg^{2+}

channels is not conserved as is evident by the recent crystal structures of prokaryotic Mg^{2+} channels (Fig. 1.5). For instance, the functional unit of CorA Mg^{2+} channel is a pentamer (Eshaghi et al., 2006; Payandeh and Pai, 2006; Matthies et al., 2016) whereas MgtE functions as a dimer (Hattori et al., 2007; 2009). Intriguingly, these two evolutionarily distinct Mg^{2+} transporters seem to have conceptually similar Mg^{2+} -dependent gating mechanisms with different architectures, which makes them unique. While the CorA superfamily is characterized by having a conserved glycine-methionine-asparagine (GMN) motif which is known to be essential for channel function (Palombo et al., 2013), the MgtE family of channels have no signature motifs present.

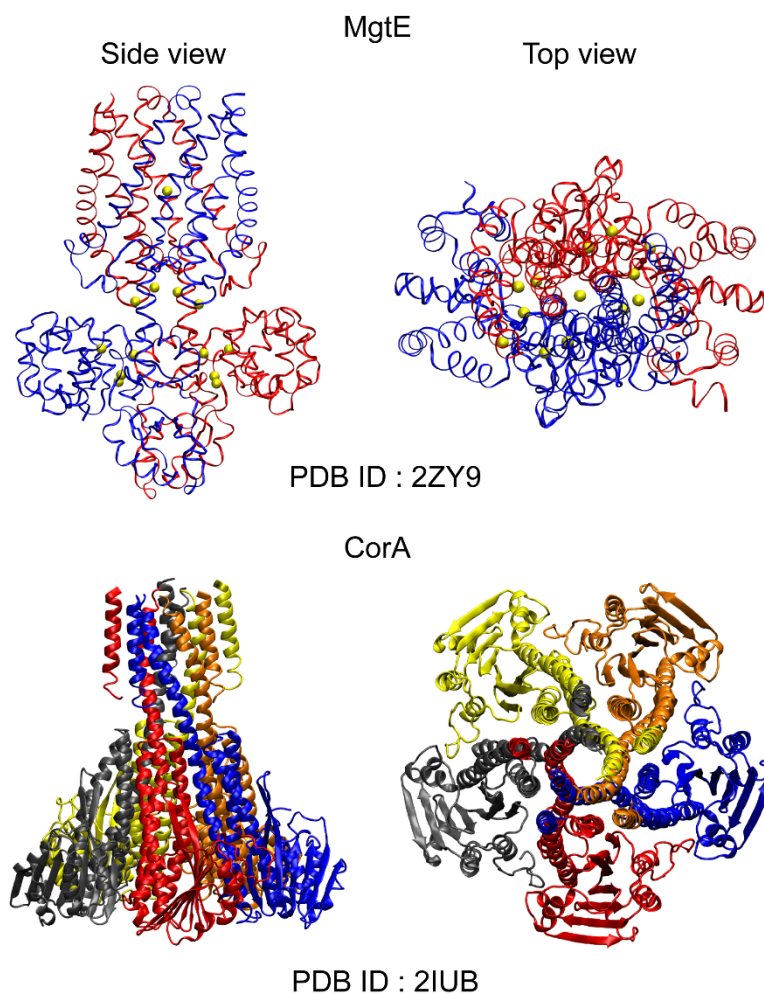


Fig. 1.5. Differences in subunit arrangement in Mg^{2+} channels.

Schematic representations of the Mg^{2+} bound homodimeric MgtE and the homopentameric CorA. The colors represent the different subunits of the channels.

1.6.1. Diversity and regulation of the CorA Mg²⁺ channel

CorA is one of the most abundant Mg²⁺ channels, forming a large superfamily of proteins with about 800 sequences currently known in eubacteria (Moomaw and Maguire, 2008). CorA was initially named after the cobalt-resistant mutants in which it was identified (Nelson and Kennedy, 1971, Park et al., 1976). CorA expression has been known to be modulated by RNase III activity (Lim et al. 2012). Importantly, the *corA* gene has also been implicated as a virulence modulator in *Salmonella* and has been found in almost half of all prokaryotic genomes (Payandeh et al., 2013). The CorA family of proteins can be broadly classified into two sub-groups and a distantly related third group (to which ZntB belongs). While the proteins in both the sub-groups function primarily as a Mg²⁺-transporter but discrepancies like lack of amino acid sequence homology in the N-terminus and the presence or absence of the conserved residue D277 which forms the ‘aspartic ring’, places these proteins in two distinct sub-groups. Those having high sequence homology to CorA from *Thermotoga maritima* are placed into group A while those having high sequence similarity to CorA from *Escherichia coli* and *Salmonella typhimurium* form group B (Niegowski and Eshaghi, 2007).

Interestingly, the distant homolog of CorA, ZntB which functions primarily as Zn²⁺ transporter is placed as an extension of the CorA superfamily of proteins due to its conserved GXN motif where X is methionine (M) for the two sub-groups of the CorA superfamily and isoleucine (I) for the ZntB transporter. Recently, extensive functional characterization of the ZntB from *E.coli* has shown that ZntB can not only transport Zn²⁺ but also Mg²⁺, although the transport of Zn²⁺ is preferred to Mg²⁺ when both are present (Stetsenko and Guskov, 2020). Interestingly, while Mg²⁺ transport in CorA is driven by an electrochemical gradient, ZntB from

E. coli can co-transport H⁺ along with Zn²⁺ suggesting divergent evolution mechanisms of these two channels (Stetsenko and Guskov, 2020).

The CorA family is not only present in bacteria but also throughout the other domains of life. Mrs2, which is required for normal mitochondrial functioning and Mg²⁺ homeostasis (Kolisek et al., 2003) and also is a genetic marker for embryonic stem cells (Assou et al., 2009) and is linked to multidrug resistance in cancer (Wolf and Trapani, 2012), is an orthologue of CorA (Bui et al., 1999). The CorA-like yeast plasma membrane protein Alr1 and Alr2 has been implicated in cellular Mg²⁺ homeostasis (Graschpof et al., 2001; Liu et al., 2002; Wachek et al., 2006) while the Mnr2 protein in vacuoles is known to regulate intracellular Mg²⁺ stores (Pisat et al., 2009). In plants, the CorA family has diversified and can most likely participate in divalent cation transport in many different cellular membranes (Knoop et al., 2005). Additionally, in the intracellular parasite *Leishmania major*, CorA-like gene products have been implicated as virulence modulators (Zhu et al., 2009).

Most of the structural information on CorA comes from the crystallographic snapshots of CorA from *T. maritima* (TmCorA) (Eshaghi et al., 2006; Lunin et al., 2006) and *Methanocaldococcus jannaschii* (MjCorA) (Guskov et al., 2012). Essentially both the structures are similar and are homopentamers made up of two transmembrane helices, TM1 and TM2. Upon oligomerization, the TM1 helices form a ~55 Å long central ion pore with the conserved GMN motif which is the putative selective filter for the CorA family of proteins (Knoop et al., 2005). The overall structure reveals a funnel-like appearance with the TM1 helix extending into the cytosol and forms the large extracellular domain of CorA which forms a seven-stranded parallel/anti-parallel β-sheet between two sets of α-helices (Lunin et al., 2006).

CorA contains two Mg^{2+} binding sites in the extracellular domain per monomer and therefore a total of ten Mg^{2+} binding sites for the complete pentamer (Payandeh et al., 2013). Therefore, the extracellular domain of CorA acts as a regulatory domain by closing the channel in presence of excess intracellular Mg^{2+} by shielding the electrostatic repulsion conferred by the acidic residues. It has been proposed that in absence of Mg^{2+} , CorA undergoes structural changes which expands the ion pore throughout the length of the permeation pathway (Dalmas et al., 2014). Interestingly, single-particle high-resolution cryo-EM structure of CorA has revealed a break in the five-fold symmetry of CorA upon opening of the channel in absence of Mg^{2+} (Matthies et al., 2016). Importantly, based on the nature of symmetry break (different degrees of motions of the subunits), TmCorA has been assigned two or more possible conformations of open states (Rangl et al., 2019). Therefore, it is proposed that in absence of Mg^{2+} , CorA undergoes a conformational wave which widens the channel pore for Mg^{2+} permeation.

1.6.2. The MgtE Mg^{2+} channel

1.6.2.1. Diversity and distribution of the MgtE Mg^{2+} transporter system

The *mgtE* gene is located in a broad range of Gram-positive and Gram-negative bacteria (Smith et al., 1995; Townsend et al., 1995), suggesting the importance of the *mgtE* gene in bacterial physiology as well as virulence as seen in *Borrelia burgdorferi* (Aron et al., 1996). MgtE has been implicated in many diverse functions such as functioning of electron transport chain (Tai et al., 2010), adherence of *Aeromonas hydrophila* to host (human) cells (Merino et al., 2001), and modulating the Type III secretion machinery in *Salmonella* (Anderson et al., 2010). Recently, a dual-function of MgtE has been found in *P. aeruginosa*, where it not only functions as a Mg^{2+} transporter but also a virulence modulator (Coffey et al., 2014). Overall, these

observations and findings suggest an important role of MgtE in bacterial physiology and pathogenesis. Importantly, the *mgtE* gene is present in about half of all prokaryotic species and therefore is thought to be the primary Mg^{2+} transport system in prokaryotes.

The distribution of *mgtE* is not only restricted to prokaryotes but also is found in eukaryotes, as an ortholog of the SLC41A1 gene. It has been found that the transmembrane domain of MgtE has a consensus with the predicted SLC41A1 amino acid sequence in two particular stretches of sequences, namely D1 and D2, having a sequence similarity of 52% and 46%, respectively (Wabakken et al., 2003). Interestingly, SLC41A1 can functionally compensate for the absence of Mg^{2+} transporters in *Salmonella enterica* making it a Mg^{2+} transporter. Also, SLC41A1 has been shown to mediate Mg^{2+} efflux when over-expressed in HEK293 making it a Mg^{2+} efflux channel (Kolisek et al., 2008) as opposed to the bacterial MgtE ortholog which imports Mg^{2+} into the cell (Hattori et al., 2009).

It is speculated that the SLC41A1 Mg^{2+} transporter has undergone a gene duplication and fusion event from the source *mgtE* gene (Payandeh et al., 2013). However, the major difference from MgtE is that it lacks a large cytoplasmic domain (~259 residues for MgtE) with a regulatory N-domain but predicted to have a rather short N-terminal cytoplasmic region of ~92 residues (Mandt et al., 2011) thus suggesting an alternate mechanism of regulation for SLC41A1. Interestingly, it has been found that the predicted short N-terminal cytoplasmic domain (~92 residues) of SLC41A1 might be involved in a Mg^{2+} dependent endosomal recycling mechanism which is proposed to be the regulation mechanism for SLC41A1 (Mandt et al., 2011). MgtE can also functionally compensate for the absence of TRPM-7 in vertebrate B-cells (Sahni et al., 2012). In addition, SLC41A1 has also been characterized to function as a Na^+/Mg^{2+} exchanger (Kolisek et al., 2012). Further, as previously discussed, SLC41A1 has been implicated in

Parkinson's disease (Kolisek et al., 2013), head and neck cancer (Lin et al., 2015), and the attenuation of the pro-survival signal in cells (Sponder et al., 2018). Therefore, structural and functional studies on the bacterial ortholog MgtE can give valuable insight into the functional dynamics and regulation of the SLC41 protein family.

Table 1.1. Solved structures of MgtE in various conditions

Technique	Condition	Resolution	Residues	PDB ID	Detergent for extraction	Solved in	Reference
X-ray crystallography	Mg ²⁺ -bound	3.5 Å	7-448 (full-length)	2YVX	DDM ^a	DDM ^a	Hattori et al., Nature 2007
X-ray crystallography	Mg ²⁺ -bound	2.9 Å	23-449 (full-length)	2ZY9	DDM ^a	NTM ^a	Hattori et al., EMBO J. 2009
X-ray crystallography	Mg ²⁺ -ATP bound	3.6 Å	23-449 (full-length)	5X9G	DDM ^a	NTM ^a	Tomita et al., Nature Commun. 2017
X-ray crystallography	Mg ²⁺ -free	3.9 Å	5-252 (cytosolic domain)	2YVZ	NA ^b	NA ^b	Hattori et al., Nature 2007
X-ray crystallography	Mg ²⁺ -bound	2.9 Å	5-252 (cytosolic domain)	2YVY	NA ^b	NA ^b	Hattori et al., Nature 2007
X-ray crystallography	Mg ²⁺ -ATP bound	3.0 Å	5-252 (cytosolic domain)	5X9G	NA ^b	NA ^b	Tomita et al., Nature Commun. 2017
X-ray crystallography -LCP	Mg ²⁺ -bound	2.3 Å	271-449 (TM-domain)	4U9L	DDM ^a	Monoolein ^c	Takeda et al., Nature Commun. 2014
X-ray crystallography -LCP	Mn ²⁺ -bound	2.2 Å	271-448 (TM-domain)	4U9N	DDM ^a	Monoolein ^c	Takeda et al., Nature Commun. 2014
X-ray crystallography -LCP	Ca ²⁺ -bound	3.2 Å	271-448 (TM-domain)	4WIB	DDM ^a	Monoolein ^c	Takeda et al., Nature Commun. 2014
Cryo-EM	Mg ²⁺ -free	3.7 Å	271-448 (full-length)*	6LBH	DDM ^a	PMAL-C8 ^d	Jin et al., 2021

*Full-length MgtE construct was used for solving the structure, but only the cryo-EM density of TM-domain could be resolved.

^aDetergents used for solving structure.

^bNot applicable. Since only the cytoplasmic domain construct was used, detergents were not used for solving structures.

^cCrystal structure was solved by the lipidic cubic phase (LCP) method using monoolein. ^d Cryo-EM structure of MgtE was solved in the presence of PMAL-C8 amphipol.

1.6.2.2. Structure of the MgtE Mg²⁺ ion channel

Details of the structural studies on *Thermus thermophilus* MgtE are summarized in Table 1.1. It is evident from the three-dimensional crystallographic snapshot of the full-length MgtE in presence of Mg²⁺ in detergent micelles that it is a homodimeric channel (Fig. 1.6) of 450 amino acids with a molecular mass of approximately 50 KDa having a transmembrane C-terminal (TM) domain (made of five helices per monomer, labeled TM1-5) and a cytosolic N-terminal domain. The cytosolic domain is divided into two sub-domains: The N-domain and the cystathione-β synthase (CBS) domain. Interestingly, the N domain which forms a right-handed superhelix, shares similar structural features with the human FancF protein which is associated with signaling during DNA damage (Kowal et al., 2007). The CBS domain is repeated twice to further divide the CBS domain into CBS1 and CBS2 sub-domains (Hattori et al. 2007). Interestingly, the CBS domain is not exclusive to MgtE but has been found to play important regulatory roles in the human chloride channel (Bennetts et al., 2005), ATP binding cassette (ABC) transporters, and the evolutionary conserved Mg²⁺ transporters (Ignoul and Eggermont, 2005), cyclin M (CNNM) (Funato and Miki, 2019).

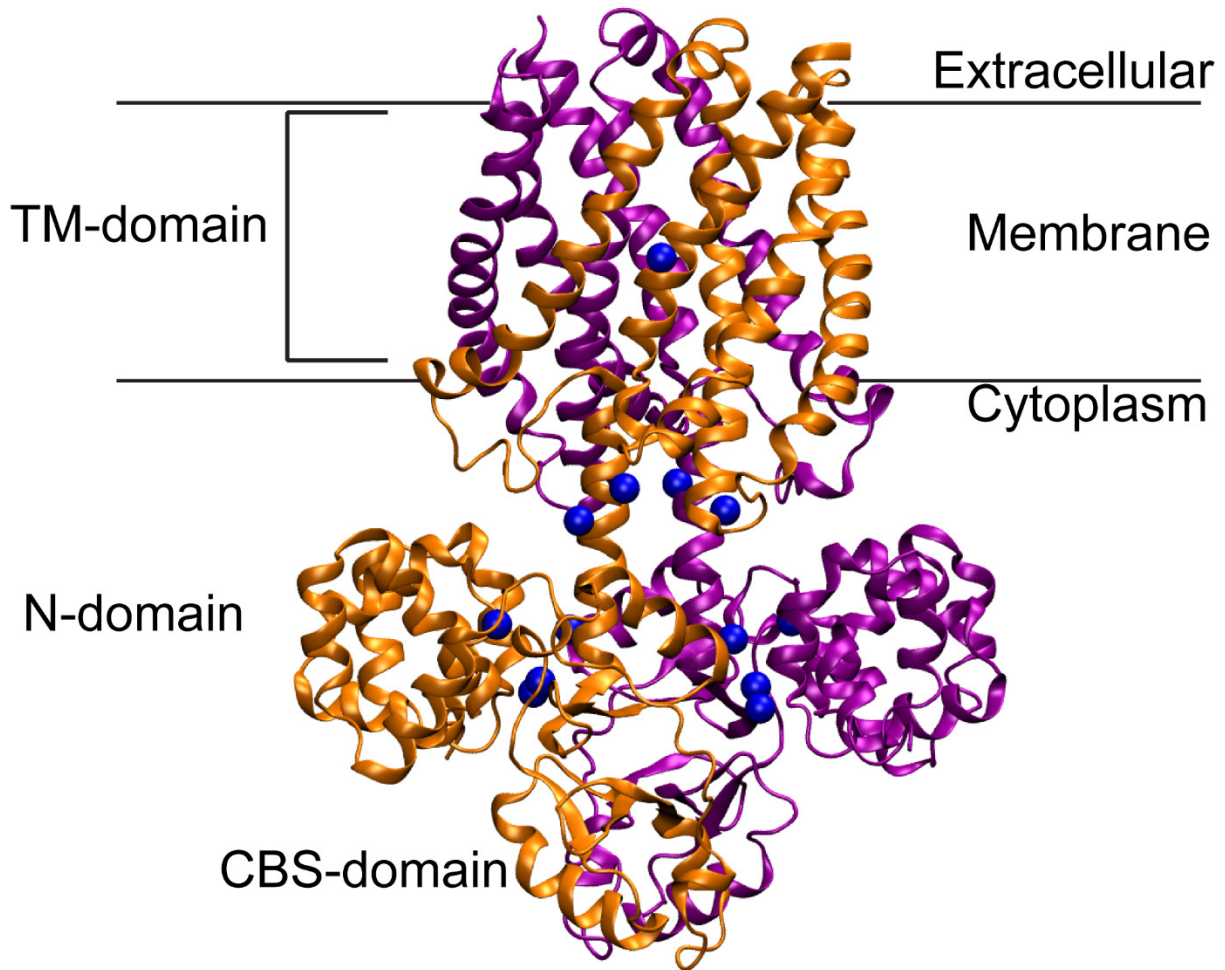


Fig. 1.6. Closed-state crystal structure of MgtE. Cartoon representation of the Mg²⁺-bound (blue spheres) crystal structure of homodimeric MgtE (PDB ID: 2ZY9) in detergent micelles at 2.94 Å showing the various domains of MgtE. The Mg²⁺-bound form represents the closed state of MgtE. The two subunits are represented by orange and purple colors.

A major part of the cytosolic domain (52 out of 244 residues) is made up of aspartic and glutamic acid residues rendering the cytosolic domain primarily acidic and thus facilitating interaction with the positively charged Mg^{2+} ions. The linker region between the cytosolic and the transmembrane domain forms a stretch helix, also referred to as the connecting or plug helix, lies perpendicular to the membrane interface (interacting with TM5) and is lined with several conserved acidic residues (D246, D247, D250, E253, E255, E258, and D259) forming an ion-conducting pore connecting the cytosolic domain to the transmembrane domain. The TM helices of MgtE are very unique in the way that they are connected by short loops (Fig. 1.7a). Further, the TM-domains of MgtE dimerize by hydrophobic interactions while hydrogen bonds between R285 and N402 (of adjacent monomer) and E359 (of adjacent monomer) and Y273 stabilize the homodimer channel (Fig. 1.7b). Interestingly, R285 and E359 are conserved in the MgtE family of ion channels amongst the eubacterial and archaeal origins. The transmembrane helices undergo a twist at the glycine or proline residues which might provide flexibility during the gating process or even may narrow the pore to increase ion selectivity.

The transmembrane helices form a putative ion-conducting pore which widens to about 15 Å towards the periplasmic opening and narrows to about 6 Å towards the cytosolic end. The periplasmic end is lined with hydrophobic residues with carbonyl groups facing towards the pore. In the middle of the pore the negatively charged residue, D432 of each monomer have their negatively charged side chains facing the pore while the cytoplasmic end of the pore is lined with hydrophilic residues. It might be presumed, as with the other ion channels, the orientation of the side chains is such that they can support the high energetic cost associated with dehydration of magnesium ion while transport.

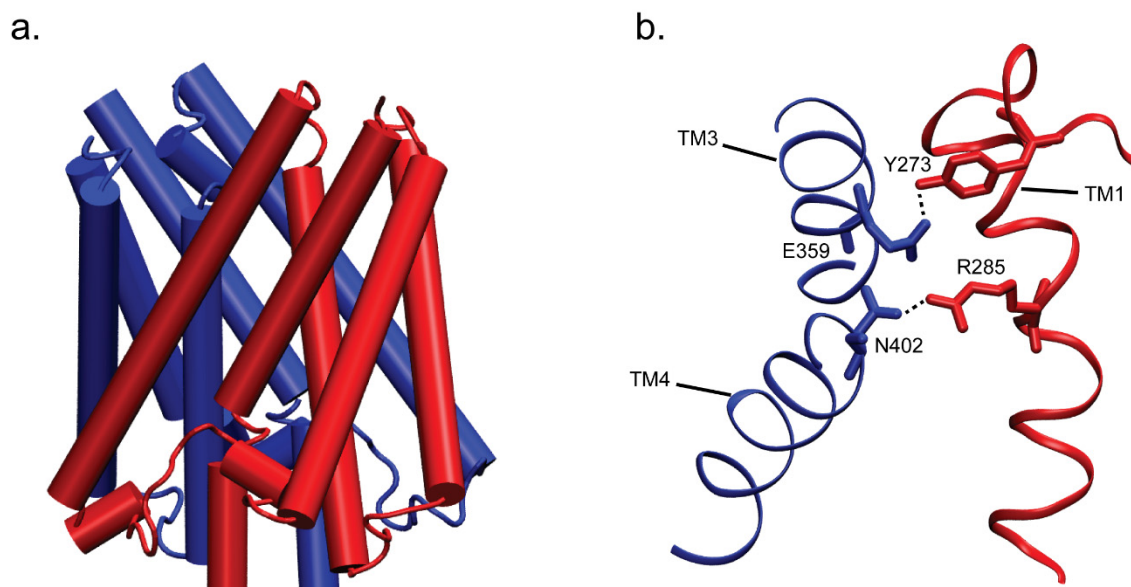


Fig. 1.7. TM-domain of MgtE. (a) Cartoon representation of the TM-domain of MgtE showing the transmembrane helices (cylinders) connected by short loops (strings). (b) Shown are the hydrogen bonds (depicted as dashed lines) between the TM-domains of the two monomers. Red and blue colors indicate the subunits of the MgtE homodimer (PDB ID: 2ZY9).

1.6.2.3. Cytosolic metal binding sites of MgtE

While the initial structure solved in dodecyl- β -maltopyranoside (DDM) micelles at a resolution of 3.5 Å shows the presence of 5 magnesium binding sites per monomer in the cytosolic domain (Hattori et al., 2007), the X-ray crystallographic snapshot solved at a higher resolution of 2.9 Å in n-nonyl- β -D-thiomaltoside (NTM) shows 6 Mg^{2+} binding sites (Mg2-Mg7) in the cytoplasmic domain per monomer (Hattori et al., 2009). Additionally, one binding site is present at the transmembrane domain (Mg1) where Mg^{2+} is coordinated by the side chains of D432 and carbonyl groups of A428 on TM5 of both the monomers.

Mg2 is located 6 Å away from Mg3 at the interface between the transmembrane and cytosolic domain. Mg2 is coordinated by D214 (at CBS domain), E255, and E258 (of plug helix). Mg3 on the other hand is coordinated by side chains of E216 (CBS domain), E259 (plug helix), and D418 (fourth loop of the transmembrane domain). Mg4 and Mg5 are at the interface between the N and CBS domains. Mg4 interacts with the side chains of D91 (N domain) and D247 (plug helix). Mg5 is recognized by the main chain carbonyl groups of A223 and the side chains of D226 (both in CBS domains). Mg6 resides 13 Å away from the Mg5 site and is coordinated by side chains of D95 (N domain), the main-chain carbonyl group of G136, and four water molecules. The Mg7 binding site was observed between E59 of the N-domain and D226 in the CBS domain from the adjacent subunit.

1.6.2.4. *MgtE* is a Mg^{2+} selective ion channel

Excellent biochemical, genetic and electrophysiological characterization of MgtE by Nureki and co-workers established the selective nature of the channel (Hattori et al., 2009). Initial genetic screens using a triple knock-out variant of *Escherichia coli* K12 strain which lacks the essential genes for Mg^{2+} transport (rendering it a Mg^{2+} auxotroph), showed growth complementation in presence of full-length wild-type MgtE indicating the Mg^{2+} transport capability of MgtE. Patch-clamp analysis of magnesium transporter deficient auxotrophic mutant *E. coli* spheroplasts complemented with only the MgtE gene showed that magnesium influx was depended only on magnesium and not on nickel, manganese, and calcium and that the current representing the open state increased with increasing negative membrane potential (Hattori et al. 2009). Moreover, a conductance of ~96 pS obtained from the slope of the current-voltage relationship at -40 mV corresponded to a transport efficiency of $\sim 3 \times 10^7$ ions at -60

mV indicating the channel-like properties of MgtE. Interestingly, patch-clamp performed with Co^{2+} also showed a representative current at a lower conductance of ~ 22 pS. This suggests that MgtE might be involved in the uptake of Co^{2+} as a micronutrient (Smith et al., 1995). Importantly, Cobalt (III) hexamine which is an analog to fully hydrated magnesium ion completely inhibited MgtE, indicating that a fully hydrated Mg^{2+} ion is initially recognized by the channel (Hattori et al., 2009).

1.6.2.5. Mg^{2+} -induced cytoplasmic domain movement

Three-dimensional X-ray crystal structures of the isolated cytoplasmic domain of MgtE from *T. thermophilus* (see Table 1.1) determined in the absence of Mg^{2+} (open/apo form) and presence of Mg^{2+} (closed/ligand-bound form) revealed large domain rearrangements between the two states. The N-domain in the apo/open form swings away from the CBS-domain after undergoing a $\sim 120^\circ$ rotation. The interactions between the CBS domains and N-domain dissociate probably due to inter-subunit repulsion by the highly acidic subunits in the absence of Mg^{2+} . In addition, the plug helices also have undergone a significant displacement thereby ‘unplugging’ the N-domain from the otherwise tightly bound CBS domains which would allow the permeation of Mg^{2+} . Paramagnetic relaxation enhancement (PRE) experiments suggest a dynamic interaction between the CBS- and N- domains in the absence of Mg^{2+} in solution (Imai et al., 2012). Further, molecular dynamics simulations performed in the presence of Mg^{2+} strongly support the notion that the N-domain stabilizes the closed conformation of the channel by restricting the movement of the CBS domain (Ishitani et al., 2008). Importantly, the Mg5 binding site which lies between the CBS domains of both the subunits seems to be critical for stabilizing the closed conformation of MgtE (Ishitani et al., 2008). Interestingly, a monovalent

cation (Na^+) placed at the Mg5 site could not stabilize the closed conformation of the CBS domain, indicating the specificity of divalent cations, particularly Mg^{2+} , for the cytoplasmic domain which is further supported biochemically by the fact that increasing Na^+ concentration could not protect MgtE from trypsin protease (Ishitani et al., 2008). Together, these studies suggest a possible Mg^{2+} -sensing regulatory mechanism of the cytoplasmic domain of MgtE.

Interestingly, solution NMR studies of full-length MgtE in detergent micelles revealed that Mg^{2+} -dependent structural changes are not only restricted to the cytoplasmic domain but also involve a conformational equilibrium with the transmembrane domain which is suppressed by Mg^{2+} binding (Maruyama et al., 2018). Importantly, all portions of MgtE do not respond equally to the same concentrations of Mg^{2+} . While NMR signals associated with residues lying close to the Mg1 site saturate at lower concentrations of Mg^{2+} , residues of the N- and CBS-domain show signal saturation at higher Mg^{2+} concentrations (>4 mM). Further, cooperative binding of Mg^{2+} to the cytoplasmic binding sites (Mg2-7) enables the stabilization of the closed conformation of MgtE suggesting that the cytoplasmic domain might function as a ' Mg^{2+} -sensor' (further discussed below).

1.6.2.6. Negative feedback regulation of MgtE by Mg^{2+}

The Mg^{2+} sensing mechanism of MgtE was tested electrophysiologically in inside-out patches excised from *E. coli* spheroplasts by decreasing the difference in concentration of Mg^{2+} between the bath (analogous to the intracellular compartment) and the pipette solutions (analogous to extracellular medium) (Hattori et al., 2009). Mg^{2+} conduction was diminished to a near zero at concentrations of 5 to 10 mM Mg^{2+} in the bath solution. This shows negative feedback imposed on MgtE in response to decreasing difference in Mg^{2+} concentration between

the periplasm and cytosol. To test the specificity of this feedback, currents were recorded using the near cognate of Mg^{2+} , Ca^{2+} which showed the regulation at a much higher concentration than what is generally found at physiological conditions while experiments with monovalent cations like Na^+ and K^+ did not give any conduction. Thus, proving that MgtE acts not only as a divalent cation sensor but is highly specific to regulation in response to Mg^{2+} concentrations present in the physiological range.

1.6.2.7. Cytoplasmic domain of MgtE as a divalent cation sensor

Although several Mg^{2+} binding sites are present at the cytoplasmic domain of MgtE (Hattori et al., 2007; 2009), the importance of this domain as a gating modulator was realized after extensive functional characterization of key mutants in the cytoplasmic domain (Hattori et al., 2009). The Mg^{2+} at Mg5 binding site is coordinated by the γ -carboxyl group of D226 and main chain carbonyl group of A223 of one subunit, and the main chain carbonyl group of D250 of the other subunit. Mutations in the Mg5 binding site (D226N/D250A) abolished the negative regulation by Mg^{2+} evident by similar open probabilities in low or high intracellular Mg^{2+} . Similarly, mutating key residues of the Mg2 and Mg3 Mg^{2+} binding sites (E238Q at Mg2 or D259N at Mg3) present on the plug helices, which are hypothesized to be neutralized when bound to Mg^{2+} stabilizing the closed state of the channel, inhibits the Mg^{2+} -dependent negative regulation of MgtE. Interestingly, deleting the N-domain resulted in much higher open probabilities irrespective of intracellular Mg^{2+} concentration, therefore, indicating the loss of Mg^{2+} -dependent negative regulation of MgtE. Therefore, the cytoplasmic domain, particularly, the N-domain can be hypothesized to be acting as a ' Mg^{2+} -sensor' and a gating modulator for the Mg^{2+} -dependent gating of MgtE.

1.6.2.8. MgtE ion pore

Nureki and co-workers showed that mutations of the conserved polar residues involved in dimer interactions (R285, Q333, and E359) to alanine, abolished the growth complementation, thereby supporting the fact that MgtE functions as a dimer (Hattori et al., 2009). Interestingly, it was seen that mutating the hydrophobic residues near the periplasmic side (F318A, P321A, L324A) and the residue which is central to the ion-conducting pore (D432A and N329A) abolished the growth complementation indicating that these residues are crucial in forming the ion-conducting pore which was further shown by loss of transporter activity by patch-clamp analysis (Hattori et al., 2009). Importantly, the presence of the Mg1 site at D432 suggests this site to be an ion-selective site of the MgtE ion pore.

Interestingly, unlike other ion channels like members of the K⁺ channel family; KcsA (Zhou et al., 2001, Morais-Cabral et al., 2001), MthK (Ye et al., 2010), and NaK (Alam and Jiang, 2009) which conduct K⁺ after stripping it off its hydration, MgtE recognizes a fully hydrated Mg²⁺ at the Mg1 site in the ion pore as determined by the Mg²⁺ high-resolution crystal structure of MgtE-transmembrane domain in monoolein lipids using the lipid cubic phase method (LCP) of crystallography (Takeda et al., 2014). Further, hydrogen bonds between the first and second hydration shells of the hexacoordinated water molecules of Mg²⁺ and carboxyl atoms of D432 (primary residue forming the Mg1 site), backbone carbonyl oxygen atoms of P321 and L324 of TM2 and A428 of TM5 stabilize and thus help in recognition of the hydrated Mg²⁺ ion having octahedral geometry (Takeda et al., 2014). Interestingly, although the size of fully hydrated Mg²⁺ (~ 6 Å) is slightly larger than the distance between the D432 residues in the ion pore (~ 5 Å), electrostatic interactions between the negatively charged D432 and the

contributing hydrogen bonds with the hydration shells of Mg^{2+} and M1 site might reduce the imposed steric barrier.

Recently, a 3.7 Å cryo-EM structure of MgtE-Fab complex in Mg^{2+} -free conditions is available in which the cryo-EM density is only detectable for the TM-domain (see Table 1.1). It is evident from the cryo-EM structure that there is a ‘partial opening’ of the ion pore where the pore is open towards the cytoplasmic end while the pore remains closed towards the periplasmic end (Jin et al., 2021). Interestingly, it was observed that the cytoplasmic pore opening was facilitated by the TM2 and the TM5 helices. Glycine residues of these helices (G325 and G328 of TM2 and G435 of TM5) were found to be responsible for the kink motions involved in the movement of the TM2 and TM5 helices. Considering the fact that MgtE is in equilibrium with both the open and closed state in absence of Mg^{2+} (Hattori et al., 2009) it is possible MgtE may have a partially closed non-conductive state without Mg^{2+} to stabilize the closed conformation and in the presence of high intracellular Mg^{2+} the non-conductive closed conformation of the channel is favored. Therefore, it can be presumed that in presence of low-intracellular Mg^{2+} there are myriad of possible conformations of the cytoplasmic domain, which was also evident from the jagged topography seen in the high-speed atomic force microscopy (HS-AFM) image of MgtE (Haruyama et al., 2019), while the closed conformation of MgtE is favored in presence of high (>10 mM) intracellular Mg^{2+} concentration.

1.6.2.9. Regulation of MgtE gating at the periplasmic site

The high-resolution X-ray crystallographic snapshot of the MgtE-transmembrane domain in monoolein environment in the presence of Mn^{2+} and Ca^{2+} showed strong electron densities for these divalent cations at the Mgl site in their fully hydrated forms (see Table 1.1. and ref

[Takeda et al., 2014]). The interaction between hydrated Ca^{2+} and the Mg1 site is unstable compared to that of Mn^{2+} and Mg^{2+} arising due to the otherwise dynamic coordination number of Ca^{2+} with water molecules (Katz et al., 1996; Pavlov et al., 1998; Jalilehvand et al., 2001), resulting in a lower resolution Ca^{2+} bound structure of MgtE (3.2 Å) compared to the Mn^{2+} bound form (2.2 Å).

Interestingly, other than the Mg1 site, Mn^{2+} was found to be bound to M2 (consisting of side chains from Q304 and E307), M2' (consisting of side chains from E307, E311, D438, and main chains of R345 and D346), and M3 (consisting of side-chain carboxylate group of E275) sites at the periplasmic site of MgtE while Ca^{2+} was bound to the M3 site (Takeda et al., 2014). However, Mg^{2+} was not observed in any of the above sites thereby suggesting a cation selectivity mechanism mediated by side-chain coordination at these sites. While wild-type MgtE showed no transport activity of Mn^{2+} and Ca^{2+} , mutating the residues of the M2 (M2A), M3 (M3A), and both M2 and M3 (M2M3A) sites resulted in a high permeability of Mn^{2+} and Ca^{2+} , although Mg^{2+} transport activity was unaffected irrespective of the wild-type or mutants forms. Additionally, in presence of Mn^{2+} , Mg^{2+} permeation was inhibited in wild-type MgtE, while the inhibitory effect was greatly reduced for mutant forms (M2A, M3A, and M2M3A). However, the presence of Ca^{2+} did not affect the Mg^{2+} transport activity irrespective of wild-type or mutant forms of MgtE (Takeda et al., 2014). Therefore, it is suggested that the Mn^{2+} stabilizes the closed-form of MgtE preventing entry of Mg^{2+} . Overall, these observations suggest an alternate gating mechanism at the periplasmic site regulated by Mn^{2+} other than the canonical Mg^{2+} -dependent negative regulation of MgtE.

1.6.2.10. Modulation of MgtE gating by ATP

It is known that CBS domains present in various enzymes and transporters like human CLC5 Cl⁻ transporter contain a regulatory nucleotide-binding site (Meyer et al., 2007). However, the nucleotide-mediated regulation of MgtE was unclear. Isothermal titration calorimetry (ITC) studies showed that while Adenosine triphosphate (ATP) binds to MgtE with a high affinity (K_d of 0.415 mM) and Adenosine diphosphate (ADP) binds with a slightly lower affinity (K_d of 0.763 mM), no interaction was observed for Guanosine triphosphate (GTP) (Tomita et al., 2017). Similar results were recapitulated biochemically using protease protection assay which showed sufficient protection in presence of ATP and ADP but not with GTP. X-ray crystallographic snapshot of the full-length and cytoplasmic domain of MgtE co-crystallized with ATP (see Table 1.1), showed its presence in the interface of the N-domain of one subunit and CBS-domain of the adjacent subunit. Interestingly, the interaction of ATP with the cytoplasmic domain is independent of the Mg²⁺ ions (Tomita et al., 2017). Further, the superimposition of the GTP structure on the ATP structure showed a steric clash between the amino group of the guanine base with the ATP binding pocket. It is to be noted that the stable presence of ATP in the crystal structure is indicative of the fact that MgtE lacks ATPase activity which was also supported biochemically by ATP hydrolysis assay (Tomita et al., 2017).

Patch-clamp experiments of MgtE in presence of 3 mM ATP showed channel inactivation at a much lower concentration of intracellular Mg²⁺ (3 mM) than seen for MgtE in absence of ATP (10 mM Mg²⁺) suggesting an enhancement of Mg²⁺ affinity in presence of ATP (Tomita et al., 2017). The molecular interaction of ATP with the cytosolic domain of MgtE was assessed by mutating key residues (F227, R187, and D188) in the binding pocket of the cytoplasmic domain systematically characterizing them biochemically and by patch-clamp

experiments. Interestingly, while mutating F227 to alanine abolished ATP-dependent gating modulation, D188A behaved similarly to wild-type MgtE. F227A mutant showed no binding affinity to MgtE but R187E mutant showed a weaker binding affinity suggesting the importance of binding of the side-chain rather than the main chain of the arginine residue to γ -phosphate group of ATP. Similarly, patch-clamp and biochemical experiments showed that F227A mutant completely diminished the enhanced Mg^{2+} affinity of MgtE in presence of ATP, thereby suggesting the pivotal role played by this residue in binding ATP. Intriguingly, when R187 was replaced with negatively charged glutamate (R187E), it was seen that irrespective of the presence or absence of ATP the open probabilities of the channel were similar to that of wild-type MgtE in presence of 3 mM ATP, thereby indicating that introduction of a negative charge had a similar effect to that of binding negatively charged ATP. Overall, these observations led to believe that the extra negative charge contributed by the phosphate groups after ATP binding further enhances the affinity for the positive Mg^{2+} thereby reducing the concentration of Mg^{2+} needed to close the channel (Tomita et al., 2017). This hypothesis was supported by the fact that in presence of ADP (having one less phosphate group than ATP), MgtE was gated at a higher concentration of Mg^{2+} than in presence of ATP.

1.6.2.11. Dual role of MgtE

It has been recently shown that MgtE ortholog from *Pseudomonas aeruginosa* not only transports Mg^{2+} but also has a role in biofilm formation (Coffey et al. 2014). Mutating Mg^{2+} binding sites 2 and 3 resulted in uncoupling of Mg^{2+} transport from regulation of cytotoxicity in *P. aeruginosa*. It was also reported that truncating 37 amino acids of the N-terminal of MgtE resulted in the loss of Mg^{2+} transport activity but cytotoxicity was retained. The combination of

these results indicated that MgtE has a moonlighting activity of regulating cytotoxicity in addition to its primary activity as a divalent cation transporter. The authors also found that the expression of *mgtE* gene is regulated by magnesium concentration. Hence, it might be speculated that low magnesium conditions found in a cystic fibrosis lung triggers MgtE expression and plays an important role in the virulence of *P. aeruginosa* (Coffey et al., 2014).

1.7. Objectives

While a good amount of effort has been given to understand the gating and permeation mechanisms of MgtE, the structural dynamics of MgtE in membranes upon gating is not yet fully understood. To gain a deeper insight into understanding the structural and functional dynamics of MgtE Mg^{2+} channel, the present thesis has been undertaken with the following objectives:

- It is well-known that extraction of membrane proteins from the native membrane source remains the biggest obstacle in obtaining large quantities of pure, stable and functional proteins that are needed for characterizing the functionally-relevant structural dynamics utilizing sophisticated biophysical approaches. In this context, detergents serve as an indispensable tool for the membrane solubilization and extraction of membrane proteins. However, the membrane protein purification process in general, and detergent-mediated membrane solubilization in particular, is very expensive. In lieu of this, we have screened for relatively inexpensive detergents and extensively characterized the optimum purification conditions which can extract MgtE in a pure, stable and functional form that can be used for further biophysical studies in a cost-effective manner.
- Although the full-length MgtE structural snapshot is available in one functional state (closed state), the gating-related structural dynamics in physiologically-relevant membranes is poorly understood. As mentioned earlier, most of the structures of MgtE have been solved in detergent micelles and studies focused on MgtE organization and dynamics in membranes are scarce. Most importantly it is now known that micelles, despite being widely used as membrane-mimetic systems, have been shown to drastically affect the function, dynamics and structural integrity in several membrane proteins. Therefore, we sought to identify the organization and dynamics of MgtE in membrane-

mimetics. Further, we have monitored the gating-related structural dynamics of MgtE in the physiologically-relevant membrane environment. To do this, we have exploited the fluorescence properties of the native Trps (two in the cytoplasmic N-domain and the four in the transmembrane domain per monomer) of MgtE so as to obtain site-specific structural and dynamic information of full-length MgtE in response to gating in membrane-mimetics using sophisticated fluorescence techniques.

- As discussed above, the importance of the N-domain as a Mg^{2+} -sensor and stabilizing the closed state of MgtE was realized by electrophysiology, simulation and structural determination of the isolated cytoplasmic domain. However, the structural dynamics information of the N-domain in full-length MgtE when shuttling from the open to closed still remains obscure. Therefore, to understand the gating-related dynamics of the N-domain, particularly the N-domain residues around the Mg^{2+} binding sites at the subunit interface of the N- and CBS-domain, in different functional states of MgtE in physiologically relevant membranes we have systematically constructed single-cysteine mutants around the Mg^{2+} binding sites of the N-domain. We have labeled these residues with the environment sensitive dye, NBD, and monitored the gating-related dynamics of MgtE in membrane-mimetics utilizing sophisticated site-directed fluorescence approaches.

Chapter 2

Materials and methods

2.1. Materials

E. coli C41(DE3) strain was purchased from Agilent (Santa Clara, CA). n-dodecyl- β -D-maltopyranoside (DDM), Triton X-100 and Anzergent 3-14 were obtained from Anatrace (Maumee, OH). Mouse anti-6X His tag antibody and goat anti-mouse IgG H&L (HRP) was from Abcam (Cambridge, MA). Protease inhibitors were obtained from GoldBio (St. Louis, MO). Pre-stained molecular weight markers were obtained from Bio-Rad (Richmond, CA). 1-palmitoyl-2-oleoyl-*sn*-glycero-3-phosphocholine (POPC) and 1-palmitoyl-2-oleoyl-*sn*-glycero-3-phospho-(1'-rac-glycerol) (POPG) were obtained from Avanti Polar Lipids (Alabaster, AL). All other chemicals used were of the highest purity available from either Merck (Kenilworth, NJ) or Amresco (Radnor, PA).

2.2. Cloning and expression test of MgtE

The gene encoding MgtE from *Thermus thermophilus* genomic DNA from strain HB8 (ATCC 27634) was PCR-amplified and cloned into a pET28a vector (N-terminal His-tag) between NdeI and XhoI restriction sites. The MgtE construct was transformed into chemically competent *E. coli* C41 (DE3) cells by the heat shock method and grown overnight at 37 °C in Luria-Bertani (LB) broth containing 50 μ g/ml of kanamycin. The following day, 1% of the overnight pre-culture was used to start a mini-culture using LB broth containing 50 μ g/ml of kanamycin and grown at 37 °C till the cells reached optical density (OD) at 600 nm of 0.5. Protein expression was started by inducing cells with 0.5 mM isopropylthiogalactoside (IPTG) at 0.5 OD. After induction, cells were incubated under constant agitation (250 rpm) at 37 °C for 4 hours, 30 °C for 4 hours or 20 °C for 20 hours. Pre- and post-induction cells (normalized to OD 0.5) were collected, harvested and lysed using Laemmli buffer and electrophoresed in a 10%

SDS-PAGE. The gel was electro-transferred to a polyvinylidenedifluoride (PVDF) membrane for 2 hours. Membranes were blocked for 1 hour at room temperature with 3% Bovine serum albumin (BSA) in phosphate buffered saline (PBS), pH 7.4 followed by overnight incubation with mouse anti-histidine antibody (1:5000 dilution) at 4 °C. After three washes with PBS containing 0.02% Tween-20 (PBST), the membranes were incubated with goat anti-mouse antibody (1:10000 dilution) for 2 hours. After three washes with PBST, the MgtE bands were visualized using a GE Healthcare Life Sciences ImageQuant LAS 500 system.

2.3. Detergent-mediated solubilization of MgtE

Small-scale solubilization tests were performed with different detergents as follows: Wild type MgtE was expressed in 100 ml Luria-Bertani (LB) broth containing 50 µg/ml of Kanamycin and was induced at 0.5 OD with 0.5 mM of IPTG. The cells were grown overnight at 20 °C post-induction and then harvested by centrifuging at 5000 rpm and resuspended in 8 ml of 20 mM HEPES buffer. The cells were then sonicated in the presence of protease inhibitors: 1 µg/ml aprotinin, 10 µM leupeptin and 1 µM pepstatin A, and the membrane fraction was separated by ultracentrifugation at 100,000 g. The resuspended membrane fractions were then subjected to detergent solubilization by using 10 mM of DDM, Triton X-100 or Anzergent 3-14, ~50X critical micelle concentration (CMC), for 2 hours at 4 °C in different NaCl concentrations (150 to 1200 mM). The combined effect of the chemical osmolyte (10% glycerol) with high concentration of NaCl (1200 mM) during solubilization was also assessed. The detergent-soluble fraction (supernatant) was then separated by centrifugation at 30,000 g for 45 minutes at 4 °C, and was electrophoresed in a 10% SDS-PAGE followed by Western blotting as described above.

2.4. Large scale expression and purification of MgtE

The wild type MgtE was expressed in 1 L cultures and induced at 37 °C, 30 °C and 20 °C, respectively. The harvested cells were disrupted and the membrane fraction was solubilized using different detergents as described above. The supernatant containing the detergent-solubilized membrane was incubated with Ni²⁺ resin for 15 min. followed by passing it through a column. The resin was washed with 20 mM HEPES, 150 mM NaCl, 1 mM DDM, 50 mM imidazole, pH 7.0 buffer and MgtE was eluted with buffer containing 300 mM imidazole and 1 mM DDM. The eluate was then concentrated in Amicon Ultra 30K filter (Merck Millipore). To analyze whether the channel is properly folded, the purified protein was applied onto a Superdex 75 10/300 column (GE Healthcare) size-exclusion column equilibrated with 20 mM HEPES, 150 mM NaCl, 1 mM DDM, pH 7.0 buffer. The main peak of the gel filtration profiles was collected to measure the concentration of the purified MgtE (normalized to per litre of culture) using the molecular weight (~50 KDa) and molar extinction coefficient (53860 M⁻¹cm⁻¹) of wild-type MgtE in a DS-11+ microvolume spectrophotometer (DeNovix).

2.5. Mutagenesis, channel expression and purification

The gene encoding MgtE from *Thermus thermophilus* genomic DNA from strain HB8 (ATCC 27634) was cloned into a pET28a vector with a N-terminal His-tag am(Qiagen, Hilden, Germany) and single-Trp or single-cysteine mutants were generated. To generate single-Trp mutants of MgtE, we made a Trp-less mutant, where all the native Trps have been converted to phenylalanine (W37F/W79F/W282F/W288F/W352F/W380F). Then one Trp at a time was introduced back to its native site making six ‘Trp-only’ mutants. For instance, reintroducing Trp37 to the Trp-less construct would result in a construct (‘W37only’) with only one tryptophan

residue in MgtE. For Tryptophan-induced quenching (TrIQ) experiments double-mutants, that is, W37F in the respective single-cysteine mutant background, was constructed for control samples where TrIQ is not possible. The mutations were confirmed by DNA sequencing. Single-cysteine, Trpless and single-Trp mutants of MgtE were expressed and purified using the ‘dual-detergent strategy’ as described previously except that 10% glycerol was added during solubilization step for Trp-less and Single-Trp mutants. The concentration of the protein was checked in a DS-11+ microvolume spectrophotometer (DeNovix, Wilmington, DE). To analyze whether the channel is folded properly, the purified protein was applied onto a Superdex 75 10/300 (GE Healthcare, Chicago, IL) size-exclusion column equilibrated with 20 mM HEPES, 150 mM NaCl, 1 mM DDM (pH 8.0) buffer. The purified MgtE in the absence of added Mg^{2+} represents the open state and the channel is closed by incubating in presence of 20 mM $MgCl_2$ for 30-40 minutes.

2.6. Site-directed fluorescence labelling of MgtE single-cysteine mutants

The purified single-cysteine mutants of MgtE N-domain were treated with 5 mM dithiothreitol (DTT) for 1 h before labeling with IANBD amide (N,N’ -dimethyl-N-(iodoacetyl)-N’-(7-nitrobenz-2-oxa-1,3-diazol-4-yl)ethylenediamine) or monobromobimane (mBBBr), which is a thiol-reactive environment-sensitive fluorescent probe (Invitrogen, Carlsbad, CA). The excess DTT is removed by passing through a PD10 desalting column (GE Healthcare). After removing DTT, purified proteins in DDM micelles were labeled with fluorophore at a 10:1 (fluorophore/protein) molar ratio from a stock of either 42 mM IANBD or 100mM monobromobimane (mBBBr) in dimethylsulfoxide and incubated overnight at 4 °C. Excess NBD or mBBBr fluorophore was separated using a PD10 column. The labeling efficiency of the NBD or

mBBR-labeled single-cysteine mutants of MgtE N-domain were found to be more than 50% using the following equation:

$$\text{Labeling efficiency (\%)} = \frac{A_x}{\varepsilon} \times \frac{\text{MW of protein}}{\text{mg protein/ml}} \times 100, \quad \text{Eq. 1}$$

where A_x is the absorbance of NBD at 478 nm or mBBR at 380 nm and ε is the molar extinction coefficient of NBD or mBBR at that wavelength (25,000 M⁻¹ cm⁻¹ or 5000 M⁻¹ cm⁻¹, respectively).

2.7. Membrane reconstitution of MgtE and its mutants

The mutants of MgtE were reconstituted at a lipid-to-protein molar ratio of 100:1 in POPC: POPG (3:1) liposomes. Briefly, 120 nmoles POPC and 40 nmoles of POPG (160 nmoles of total lipids) in chloroform were mixed well and dried under a stream of nitrogen while being warmed gently (~35 °C). After the lipids were dried further under a high vacuum for at least 3 hr, they were hydrated (swelled) by adding 1 ml of 20 mM HEPES, 150 mM NaCl (pH 8.0 was used for single-Trp mutants while for all other cases pH 7.0 was used) buffer and vortexed vigorously for 2 min to disperse the lipids and sonicated to clarity. Protein was then added to give a molar ratio of 100:1 lipid:MgtE. The sample was left at room temperature for 30 minutes on a rotator and 200 mg of pre-washed biobeads (SM-2, Bio-Rad, Hercules, CA) were then added and the mixture was incubated on a rotator overnight at 4 °C to remove the detergent. The biobeads were removed by filtering using a Bio-Rad 5 ml column filter before use.

2.8. Circular dichroism (CD) measurements

CD measurements were carried out at room temperature in a Jasco J-815 spectropolarimeter purged with a nitrogen flow of 15 L/min. Wild-type MgtE, Trpless and

single-Trp mutants were measured at a concentration of 2 μM in 20 mM HEPES, 150 mM KCl, 1 mM DDM (pH 7.0 or 8.0) buffer to obtain a good signal-to-noise ratio. The spectra were scanned with a quartz optical cuvette with a pathlength of 0.1 cm. All spectra were recorded with a bandwidth of 1 nm and integration time of 0.5 s with a scan rate of 50 nm/min. Each spectrum is the average of 10 scans. All spectra were appropriately blank subtracted and smoothed so as to ensure that the overall shape of the spectra remains unaltered. The ellipticity data obtained in millidegree was converted to molar ellipticity ($[\theta]$) by using the following equation:

$$[\theta] = \theta_{\text{obs}} / (10Cl) \quad \text{Eq. 2}$$

where θ_{obs} is the observed ellipticity in millidegree, C is the concentration in mol/L and l is the pathlength in cm.

2.9. Limited protease protection assay

The limited protease protection assay with purified wild type MgtE, extracted using DDM, Triton X-100 or Anzergent 3-14, was carried out as follows: 5 μl of purified MgtE (2 mg/ml) was equilibrated with 0 to 32 mM MgCl_2 for 30 minutes, and 2 μl of trypsin (15.6 $\mu\text{g/ml}$) was added to each reaction mix and incubated at 4 $^\circ\text{C}$ for 17 hrs. Wild type MgtE with no added Mg^{2+} and trypsin served as a control. After the addition of 4X laemmli buffer, the samples were run on a 10% SDS-PAGE.

2.10. Mg^{2+} transport assay

The fluorescence assay for Mg^{2+} transport using the Mg^{2+} -sensitive fluorophore Mag-Fura-2 was carried out as described previously (Payandeh et al., 2008). The wild-type and Trp-less mutant of MgtE were reconstituted in POPC/POPG (3:1 mol/mol) liposomes as described

above with few modifications. Briefly, the dried lipids were hydrated (swelled) by adding 1 ml of 20 mM HEPES, 150 mM KCl, pH 8.0 buffer and vortexed vigorously for 2 min to disperse the lipids. Membrane-impermeable Mag-Fura-2 (Invitrogen) was added to a final concentration of 60 μ M to the lipid suspension and sonicated to clarity to form small unilamellar vesicles loaded with Mag-fura-2. The total lipid used was 2560 nmoles and the protein reconstitution was done at a lipid-to-protein molar ratio of 1000:1. Mag-Fura-2-loaded proteoliposomes were subsequently separated from nonencapsulated (free) Mag-Fura-2 by gel filtration on a Sephadex G-50 column (GE Healthcare, Chicago, IL) using a potassium-free buffer (150 mM N-methyl-D-glucamine chloride (NMDG-Cl), 20 mM HEPES, pH 8.0) to remove extraliposomal potassium and generate an outward potassium gradient. Fluorescence intensity measurements in a time-scan mode were made at room temperature in a PTI Quantamaster 8000 (HORIBA) spectrofluorometer in 3 ml quartz cuvette with constant stirring and a nominal bandpass of 5 by 5. Magnesium influx was initiated by adding 20 mM $MgCl_2$ after making sure that the baseline for the Mag-Fura-2 loaded proteoliposomes is flat. Continuous recording of fluorescence emission intensity of Mag-Fura-2 at 509 nm was used to monitor the rate of magnesium influx while exciting at 329 nm. Experiments with protein-free Mag-fura-2 liposomes served as control.

2.11. Steady-state fluorescence measurements

Steady-state fluorescence measurements were performed with a Hitachi F-7000 spectrofluorometer using 1 cm path length quartz cuvettes. Excitation and emission slits with a nominal bandpass of 5 nm were used for all measurements except in Mg^{2+} titration experiments in which excitation and emission slits used were 1 nm for emission maximum measurements. Background intensities were appropriately subtracted from each sample spectrum to cancel out

any contribution due to the solvent Raman peak and other scattering artefacts. Corrected spectra were recorded for measuring tryptophan fluorescence of MgtE in micelles and when reconstituted in membranes. Fluorescence anisotropy measurements were performed at room temperature using Hitachi polarization accessory. Anisotropy values were calculated from the equation (Lakowicz, 2006):

$$r = \frac{I_{VV} - GI_{VH}}{I_{VV} + 2GI_{VH}} \quad \text{Eq. 3}$$

where, I_{VV} and I_{VH} are the measured fluorescence intensities (after appropriate background subtraction) with the excitation polarizer vertically oriented and emission polarizer vertically and horizontally oriented, respectively. G is the grating correction factor and is the ratio of the efficiencies of the detection system for vertically and horizontally polarized light, and is equal to I_{HV}/I_{HH} . The apparent (average) rotational correlation times were calculated using Perrin's equation (Lakowicz, 2006):

$$\tau_c = \langle \tau \rangle r / (r_o - r) \quad \text{Eq. 4}$$

where r_o is the limiting anisotropy of Trp (0.16), r is the steady-state anisotropy, and $\langle \tau \rangle$ is the mean fluorescence lifetime taken from Table 2 and 3.

Red edge excitation shift (REES) measurements were done by measuring the emission maximum as a function of increasing excitation wavelength from 295 to 305 nm or 465 to 515 nm for tryptophan and NBD, respectively. The magnitude of REES represents the total shift in emission maximum upon the indicated change in the excitation wavelength. The REES data was fitted by a Gaussian probability distribution of the form (Catici et al., 2016):

$$f(x) = R_0 + \frac{A\sqrt{2/\pi}}{w} \exp\left(-2\left(\frac{x-m}{w}\right)^2\right) \quad \text{Eq. 5}$$

where A is the area, w is the full width at half-maximum (fwhm), m is the midpoint and R_0 is the y-intercept and m is the excitation wavelength that gives the largest change in the emission peak wavelength.

2.12. Time-resolved fluorescence measurements

Fluorescence lifetimes were calculated from time-resolved fluorescence intensity decays using HORIBA Fluoromax-3 in time-correlated single-photon counting (TCSPC) mode with a picosecond pulsed 285 nm and 456 nm Nano-LED as the light source for exciting tryptophan and NBD, respectively. Lamp profiles were measured at the excitation wavelength using Ludox (colloidal silica) as the scatterer. To optimize the signal/noise ratio, 10,000 photon counts were collected in the peak channel. All experiments were performed with a bandpass of 5-8 nm. Fluorescence intensity decay curves so obtained were deconvoluted with the instrument response function and analysed as a sum of exponential terms:

$$F(t) = \sum_i \alpha_i \exp(-t/\tau_i) \quad \text{Eq. 6}$$

where $F(t)$ is the fluorescence intensity at time t and α_i is a pre-exponential factor representing the fractional contribution to the time-resolved decay of the component with a lifetime τ_i such that $\sum_i \alpha_i = 1$. Mean (average) lifetimes $\langle \tau \rangle$ for triexponential decays of fluorescence were calculated from the decay times and preexponential factors using the following equation (Lakowicz, 2006):

$$\langle \tau \rangle = \frac{\alpha_1\tau_1^2 + \alpha_2\tau_2^2 + \alpha_3\tau_3^2}{\alpha_1\tau_1 + \alpha_2\tau_2 + \alpha_3\tau_3} \quad \text{Eq. 7}$$

The mean fluorescence lifetime, τ_H , can be directly calculated using a model-independent approach from the histogram of photons obtained during fluorescence lifetime measurements using the following equation (Fiserova and Kubala, 2012):

$$\tau_H = \frac{\sum_{i=p}^n (N_i - \text{noise}) t_i}{\sum_{i=p}^n (N_i - \text{noise})} - t_p \quad \text{Eq. 8}$$

where N_i and t_i denote the number of detected photons in the i -th channel and the corresponding value on the time axis, respectively, n is the total number of channels in the histogram, p is the channel with the highest number of detected photons (peak of the decay) and t_p is the corresponding time.

2.13. Maximum Entropy Method (MEM) analysis of fluorescence intensity decay

The fluorescence decay data analysis by MEM represents a convenient, robust, model-free and realistic approach of data analysis (Brochon, 1994; Swaminathan and Periaswamy, 1996; Smith et al., 2017). In MEM, the fluorescence intensity decay $[I(t)]$ is analysed using the model of continuous distribution of lifetimes:

$$I(t) = \int_0^{\infty} \alpha(\tau) \exp(-t/\tau) dt \quad \text{Eq. 9}$$

where $\alpha(\tau)$ represents the amplitude corresponding the lifetime τ in the intensity decay. In practice, the limits on the above integration are set based on the information regarding the system under study and the detection limit of the instrument. In our case, the lower and upper limits are

set to 0.1 ns and 10 ns, respectively. For practical purposes, the above equation can be written in terms of a discrete sum of exponentials as

$$I(t) = \sum_{i=1}^N \alpha_i \exp(-t/\tau_i) \quad \text{Eq. 10}$$

where N represents the total number of exponentials. In our analysis, N is taken as 100 exponentials equally spaced in the $\log(\tau)$ space between the lower and upper limits. MEM initially starts with a flat distribution of amplitudes $\alpha(\tau)$, i.e., each lifetime has equal contribution in the beginning and arrives at the amplitude distribution which best describes the observed experimental fluorescence intensity decay. The optimization of the amplitude distribution $\alpha(\tau)$ is carried out in successive iterations controlled by a regularization parameter γ (set to a value of 0.001) such that the χ^2 is minimized while maximizing the entropy (S). The expression used for S is the Shannon-Jaynes entropy function, which is:

$$S(\alpha) = - \sum_{i=1}^N \alpha_i \log\left(\frac{\alpha_i}{b_i}\right) \quad \text{Eq. 11}$$

where the set of values b represent a default model for the system. However, in the absence of a default model for our system, b_i are generally set to a constant value. Using constant b_i value favours equal contribution from all lifetimes which means that the introduction of structure into the distribution is discouraged. The analysis is terminated when χ^2 reaches the specified lower limit or when χ^2 and $\alpha(\tau)$ show no change in successive iterations. All MEM fits were performed on a standard PC using the open access AnalyseDistribution MATLAB code (see ref. [Smith et al., 2017] for further details).

2.14. Fluorescence quenching measurements

Acrylamide or potassium iodide (KI) quenching experiments were carried out by measurement of fluorescence intensity of MgtE in 20 mM HEPES, 150 mM NaCl, 1 mM DDM

(pH 8.0 or 7.0) buffer by sequential addition of freshly prepared stock solution (1 M) of acrylamide or KI (2.5 M) in water to each sample. After addition of the quencher, the sample was incubated in dark for about 5 minutes before taking the measurement. The excitation wavelength used was 295 nm for Trp or 465 nm for NBD and emission was monitored at the respective emission maxima. After dilution correction, the inner filter effect correction was made using the following equation (Lakowicz, 2006):

$$F = F_{obs} \text{antilog}[(A_{ex} + A_{em})/2] \quad \text{Eq. 12}$$

where F is the corrected fluorescence intensity and F_{obs} is the background subtracted fluorescence intensity of the sample, A_{ex} and A_{em} are the measured absorbance at the excitation and emission wavelengths. The absorbance of the samples was measured using a Jasco V-650 ultraviolet (UV)-visible spectrophotometer. Quenching data were analysed by fitting to the Stern-Volmer equation (Lakowicz, 2006):

$$F_o / F = 1 + K_{SV}[Q] = 1 + k_q\tau_o [Q] \quad \text{Eq. 13}$$

where F_o and F are the fluorescence intensities in the absence and presence of the quencher, respectively, K_{SV} is the Stern-Volmer quenching constant, and $[Q]$ is the molar quencher concentration. The Stern-Volmer quenching constant K_{SV} is equal to $k_q\tau_o$, where k_q is the bimolecular quenching constant and τ_o is the lifetime of the fluorophore in the absence of quencher.

Chapter 3

Biochemical and Biophysical Characterization of a Prokaryotic Mg²⁺ Ion Channel: Implications for Cost-effective Purification of Membrane Proteins

3.1. Introduction

Membrane proteins perform many important biological processes such as ion transport, electrical excitability, cell communication, signal transduction and protein secretion, and are associated with diseases like heart disease, cancer, neurodegenerative diseases etc. Importantly, membrane proteins constitute ~30% of proteins produced by genomes of lower and higher organisms (Wallin and Heijne, 1998; Fagerberg et al., 2010), and ~60% of approved drugs target membrane proteins, of which G-protein coupled receptors and ion channels constitute the largest groups (Terstappen and Reggiani, 2001; Yildirim et al., 2007; Bakheet and Doig, 2009; Bull and Doig, 2015). This highlights the importance of understanding the mechanism of membrane proteins' function, which is very critical for biomedical research and drug discovery. Despite recent successes in determining the high-resolution structures of membrane proteins, the study of membrane proteins at atomic level is still quite challenging due to poor expression and extraction, low yield of functional protein, the complexity and heterogeneity of source membranes (Carpenter et al., 2008) and the low success rate of forming well-ordered 3D crystals (Moraes et al., 2014).

In particular, extraction of membrane proteins from the native membrane source remains the biggest obstacle in obtaining large quantities of pure, stable and functional proteins that are needed for characterizing the functionally-relevant structural dynamics utilizing sophisticated biophysical approaches. In this context, detergents serve as an indispensable tool for the membrane solubilization and extraction of membrane proteins (Helenius and Simons, 1975; Garavito and Ferguson-Miller, 2001; Seddon et al., 2004; Prive, 2007; Arachea et al., 2012; Stetsenko and Guskov, 2017). However, the membrane protein purification process in general, and detergent-mediated membrane solubilization in particular, is very expensive. Any

improvement in the extraction of pure, stable and functional membrane proteins in a cost-effective manner is, therefore, expected to facilitate the structure-guided approaches that are in need for the drug discovery pipeline.

In this work, we have tested the effect of relatively inexpensive detergents such as Triton X-100 and Anzergent 3-14 and a widely used expensive detergent, DDM (n-dodecyl- β -D-maltopyranoside) in successful extraction of the magnesium ion channel MgtE from *E. coli* membranes with structural and functional integrity. MgtE is a homodimeric Mg^{2+} channel of 450 amino acids with a monomeric molecular mass of ~ 50 KDa having a transmembrane C-terminal domain and a cytosolic N-terminal domain. The putative closed state three-dimensional X-ray structure of MgtE homodimer has been determined at high-resolution in detergent micelles (Hattori et al., 2007; 2009). The structure reveals that the cytosolic domain is divided into two sub domains: The N-terminal N-domain and the C-terminal cystathione- β synthase (CBS) domain. The N-domain of MgtE has six Mg^{2+} binding sites possibly making it functions primarily as a Mg^{2+} sensor. Electrostatic repulsion amongst several acidic residues of the N-domain of MgtE keep the channel open in the absence of Mg^{2+} , whereas neutralization of these charges helps to close the channel (Ishitani et al., 2008; Hattori et al., 2009). In this regard, Mg^{2+} acts not only as a permeating ion, but also the regulatory one that modulates the gating behavior of MgtE. Despite the availability of a crystallographic snapshot in one functional state, namely the closed state, the gating and permeation mechanisms in membranes are poorly understood partly due to the unavailability of structural information in other functional states.

Our results show that the relatively inexpensive detergents (Triton X-100 and Anzergent 3-14) can faithfully be used to solubilize and extract MgtE in a properly folded and stable conformation. Further, the quantity and quality of MgtE extracted using these alternative

detergents are comparable to procedures with DDM. Importantly, our results demonstrate that the secondary and tertiary structural features, along with the gating-related dynamics, are preserved suggesting that these detergents do not disrupt the functional and structural integrity of the protein during extraction.

3.2. Results

3.2.1. Temperature-dependent expression of MgtE

Previous excellent studies by Nureki and co-workers (Hattori et al., 2007; 2009) on MgtE from *T. thermophilus* have used the post-induction temperature of 20 °C to express MgtE in C41(DE3) cells. Since the objective of these studies is to obtain the crystal structure of MgtE, it is not very clear whether the post-induction temperature of 20 °C is really needed for proper purification of the protein or to obtain better crystals. We have systematically checked the expression of MgtE in C41(DE3) cells at different post-induction temperature. Our expression test results show that there is no leaky expression (pre-induction lane) and the expression of MgtE is considerably increased as a function of decreasing temperature and the maximum expression has been observed at post-induction temperature of 20 °C (Fig. 3.1a). Large scale purification of MgtE shows that the protein is pure irrespective of the post-induction temperature used as determined by SDS-PAGE (Fig. 3.1c). In addition, size exclusion chromatography profiles do not contain void volume peak, suggesting that non-specific aggregation of MgtE is not present irrespective of the temperature used for post-induction. However, the gel filtration profiles of the purified MgtE when expressed at 30 and 37 °C are slightly broader and not particularly homogeneous compared to when expressed at 20 °C. The purified MgtE elutes at ~10.6 ml with a homogenous peak when expressed at 20 °C indicating the good quality of the purified protein (Fig. 3.1b), as shown previously (Hattori et al., 2007; 2009). Importantly, significant increase (~3 fold) in the overall yield of protein per litre of culture when expressed at 20 °C, compared to when expressed at higher post-induction temperature (Fig. 3.1d). Based on these results, we have used the post-induction temperature of 20 °C to express MgtE for subsequent studies.

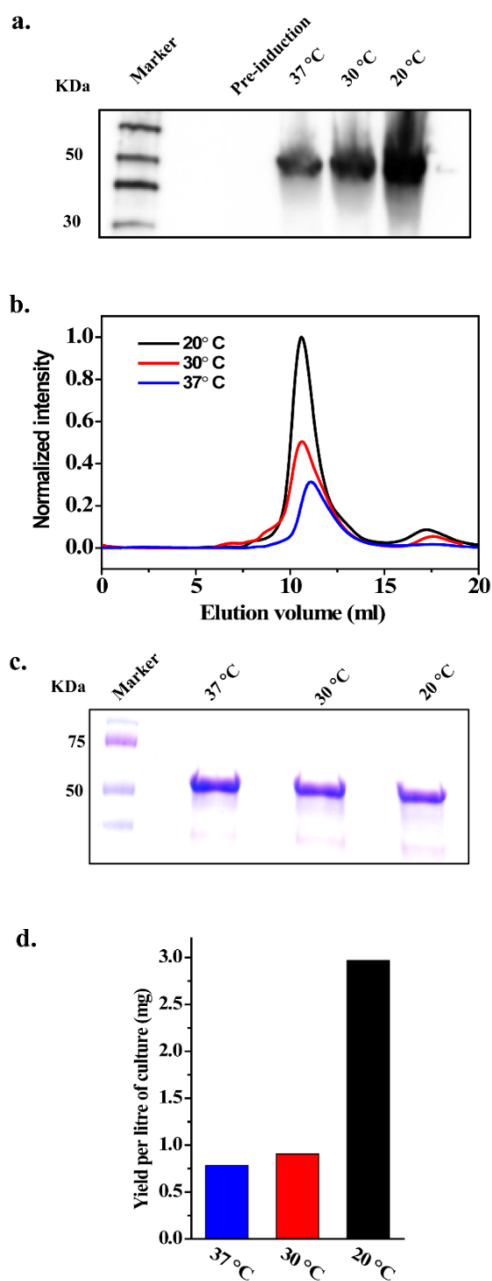


Fig. 3.1. Expression of MgtE at different temperature. (a) Western blot of MgtE expressed in C41 *E. coli* cells before (pre-induction) and after IPTG induction at different post-induction temperature as indicated. MgtE migrates as ~50 kDa band. (b) Size exclusion chromatography (SEC) of purified MgtE, expressed at different temperature, in DDM micelles, and (c) SDS-PAGE of MgtE peak fraction. (d) Yield of purified MgtE obtained per litre of culture grown. See Chapter 2 for details.

3.2.2. *Extraction of MgtE from membranes by detergents*

The molecular structures of detergents used in this study are shown in Fig. 3.2. While DDM is a popular, nonionic detergent for both purification and crystallization of many membrane proteins (Stetsenko and Guskov, 2017), Anzergent 3-14 is a promising zwitterionic detergent that has been used for the crystallization of a voltage-sensing domain (Li et al., 2014). Triton X-100 is probably the oldest classical nonionic detergent that has been widely used in membrane biology (Brown and London, 1998; Raghuraman et al., 2004; Jacobson et al., 2007) but significantly underrepresented in the use of membrane protein extraction and purification. We have chosen these relatively mild detergents in such a way that the properties such as the CMC, aggregation number and micellar size are comparable (Brito and Vaz, 1986; Stetsenko and Guskov, 2017; Le Maire et al. 2000).

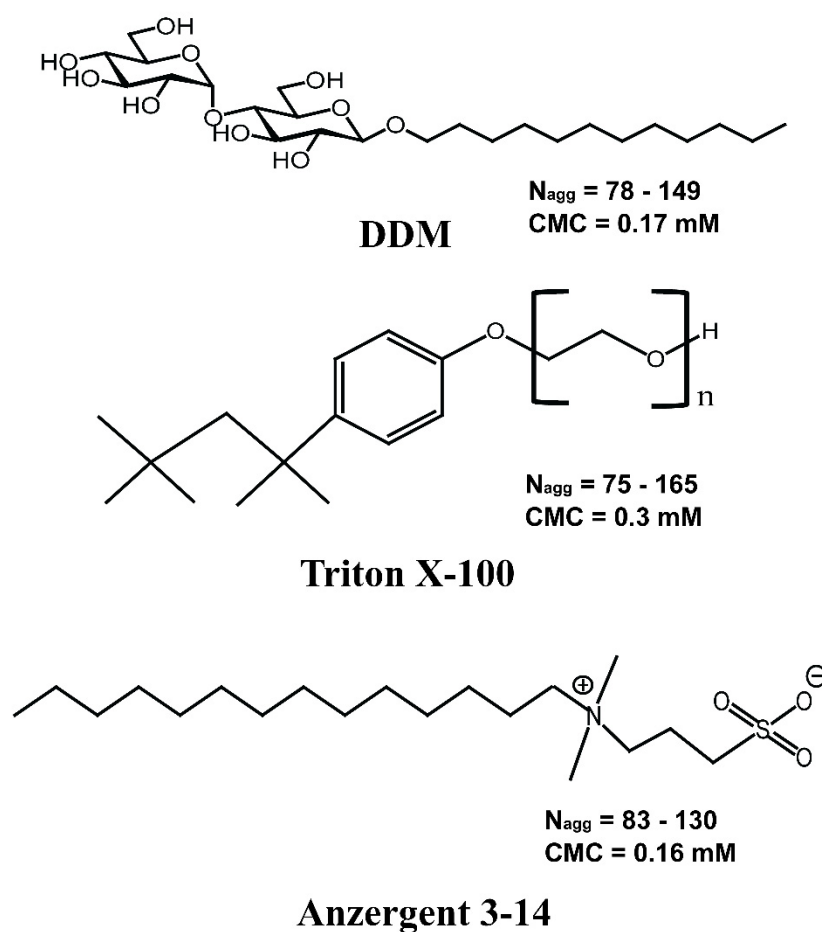


Fig. 3.2. Molecular structure of detergents used to extract MgtE. DDM, *n*-dodecyl- β -D-maltopyranoside; Triton X-100, α -[4-(1,1,3,3-tetramethylbutyl)phenyl]- ω -hydroxy-poly(oxy-1,2-ethanediyl), where $n = 9-10$ units of ethylene oxide; Anzergent 3-14, *n*-tetradecyl-*N,N*-dimethyl-3-ammonio-1-propanesulfonate. N_{agg} and CMC represent the aggregation number and critical micelle concentration, respectively.

Our results on solubilization screening of MgtE show that DDM extracts MgtE well and the protein migrates as a ~50 KDa band (Fig. 3.3a) – expected for a MgtE monomer with 450

amino acids, which is in excellent agreement with the previously published reports (Hattori et al., 2007; 2009). Importantly, Triton X-100 (Fig. 3.3b) and Anzergent 3-14 (Fig. 3.3c) detergents could faithfully extract MgtE as efficiently as the more expensive DDM when all detergents being used at $\sim 50X$ CMC for solubilization. Considering the fact that these detergents, Triton-X-100 in particular, are inexpensive, our results show a great promise to purify magnesium channels in a cost-effective manner.

It has been shown that high concentration of salts added during the detergent-mediated solubilization step increases the extraction efficiency of membrane proteins (Stauffer et al., 1991; Tilegenova et al., 2016). Extraction of membrane proteins from their native membranes to membrane-mimetic environments like detergent micelles subjects the protein to chemical and mechanical stress which might compromise the stability of the extracted protein. Polyhydric alcohols like glycerol are, therefore, used as chemical chaperones to stabilize proteins, *i.e.*, protect the protein from unfolding (Welch and Brown, 1996; Street et al., 2006). We have used a range of sodium chloride concentrations (150 to 1200 mM) and the chemical chaperone, glycerol, at the time of solubilization, to see their individual or combined effect on the efficiency of detergent-mediated extraction of MgtE. It is interesting to note that there is no appreciable change in the extraction efficiency of MgtE regardless of concentration of NaCl used during membrane solubilization (Fig. 3.3a-c). Even addition of 10% glycerol in the presence of high concentration of NaCl (1.2 M) does not significantly affect the extraction efficiency (Fig. 3.3d) irrespective of the detergent used during solubilization. This suggests that detergents, and not the tested additives, play an important role in MgtE solubilization.

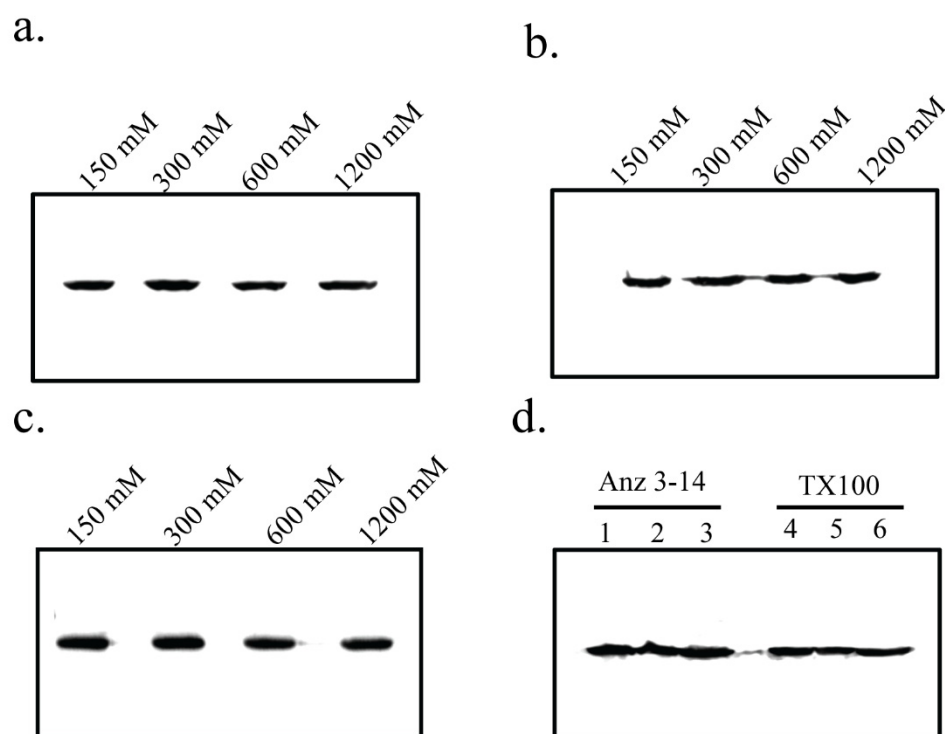


Fig. 3.3. Effect of salt and glycerol on detergent solubilization of MgtE. Western blot analysis of MgtE extracted using (a) DDM, (b) Triton X-100 and (c) Anzergent 3-14 detergents during solubilization as a function of increasing NaCl concentration, as indicated. (d) Anzergent 3-14 and Triton X-100 extracted MgtE in the absence (lanes 1 and 4) and presence of 10% glycerol (lanes 2 and 5); and a combination of 10% glycerol and 1.2 M NaCl (lanes 3 and 6). Similar results were obtained for DDM as well (not shown). MgtE migrates as ~50 KDa band. See Chapter 2 for other details.

3.2.3. *MgtE* extracted by alternative detergents is stably folded and α -helical

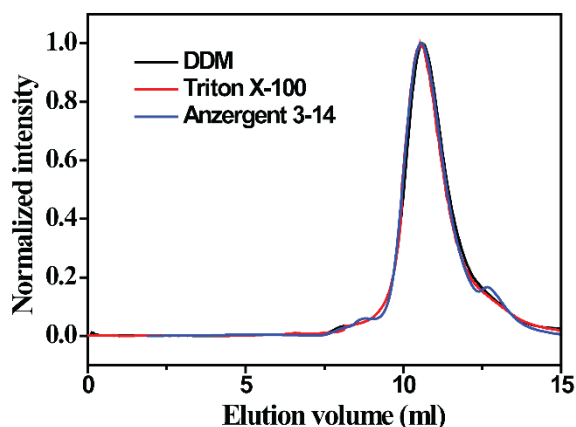
Although *MgtE* is extracted well by Triton X-100 and Anzergent 3-14 detergents, it migrates as a monomer (a single band at 50 KDa) in presence of a harsh anionic detergent, sodium dodecylsulfate (SDS), commonly used in SDS-PAGE. Since SDS is known to destabilize oligomers, and *MgtE* channel functions as a dimer in physiological conditions (Hattori et al., 2009; Moomaw and Maguiure, 2008; Payandeh et al., 2013), we have therefore tested the structural integrity of *MgtE* using size exclusion chromatography (SEC) and CD spectroscopy. We have adopted ‘dual-detergent strategy’ by employing inexpensive detergents (Triton X-100 and Anzergent 3-14) for membrane solubilization and subsequently changed to DDM during purification. This is particularly important for Triton X-100 because of the presence of the aromatic ring (see Fig. 3.2) that absorbs strongly in the UV region and interferes with protein quantification and size exclusion chromatography (Stetsenko and Guskov, 2017). Further, this gives an opportunity to directly compare the effects of inexpensive detergents in preserving the structural and functional integrity to that of previously used expensive detergent, DDM.

SEC analysis is used to assess the stability of a protein since it separates proteins based on their native hydrodynamic radius without perturbing the tertiary or quaternary structure of the protein. We observe that there is no protein in the void volume (~6-8 ml of elution) suggesting that there is no non-specific aggregation of *MgtE* (Fig. 3.4a). It has previously been shown that *MgtE* in DDM buffer migrates as a dimer in SEC analysis (Hattori et al., 2007; 2009). Our results show that *MgtE*, which is extracted by Triton X-100 and Anzergent 3-14, displays predominantly a single, homogenous peak that is consistent with DDM-extracted *MgtE* gel

filtration profile, suggesting that even the cheapest detergent (Triton X-100) preserved the dimeric conformation of the channel (Fig. 3.4a).

It is well established that the surface charge of micelles play an important role in stabilizing the secondary structure of membrane interacting proteins (Raghuraman et al., 2004). To investigate whether MgtE extracted with nonionic Triton X-100 and zwitterionic Anzergent 3-14 has similar secondary structure, we carried out far-UV CD spectroscopy in the wavelength range of 200 to 250 nm. The CD spectra of MgtE shows a characteristic α -helical conformation indicating that the secondary structure of MgtE, which is extracted by Triton X-100 and Anzergent 3-14, is well preserved and similar to that of DDM-extracted MgtE (Fig. 3.4b). This suggests that Triton X-100 and Anzergent 3-14 detergents are not only extracting MgtE well from membranes, but also extract in a proper, stable form during solubilization.

a.



b.

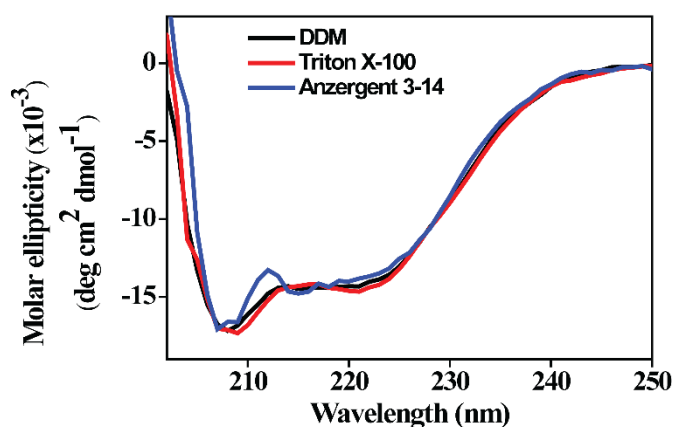


Fig. 3.4. Stability of MgtE extracted using various detergents. (a) SEC of MgtE extracted with either DDM, Triton X-100 or Anzergent 3-14 during solubilization are shown. (b) Representative far-UV CD spectra of MgtE extracted using various detergents during solubilisation. CD spectra were recorded using $2 \mu\text{M}$ MgtE in DDM micelles. See Chapter 2 and Eq. 2 for other details.

3.2.4. Mg^{2+} -induced protease protection of MgtE

Limited proteolysis assay is a commonly used sensitive technique to monitor protein dynamics to determine conformational changes and structural reorganization induced by ligands (Hubbard, 1998; Fontana et al., 2004). Trypsin is a serine protease that recognizes and hydrolyzes at exposed basic amino acids (arginine and lysine) on a protein. When the ligand-

induced conformational changes in a protein involve shielding these basic amino acids, the protein gets protection from the action of trypsin, which is directly indicative of the ligand-mediated function of protein (Dieckmann et al., 1999). The N-domain of MgtE has many such basic amino acids which might be exposed when it shuttles from closed to open state. Therefore, in the open state of MgtE, *i.e.*, in the absence of Mg^{2+} , the N-domain gets chopped off into several fragments generating a truncated MgtE (ΔN). Since Mg^{2+} is not only a permeating ion, but also a gating regulator (Hattori et al., 2009; Ishitani et al., 2008) and N-domain is proposed to be the Mg^{2+} sensor due to the presence of several Mg^{2+} -binding sites (Hattori et al., 2009), MgtE undergoes a transition from open to closed state in the presence of Mg^{2+} . This results in an increased protection of MgtE from protease as a function of increasing Mg^{2+} concentration as shown previously for DDM-extracted wild type MgtE (Ishitani et al., 2008; Tomita et al., 2017). Figure 3.5 shows that MgtE is susceptible to proteolysis in the absence of Mg^{2+} (open state) as expected in case of DDM, Triton X-100, Anzergent 3-14-extracted MgtE. Upon increasing the Mg^{2+} concentration (0-32 mM), MgtE gets more pronounced protection from trypsin, and interestingly, with the appearance of the full-length MgtE at more than 8 mM Mg^{2+} . It should be noted that the appearance of full-length MgtE in trypsin protection assay has been observed in the literature only in the presence of ATP (Tomita et al., 2017), whereas the protection of full-length MgtE is apparent at concentrations of 16 mM Mg^{2+} or more even in the absence of ATP (Fig. 3.5). Considering that MgtE fully closes at a concentration of 10 mM Mg^{2+} and above (Hattori et al., 2009), our results capture the ligand-induced conformational changes associated with gating. This is true whether DDM, Triton X-100 or Anzergent 3-14 is used to extract MgtE during solubilization (Fig. 3.5), demonstrating that the alternative, inexpensive detergents like Triton X-100 and Anzergent 3-14 extracts MgtE probably in a stable and functional form.

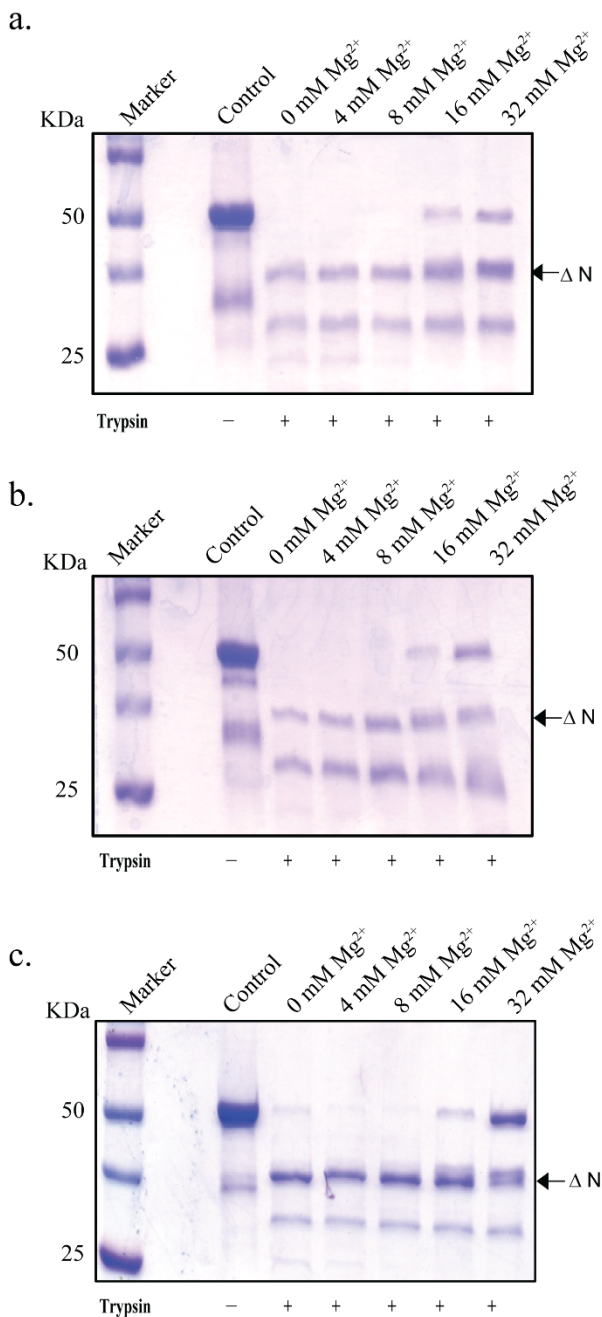


Fig. 3.5. Protease protection assay of MgtE in DDM micelles. SDS-PAGE shows trypsin-treated MgtE (10 μg) extracted by (a) DDM, (b) Triton X-100 and (c) Anzergent 3-14, during solubilisation, in the absence and presence of trypsin (16 $\mu\text{g/ml}$) with increasing concentration of Mg^{2+} as indicated. The ΔN (~37 KDa band) represents MgtE lacking N-domain. Control samples do not contain trypsin and MgCl_2 . See Chapter 2 and text for details.

3.2.5. Organization and dynamics of MgtE

Aromatic residues like tryptophan are known to localize at the protein-membrane interface in a membrane protein (Killian and von Heijne, 2000; Chattopadhyay and Raghuraman, 2004; Raghuraman et al., 2005). They form a so-called “aromatic belt” around the protein and is known to stabilize the protein at the membrane interface. Hence, the orientations of these residues can act as a reporter of the conformational homogeneity of a membrane protein. We used steady-state fluorescence approaches to monitor the organization and dynamics of MgtE during gating by utilizing the intrinsic tryptophan fluorescence. MgtE has six tryptophan residues per monomer of which four are at the membrane interface and the remaining two are in the N-domain. As mentioned earlier, MgtE can be stabilized in open and closed states in the absence and presence of Mg^{2+} , respectively.

The fluorescence emission maximum¹ and polarization values of open and closed states of MgtE that has been extracted with different detergents are shown in Table 3.1. The ‘average’ tryptophan emission maximum of MgtE in open state is 334 nm irrespective of the detergents used for membrane solubilization and MgtE extraction. Interestingly, the emission maximum of tryptophan is red shifted by ~3 nm upon closing the channel in the presence of 20 mM Mg^{2+} . The observed tryptophan fluorescence emission maximum (334 to 337 nm) is indicative of the interfacial localization of tryptophan residues as shown previously for ion channel-forming peptides in membrane-mimetic systems (Raghuraman and Chattopadhyay, 2004a,b,c; Kelkar and Chattopadhyay, 2007). Considering four of the six tryptophan residues of MgtE per monomer is expected to be localized at the membrane interface based on the crystal structure of closed state MgtE in detergent micelles (Hattori et al., 2009), our results indicate that the positions of tryptophans at the membrane interface might not change considerable during gating. Apart from

red shifted emission maximum, the closed state is also accompanied by ~15% increase in fluorescence intensity (Fig. 3.6). This suggests that the polarity of the microenvironment around the tryptophan residues is altered, which could be due to ligand-induced conformational changes (see Fig. 3.5). Further, we have carried out fluorescence polarization measurements, which has recently been shown to be a powerful approach for monitoring the dynamic behavior of ion channel gating (Raghuraman et al., 2014). The polarization values of MgtE, shown in Table 3.1, generally indicate that the average rotational mobility of tryptophan is representative of motionally restricted environments. Interestingly, the polarization values significantly increase in the closed state reflecting a reduced conformational flexibility of tryptophan residues when the channel transitions from open to closed state (Table 3.1). In other words, this indicates that, on average, the rotational dynamics of tryptophan residues gets more restricted during gating. We therefore propose that the higher dynamics of tryptophan residues is a characteristic feature of the open state of the MgtE channel. Importantly, all these gating-related dynamic changes triggered by Mg^{2+} in tryptophan fluorescence are consistent among MgtE extracted using different detergents (Fig. 3.6 and Table 3.1).

Table 3.1. Fluorescence emission characteristics of MgtE

Solubilization detergent	Emission maximum (nm)		Fluorescence polarization [#]	
	Open	Closed	Open	Closed
DDM	334	337	0.142 ± 0.008	0.164 ± 0.009
Triton X-100	334	337	0.127 ± 0.006	0.141 ± 0.007
Anzergent 3-14	334	336	0.130 ± 0.001	0.152 ± 0.009

[#]Calculated using Eq. 3 (see Chapter 2). The polarization value represents mean ± SE of three independent measurements. The excitation wavelength was 295 nm and the emission was monitored at respective emission maximum. The concentration of MgtE used was 1.6 μM in all cases.

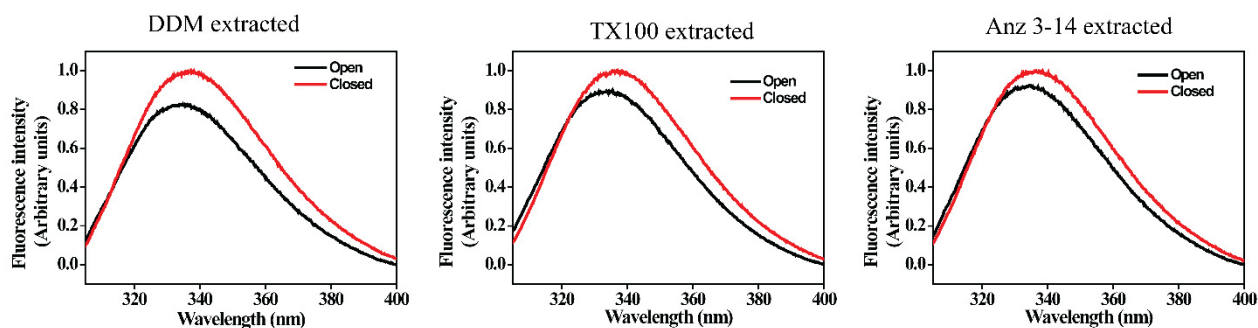


Fig. 3.6. Steady-state tryptophan fluorescence of MgtE. Intrinsic tryptophan fluorescence emission spectra of MgtE extracted using DDM, Triton X-100 and Anzergent 3-14 detergents during solubilization. The fluorescence spectrum corresponding to open (no Mg^{2+}) and closed ($20\text{ mM } Mg^{2+}$) states of MgtE is shown in black and red, respectively. The excitation wavelength used was 295 nm. Purified MgtE ($1.6\text{ }\mu\text{M}$) in 20 mM HEPES , 150 mM NaCl and $1\text{ mM DDM pH } 7.0$ buffer was used in all cases. See Chapter 2 for other details.

In general, fluorescence lifetime of tryptophan is well known to be sensitive to solvent, temperature and excited state interactions (Beechem and Brand, 1985; Raghuraman and Chattopadhyay, 2003). The fluorescence lifetimes of MgtE in DDM micelles are shown in Table 3.2. As seen from the table, all fluorescence decays were fitted with a triexponential function and the mean fluorescence lifetimes were calculated using Eq. 7 (see Chapter 2) and are shown in Table 3.2. The high values of lifetimes indicate that the tryptophan residues are not completely exposed to aqueous environments, a phenomenon which is fairly common for most membrane proteins because they preferentially localize at the membrane-mimetic interface. Apart from conventional calculation of mean fluorescence lifetimes, we have also calculated the tryptophan

fluorescence lifetimes (τ_H), obtained from the histogram of photons counted during the measurement using Eq. 8 (see Chapter 2) (Table 3.2), using a recently developed model-independent approach (Fiserova and Kubala, 2012). Obviously, model-dependent and model-independent analyses of lifetimes yield slightly different values of lifetimes. However, tryptophan lifetimes obtained using both these approaches for MgtE extracted using Triton X-100 and Anzergent 3-14 detergents are very much comparable to the values obtained for MgtE extracted using DDM. Since fluorescence lifetime serves as a faithful indicator of the local environment in which given fluorophore is placed (Prendergast, 1991; Raghuraman and Chattopadhyay, 2003), the remarkable similarity of tryptophan fluorescence lifetimes of MgtE extracted using different detergents clearly suggest that the structural properties (tertiary structure in this case) of MgtE is preserved even upon extraction using inexpensive detergents. This is in excellent agreement with our previously discussed CD results (see Fig. 3.4b).

Table 3.2. Fluorescence lifetimes of MgtE in open state

Solubilization detergent	α_1	τ_1 (ns)	α_2	τ_2 (ns)	α_3	τ_3 (ns)	$\langle\tau\rangle^{\$}$ (ns)	$\tau_H^{\%}$ (ns)
DDM	0.28	2.26	0.63	6.24	0.09	0.67	5.62	4.93
Triton X-100	0.26	2.69	0.61	6.37	0.13	0.91	5.68	4.99
Anzergent3-14	0.32	3.21	0.53	6.60	0.15	0.91	5.69	4.99

The concentration of MgtE was 1.6 μ M. The excitation wavelength was 295 nm and the emission was monitored at 334 nm. See Chapter 2 for other details.

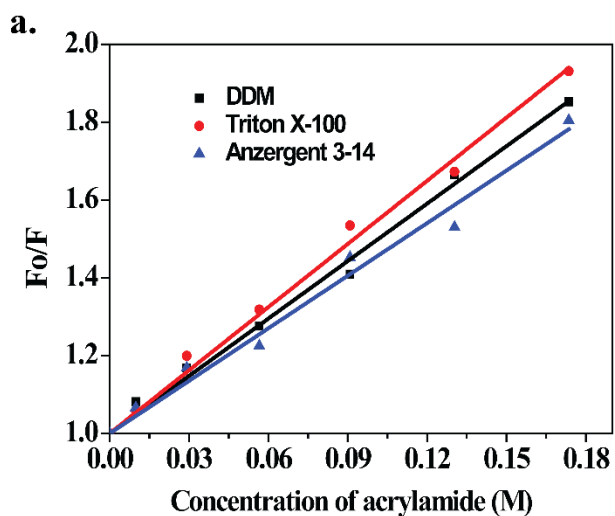
^{\\$}Calculated using Eq. 7; ^{\%}Calculated using Eq. 8.

3.2.6. Acrylamide quenching of MgtE tryptophan fluorescence

The above results show that the tryptophan residues in the transmembrane region of MgtE reside at the membrane-mimetic interface. To examine the accessibility and location of MgtE in DDM micelles, fluorescence quenching experiments were performed with acrylamide, which is a widely used neutral aqueous quencher of tryptophan fluorescence (Eftink, 1991). Figure 3.7a shows representative Stern-Volmer plots of acrylamide quenching of tryptophans of MgtE extracted using different detergents. The slope of such a plot (K_{SV}) is related to the degree of exposure (accessibility) of MgtE tryptophans to aqueous phase. In general, the higher the slope, the greater the degree of exposure, assuming that there is not a large difference in fluorescence lifetime. In fact, the bimolecular quenching constant (k_q) is a more accurate measure of the degree of exposure since it takes into account the differences in fluorescence lifetime. Since the tryptophan lifetimes of DDM, Triton X-100 and Anzergent 3-14-extracted MgtE are near identical in our case (see Table 3.2), the quenching results and interpretation due

to K_{sv} values do not suffer from lifetime-induced artifacts. The calculation of k_q is therefore not considered in our case.

It is well documented that the K_{sv} value for a completely exposed tryptophan is $\sim 18 \text{ M}^{-1}$, whereas the corresponding value for tryptophan localized at the micellar interfacial region is in the range of $\sim 4\text{-}7 \text{ M}^{-1}$ depending on the surface charge of micelles (Raghuraman and Chattopadhyay, 2004a). We have obtained the K_{sv} values of 4.5 M^{-1} , 4.9 M^{-1} and 5.4 M^{-1} for MgtE extracted using DDM, Triton X-100 and Anzergent 3-14, respectively. These values are well within the range observed for tryptophan localized at the membrane interface. This conclusively shows that the MgtE tryptophans, especially the ones present in transmembrane region, resides at the micellar interface as inferred (see Fig. 3.6 and Table 3.1). In addition, the magnitude of K_{sv} values also suggests that two of the cytoplasmic tryptophans might also be shielded from the aqueous phase in the open state of MgtE. This view is supported by $\sim 35\text{-}40\%$ overall quenching observed in the presence of 130 mM of acrylamide (Fig. 3.7b). Taken together, these results suggest that the solvent accessibility of the MgtE tryptophans are similar in all cases and reflect that the conformational homogeneity of MgtE remained constant regardless of the detergents used to extract. Overall, the inexpensive detergents, particularly Triton X-100, extracts MgtE in a stable and functional form without compromising the structural integrity.



b.

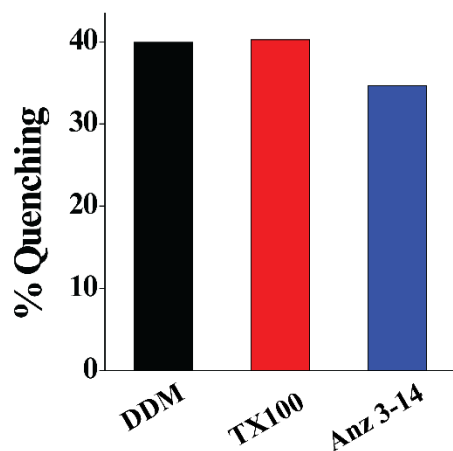


Fig. 3.7. Acrylamide quenching of MgtE tryptophan fluorescence. (a)

Representative data for Stern-Volmer analysis of acrylamide quenching of MgtE tryptophan fluorescence in DDM micelles.

F_0 is the fluorescence in the absence of quencher, F is the corrected fluorescence in the presence of quencher. The excitation wavelength was 295 nm and emission was monitored at 334 nm. The concentration of MgtE used was 1.6 μM . (b) Degree of tryptophan fluorescence quenching by acrylamide (at 130 mM) is shown. See Chapter 2 and text for other details.

3.3. Discussion

Membrane proteins are potential drug targets. However, they represent less than 2% of the reported crystal structures in the Protein Data Bank (PDB) because the structural characterization of membrane proteins using sophisticated biophysical approaches is remarkably challenging and quite expensive. The structural studies of any membrane protein require the protein to be extracted from its native membrane into a membrane-mimetic stable environment (Arachea et al., 2017). The membrane solubilization and subsequent membrane protein extraction is achieved by using detergents, which are soluble amphiphiles and above a critical concentration (strictly speaking, a narrow concentration range), known as critical micelle concentration (CMC), self-associate to form thermodynamically stable, noncovalent organized molecular aggregates called micelles (Helenius and Simons, 1975; Garavito and Ferguson-Miller, 2001; Raghuraman et al., 2004; Alam et al., 2015). The solubilization step of membrane protein purification typically requires the detergent concentration to be above the CMC. As a result, a higher concentration of specialized nonionic detergents (~5 to more than 100X CMC) is needed to extract the membrane protein from the source membrane to create water-soluble protein-detergent complexes (Garavito and Ferguson-Miller, 2001; Prive, 2007) compared to concentration of detergents needed in the downstream steps of purification.

Although detergent solubilization of membrane proteins is arguably the ‘rate-limiting’ step for a successful membrane protein purification, the detailed mechanisms of the action of detergents on membrane components have not been fully understood (Garavito and Ferguson-Miller, 2001; Prive, 2007). In addition, despite the commercial availability of large number of detergents, there is no ‘universal detergent’ that can be used to extract the different classes of membrane proteins. This is obvious from the fact that the extraction efficiency of expressed

membrane proteins can vary dramatically with different detergents (Arachea et al., 2017), and clearly highlights the importance of detergent screening to identify the best detergent for determining the extraction efficiency and stability of a target protein. The membrane protein purification process is therefore very expensive and the bulk of the purification cost lies in the choice of detergents suitable for extraction, purification and crystallization.

The most commonly used detergents for membrane protein purification and crystallization are alkyl maltosides (n-dodecyl- β -D-maltopyranoside, DDM and n-decyl- β -D-maltopyranoside, DM) and glycosides (n-octyl- β -D-glucopyranoside, OG and n-nonyl- β -D-glucopyranoside, NG) (Morales et al., 2014; Stetsenko and Guskov, 2017). These nonionic detergents are very expensive and alternative, inexpensive detergents are therefore required to reduce the purification cost, yet extracting stable and functional protein, to facilitate the structural studies of membrane proteins. Triton X-100 is one of the oldest, classical nonionic (uncharged) detergent containing polyoxyethylene chains as hydrophilic moieties characterized by a low CMC of ~ 0.3 mM [19,48]. It has been extensively used to explore the detergent resistant (insolubility) membranes and functional membrane domains in cell biology (Simons and Ikonen, 1997; Brown et al., 1998; Jacobson et al., 2007;). In general, the extraction efficiency of a target membrane protein by a detergent is directly related to the hydrophobicity of the micellar core, which is significantly higher for Triton X-100 compared to DDM, DM and OG (Feroz et al., 2018). Although it has been used to solubilize several membrane proteins in the functional state before the explosion of membrane protein structural biology (Banerjee, 1999), use of Triton X-100 in membrane protein purification is significantly underrepresented (only $\sim 2\%$ compared to $\sim 40\%$ in case of DDM) for a few practical reasons (Stetsenko and Guskov, 2017). These include its chemical heterogeneity and the interference with the protein quantitation

due to its strong absorption in the UV region of the electromagnetic spectrum (Prive, 2007, Stetsenko and Guskov, 2017; Feroz et al., 2018).

Interestingly, Triton X-100-mediated extraction of stable and functional membrane proteins has recently made significant strides (Tilegenova et al., 2016; Elberson et al., 2017). It has been shown that, for a well-characterized potassium channel KcsA (Chakrapani et al., 2007; Cuello et al., 2010; Raghuraman et al., 2012; Raghuraman et al., 2014), inexpensive detergents like Triton X-100 can be used to extract large amounts of stable and functional protein in the presence of high concentration of salt and glycerol (Tilegenova et al., 2016). In addition, Triton X-100 is also shown to increase the quality and quantity of the pentameric ligand-gated ion channels (pLGIC) of prokaryotic origin (Elberson et al., 2017). In this work, we have tested the potential applicability of such inexpensive detergents (Triton X-100 and Anzergent 3-14) along with additives such as salt and glycerol in the extraction of a Mg^{2+} -selective ion channel MgtE. Further, we have utilized ‘dual-detergent strategy’, CD spectroscopy, steady-state and time-resolved tryptophan fluorescence to demonstrate the feasibility of these detergents to be used to produce large amounts of stable and functional protein for structural characterization in a cost-effective manner.

Our current knowledge on molecular basis of Mg^{2+} transport comes from the functional and structural studies on prokaryotic CorA and MgtE Mg^{2+} channels (Moomaw and Maguire, 2008; Payandeh et al., 2013). It is now known that MgtE, like CorA, is the primary Mg^{2+} transport system in ~50% of all prokaryotic species. In addition, unlike K^+ and Na^+ channels, the architecture of the Mg^{2+} transporters is not conserved as is evident by the recent crystal structures of prokaryotic Mg^{2+} channels. For instance, the functional unit of CorA Mg^{2+} channel is a pentamer (Eshaghi et al., 2006; Payandeh and Pai, 2006; Matthies et al., 2016) whereas

MgtE is a dimer and only the structural snapshot of the closed state of MgtE in detergent micelles is available (Hattori et al., 2007; 2009). It is intriguing that these two evolutionarily distinct Mg^{2+} transporters seem to have conceptually similar Mg^{2+} -dependent gating mechanisms with different architectures, which makes them unique. Since the molecular mechanism of Mg^{2+} gating and transport across membranes remains obscure due to paucity of structural information, our study related to biochemical and biophysical characterization of MgtE assumes significance.

Our results demonstrate that the post-induction temperature is crucial for a significant expression of MgtE. Importantly, we show that inexpensive detergents, particularly Triton X-100, could potentially be used in the detergent solubilization step to extract MgtE in a stable and functional form as has been shown for Triton X-100-mediated extraction of K^+ and ligand-gated ion channels (Tilegenova et al., 2016; Elberson et al., 2017). However, in our case, the extraction efficiency is not affected by the presence of high concentration of salt and glycerol and this is true irrespective of the detergents used during solubilization. This is in agreement with a recent study in which it has been shown that the effect of salt on Triton X-100-mediated extraction of pLGIC is negligible (Elberson et al., 2017). This is not surprising since it is well-known that the optimal extraction conditions for one membrane protein may not be applicable to other members of the same class or different classes of membrane proteins (Arachea et al., 2012; Feroz et al., 2018). Taken together, our results strongly support the use of Triton X-100 as an inexpensive, alternative detergent for the purification of MgtE without compromising the structural integrity of the channel and Mg^{2+} -induced gating-related conformational dynamics. Considering that the cost of Triton X-100 is ~200 fold cheaper than the widely used expensive DDM, it will be worthwhile to include Triton X-100 for routine detergent screening for membrane protein extraction. Overall, our results will have potential implications for the cost-

effective purification of membrane proteins in general, and MgtE family of magnesium channels, in particular.

Chapter 4

Gating-related Structural Dynamics of the MgtE Magnesium Channel

in Membrane-Mimetics Utilizing Site-Directed Tryptophan Fluorescence

4.1. Introduction

Ion channels perform vital physiological functions like ion transport, electrical excitability and cellular signaling, and their dysfunction is often related to several life-threatening diseases. Importantly, ion channel family of membrane proteins are crucial targets for therapeutics (Bakheet and Doig, 2009; Bull and Doig, 2015). In general, the structure, dynamics and associated function of ion channels are affected by its surrounding membrane environment, protein-protein interactions within the structure as well as lipid-protein interactions with the membrane bilayer. Hence, knowledge of the impact of membrane environment on the protein structure and dynamics with respect to change in orientation of amino acid residues, structural transitions between functional states is of vital importance to understand the intricate functioning of ion channels (Raghuraman et al., 2019).

Magnesium is the most abundant divalent cation present in the cell with a total intracellular concentration ranging between ~20 to 50 mM depending on the cell type, of which 1-2% constitutes the free Mg^{2+} concentration (Quamme, 2010; Romani, 2011; Groisman et al., 2013). In humans, abnormal Mg^{2+} homeostasis is reported to be associated with pathophysiological conditions, which include heart disease, diabetes, high blood pressure, and cancer (Houston, 2011; Wolf and Trapani, 2012; Sahni and Scharenberg, 2013). Among the ion channels, the mechanism of Mg^{2+} transport and homeostasis are poorly understood.

MgtE is a homodimeric Mg^{2+} ion channel with a monomer molecular weight of ~ 50 KDa (450 amino acids) and contains transmembrane (TM-domain) and cytosolic domains. Importantly, MgtE is an ortholog of the mammalian SLC41A1 transporter (Sahni and Scharenberg, 2013) which has been implicated in Parkinson's disease (Kolisek et al., 2013) and head/neck cancer (Lin et al., 2015). The high-resolution three-dimensional crystal structures of the full-length MgtE in the putative closed state have been solved in detergent micelles (Hattori

et al., 2007; 2009). It is evident from the full-length structures that the cytosolic domain is divided into two sub-domains namely the N-domain and the cystathione- β -synthase (CBS) domain, and has several Mg^{2+} binding sites. Consequently, the cytoplasmic domain, particularly the N-domain, is proposed to primarily function as a Mg^{2+} sensor. It has been proposed that while Mg^{2+} binding stabilizes the closed state of the channel, the open state(s) of MgtE channel is favored due to the electrostatic repulsion among many acidic residues in the cytoplasmic domain in the absence of Mg^{2+} (Ishitani et al., 2008; Hattori et al., 2009). This makes MgtE gating interesting since Mg^{2+} is not only a permeating ion but also negatively regulates MgtE function. Although the full-length MgtE structural snapshot is available in one functional state (closed state), the atomic model of TM-domain of MgtE based on the cryo-EM structure of MgtE-Fab complex in Mg^{2+} -free conditions using amphipols has been recently solved (Jin et al., 2021). However, the gating-related structural dynamics in physiologically-relevant membranes is poorly understood and studies focused on MgtE organization and dynamics in membranes are scarce.

In this work, we have compared the organization and dynamics of MgtE in membrane-mimetic systems such as micelles and membranes. Further, we monitored the changes in gating-related structural dynamics, hydration dynamics and conformational heterogeneity of MgtE in membranes using the intrinsic site-directed Trp fluorescence. For this purpose, we employed various sophisticated fluorescence approaches that include anisotropy, red edge excitation shift (REES), quenching and lifetime distribution analysis by Maximum Entropy Method (MEM) (Raghuraman et al., 2019). Intrinsic Trp fluorescence is extensively utilized to monitor the changes in dynamics and local structure of proteins in general and membrane proteins in particular (Raghuraman et al., 2019; Eftink, 1991a; Vivian and Callis, 2001; Chattopadhyay and

Raghuraman, 2004; Raghuraman and Chattopadhyay, 2004b; Rasmussen et al., 2007; Kozachkov and Padan, 2011; Ghisaidoobe and Chung, 2014; Biswas et al., 2020). Since MgtE is a multi-tryptophan containing ion channel and analysis of ensemble Trp fluorescence is complicated (Raghuraman et al., 2019), we have engineered six single-Trp mutants in the functional Trp-less background of MgtE to obtain site-specific information on the gating-related structural dynamics of MgtE in membrane-mimetic systems. Our results show that the organization and dynamics of the full-length MgtE is significantly altered in physiologically-relevant membrane environment compared to micelles. Further, the closed state of MgtE is highly dynamic compared to the open state in membranes, which is in sharp contrast to what has been observed in micellar environment. Furthermore, our MEM results show that the changes in the conformational heterogeneity of the tryptophan residues especially W37 at the Mg^{2+} -sensing cytoplasmic domain are dependent on the functional state of MgtE. Based on our results, we propose that the Mg^{2+} -induced gating involves ‘conformational wave’ from N-domain to TM-domain of MgtE. Overall, our work highlights the importance of membrane environment and lipid-protein interactions in the gating mechanisms of ion channels in general, and magnesium channels in particular.

4.2. Results

4.2.1. Structural integrity of single-Trp MgtE mutants is preserved

The closed state crystal structure of homodimeric MgtE (*PDB: 2ZY9*) indicating the positions of intrinsic Trp residues (Hattori et al., 2009), and the spatial arrangement of MgtE in membranes with respect to the hydrocarbon core of the lipid bilayer, as obtained from the OPM database (Lomize et al., 2012), are shown in Fig. 4.1a. As seen from the figure, MgtE has six Trp residues per monomer of which four (W282, W288, W352, W380) are present in TM-domain and two (W37 and W79) are present in N-domain. We have engineered six single-Trp mutants (W37only, W79only, W282only, W288only, W352only and W380only) by individually reintroducing each of the native Trp residues in a Trp-less background in such a way that each MgtE construct has only the desired Trp residue. For example, ‘W37only’ mutant of MgtE will contain only one tryptophan residue at position 37 and the remaining Trp residues are replaced by phenylalanine. Importantly, employing the native Trp of MgtE for fluorescence studies involves minimum structural perturbations unlike labelling with the bulky extrinsic fluorophores. Further, the advantage of using single Trp mutants is that the site-directed intrinsic tryptophan fluorescence can be used as a reporter to monitor the structural and gating-related dynamics information in a site-specific manner.

It has earlier been shown that wild-type MgtE in DDM buffer (pH 7.0) elutes as a homodimer in size-exclusion chromatography (SEC) analysis (see Chapter 3 and ref [Hattori et al., 2009]). To confirm that the structural integrity of single-Trp mutants is not compromised, we carried out SEC for all the mutants (‘W380only’ is shown as representative in Fig. 4.1b). At pH 7.0, we observe that the gel filtration profiles of purified single-Trp mutants are not homogeneous in the sense that they contain broad doublet peaks. Interestingly, when the

purification is carried out at higher pH conditions (pH 8.0), the MgtE-Trp mutants elute at ~10.6 ml with a single homogeneous peak (Fig. 4.1b) similar to wild-type MgtE, indicating the good quality of purified proteins as seen from SDS-PAGE (Fig. 4.1c). To investigate whether the purified single-Trp mutants has a similar secondary structure to that of wild-type MgtE, we carried out far-UV CD spectroscopy. The CD spectra of Trp-less and single-Trp mutants ('W79only' as a representative) along with wild-type channel in DDM micelles are shown in Fig. 4.1d, which show features of α -helical conformation, which indicates that the mutants are extracted and purified in a properly folded form. Taken together, our results show that the structural integrity of MgtE dimer conformation of the MgtE-Trp mutants is well maintained at pH 8.0, and we have used this modified purification conditions for further experiments to monitor the structural dynamics of MgtE.

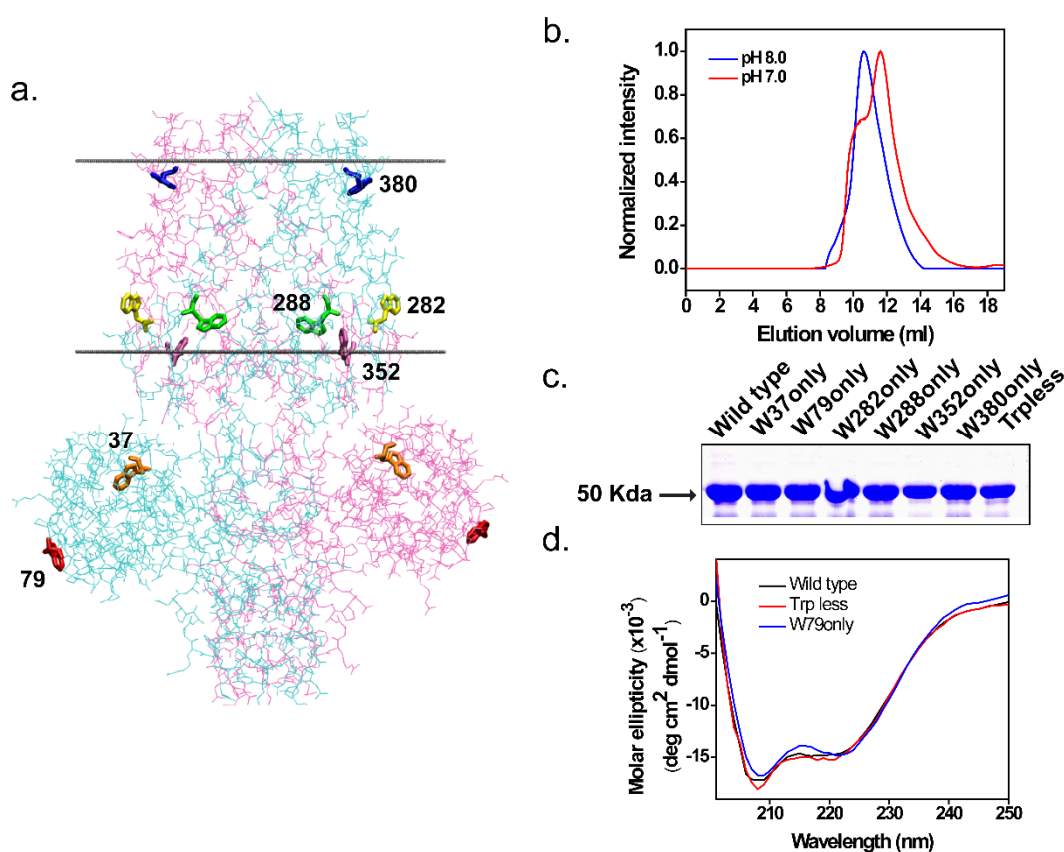


Fig. 4.1. Single-Trp mutants of MgtE. (a) Shown is the cartoon representation of membrane-incorporated closed state of homodimeric MgtE (PDB: 2YVX) obtained from OPM database showing the location of Trp residues (denoted by respective residue numbers). The two subunits of MgtE are colored as magenta and blue, and the colors of Trp residues are given as a visual aid to distinguish between various Trp residues. (b) The relative change in the elution profile with change in pH of W380only is shown by size-exclusion chromatography (SEC). (c) SDS-PAGE of purified wild-type, single-Trp mutants and Trp-less mutant of MgtE. (d) Representative far-UV CD spectra of wild-type, Trp-less and W79only mutants of MgtE. CD spectra were recorded using 2 μM of protein in DDM micelles. See Chapter 2 and Eq. 2 for other details.

4.2.2. Transport activity and ligand-induced conformational changes of Trp-less mutant of MgtE

To monitor whether the Trp-less mutant retains the functional activity similar to wild-type MgtE, we have utilized the fluorescence assay for monitoring Mg^{2+} transport using the Mg^{2+} -sensitive membrane-impermeable fluorophore Mag-Fura-2 (Fig. 4.2) and the limited protease protection assay to observe the ligand-induced conformational changes upon gating in a properly folded purified protein (see Fig. 4.1c,d). In Mg^{2+} transport experiments, the fluorescence intensity of Mag-Fura-2 encapsulated in liposomes and proteoliposomes remains stable in the absence of Mg^{2+} (Fig.4.3a). Interestingly, upon addition of 20 mM Mg^{2+} , both the wild-type and Trp-less mutant of MgtE reconstituted in Mag-Fura-2 encapsulated liposomes show a significant increase in the fluorescence intensity of the fluorescent dye over time (Fig. 4.3a). However, the control liposomes in which no protein is reconstituted, there is no increase in Mag-Fura-2 intensity upon addition of Mg^{2+} (Fig. 4.3a). This clearly indicates that both the wild-type and the Trp-less mutant of MgtE mediates the Mg^{2+} influx in the presence of inwardly directed Mg^{2+} gradient.

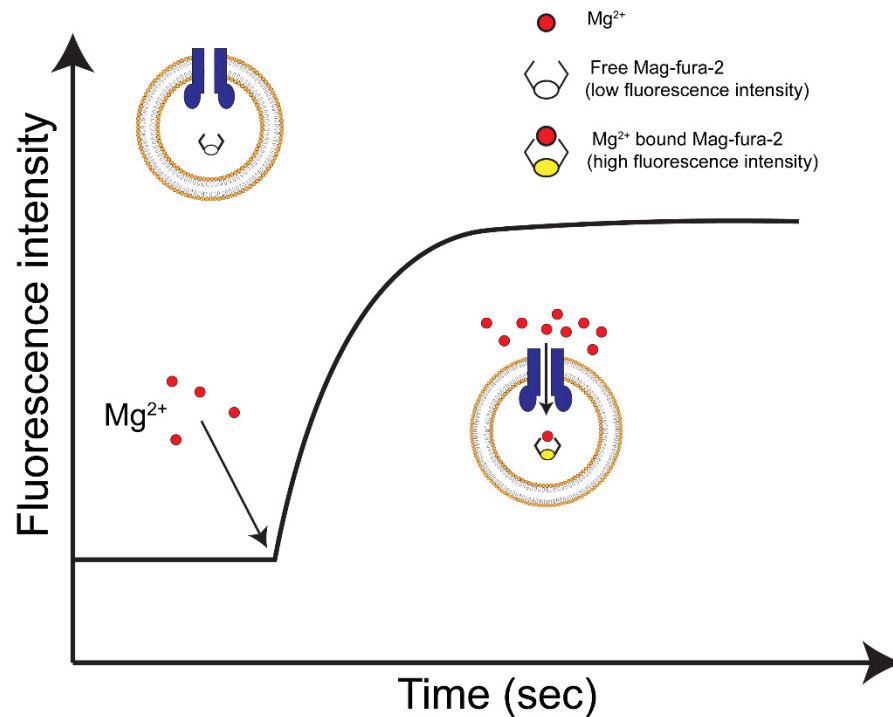


Fig. 4.2. Schematic of fluorescence transport assay. Cartoon representation showing the working principle of Mg^{2+} (red) transport assay using mag-fura-2. Upon binding Mg^{2+} the fluorescence intensity of mag-fura-2 increases (shown by yellow sphere) indicating transport of Mg^{2+} through ion channel (blue).

Since MgtE transport activity must be preceded by the ligand-induced conformational changes, we have carried out limited proteolysis assay using trypsin (Fig. 4.3b). The cytosolic domain of MgtE is proposed to act as a Mg^{2+} sensor (Hattori et al., 2007; 2009) by binding to Mg^{2+} (at high concentrations of 10 mM) and stabilizing the closed conformation of MgtE. Consequently, MgtE is protected from the protease trypsin upon increasing the concentration of Mg^{2+} . Fig. 4.3b shows the appearance of full-length MgtE band at high concentrations of Mg^{2+} ,

which shows that the Trp-less mutant of MgtE is sufficiently protected from protease at higher concentration of Mg^{2+} whereas it is sensitive to proteolysis in the absence of Mg^{2+} . This is indicative of the ligand-induced conformational changes during gating. Taken together, the Trp-less mutant functions similar to wild-type MgtE as shown previously (see Chapter 3 and ref [Hattori et al., 2009]). Since Trp-less mutant of MgtE is stably folded (see Fig. 4.1d) and functional, *i.e.*, it retains both its transport activity (Fig. 4.3a) and exhibits ligand-induced conformational changes (Fig. 4.3b), our results suggest that the Trp residues may not be a predominant factor in stability and function of MgtE, which is in agreement with Trp-less mutants of other membrane proteins (Rasmussen et al., 2007; Kozachko and Padan, 2011; Weitzman et al., 1995; Swartz et al., 2020).

It has been earlier shown, in patch-clamp electrophysiology experiments, that MgtE is fully closed at a concentration of 10 mM Mg^{2+} and above (Hattori et al., 2009). We have monitored the changes in fluorescence emission maximum of Trp residues in wild-type MgtE as a function of increasing Mg^{2+} concentrations to check whether the changes in ensemble Trp fluorescence is sensitive to the conformational changes associated with closing of the channel in micelles (Fig. 4.3c,e) and membranes (Fig. 4.3d,f). The emission maximum of Trp residues increases significantly (red shifted) until ~ 8 mM Mg^{2+} in micelles (Fig. 4.3c) and ~ 6 mM in membranes (Fig. 4.3d), beyond which there is no change. The half maximal effective concentration (EC_{50}) values associated with these changes are 3.26 mM and 2.37 mM Mg^{2+} in micelles and membranes, respectively. Interestingly, this is supported by changes in the rotational mobility of Trp residues as monitored by fluorescence anisotropy, which is a robust method to monitor the rotational dynamics and flexibility of a fluorophore and has been employed to obtain dynamic information of ion channels in different functional states (Ho et al.,

2013; Raghuraman et al., 2014; Das et al., 2020). The EC₅₀ values obtained from anisotropy measurements are very similar to the values obtained using emission maximum changes (Fig. 4.3e, f).

These results are very interesting since these spectroscopic changes are strongly correlated with the gating-induced conformational changes in MgtE. Importantly, this also suggests that the local dynamic changes (both the environment as well as segmental mobility) around the Trp residues faithfully report the global conformational changes during gating. Overall, these results conclusively show that the Trp fluorescence of MgtE could be effectively used as a sensitive reporter of conformational changes when the channel shuttles between open and closed states. It should be noted that ensemble open conformations of MgtE are possible in the absence or low concentrations of Mg²⁺. Based on this result, we use 20 mM Mg²⁺ in our single-Trp MgtE experiments to ensure that the channel is predominantly stabilized in the closed state.

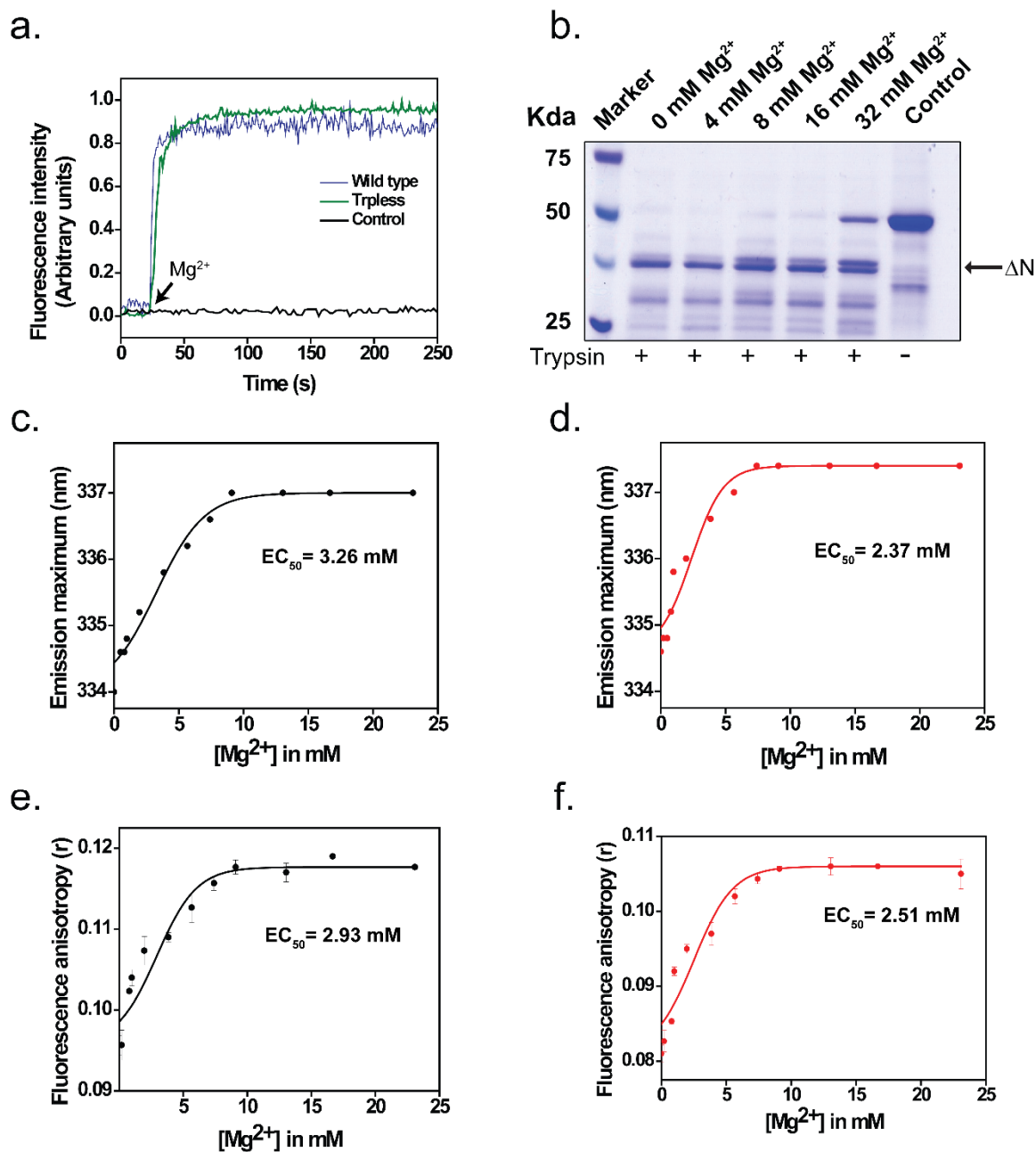


Fig. 4.3. Fluorescence transport assay and ligand-induced conformational changes.

(a) Representative experiments show the change in fluorescence intensity of Mag-Fura-2 encapsulated in PC/PG liposomes, reconstituted with either wild-type or Trp-less mutant of MgtE, monitored in a time-scan mode upon addition of 20 mM $MgCl_2$ (indicated by the arrow).

Liposomes loaded with Mag-Fura-2 (but without protein) serve as control. This assay was carried out in triplicates and similar results were obtained in all cases. (b) Protease protection assay of Trp-less MgtE in DDM micelles in the absence and presence of trypsin (16 $\mu\text{g/ml}$) with increasing concentration of Mg^{2+} as indicated. The ΔN (~37 KDa band) represents MgtE lacking N-domain. Control sample does not contain trypsin and MgCl_2 . (c,d) Changes in ensemble Trp fluorescence emission maximum and (e,f) anisotropy of wild-type MgtE as a function of increasing Mg^{2+} concentration in DDM micelles (black) and PC/PG liposomes (red) are shown. The solid line represents the best fit curves of Hill equation to the data using OriginPro 8.0. Values represent mean \pm SE of three independent measurements, and the emission maximum values contain negligible errors. The estimated Mg^{2+} concentrations reaching the half-maximal values of changes (EC_{50}) are shown in each graph. See Chapter 2 for other details.

4.2.3. Microenvironment of single-Trp residues of MgtE in micelles and membranes

We monitored the fluorescence emission maximum of the Trp-less mutant of MgtE in micelles upon excitation at 280 nm to ensure that the fluorescence emission spectrum is devoid of any characteristic Trp fluorescence (Fig. 4.4a). As expected, the fluorescence emission maximum of this mutant, which does not contain any Trp residues, is 308 nm, which is the characteristic emission maximum for Tyr fluorescence (Ross et al., 1992). Fig. 4.4b shows the representative emission scans of the wild-type and single-Trp mutants of MgtE in the open state in detergent micelles when excited at 295 nm. The ‘average’ tryptophan emission maximum of wild-type MgtE in open state is 334 nm as shown previously (see Chapter 3). On the other hand, the Trp-less mutant of MgtE lacks the Trp fluorescence emission characteristic of the wild-type,

thereby providing a background for monitoring the structural dynamics of MgtE. Interestingly, it appears that the W282 in the TM-domain is the dominant contributor to the wild-type fluorescence since the fluorescence intensity of ‘W282only’ mutant is ~80% of the wild-type. In contrast, the fluorescence intensity of the cytoplasmic N-domain W37 is the lowest among all the single-Trp mutants (Fig. 4.4b) although the fluorescence emission maximum of this mutant (333 nm) indicates the nonpolar environment around W37. Since W37 is present in the soluble domain of MgtE, the unique combination of nonpolar localization and reduced fluorescence intensity of ‘W37only’ mutant could be attributed to the presence of several nonpolar and charged amino acids - efficient quenchers of Trp fluorescence (Vivian and Callis, 2001) - within 4Å of this residue, respectively (see Fig. 4.4d). Interestingly, summation of the individual spectra from the single-Trp mutants gives a spectrum that is much higher than the wild-type spectrum (Fig. 4.4c), suggesting a significantly quenched ensemble Trp fluorescence in wild-type MgtE. This could be due to the presence of neighboring charged amino acids (Fig. 4.5) and homoFRET involving the Trp residues in the TM-domain (particularly W282 and W288 whose indole ring distances in the closed state structure are ~15 Å) that form the ‘aromatic ring’ at the membrane interface along with Tyr residues (see Fig. 4.1a and ref. [Raghuraman et al., 2019]).

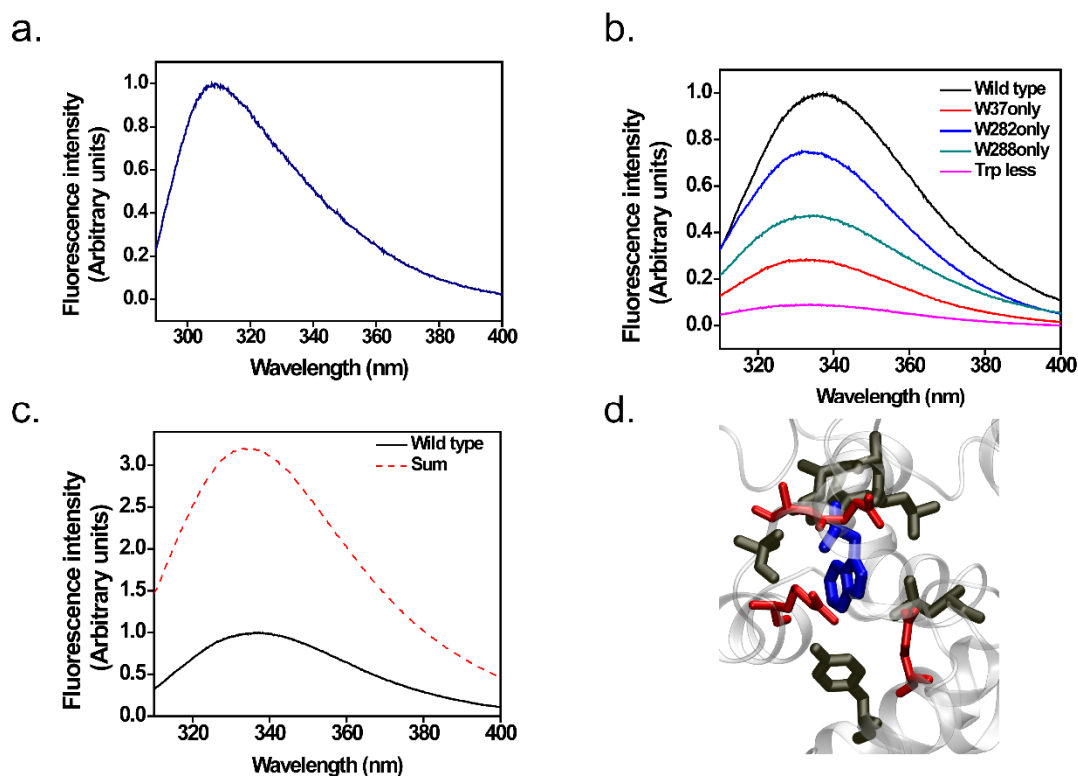


Fig. 4.4. Steady-state fluorescence of MgtE-Trp mutants. Representative fluorescence emission spectra of (a) Trp-less mutant excited at 280 nm; (b) wild-type, Trp-less and the indicated single-Trp mutants of MgtE in DDM micelles upon 295 nm excitation are shown. (c) Comparison of the wild-type spectrum of MgtE with the sum of spectra of single-Trp mutants is shown. (d) Neighboring residues within 4 Å of W37 based on the crystal structure of MgtE (PDB: 2ZY9) and the charged residues are colored red. The concentration of MgtE was 1.6 μM in all cases. See Chapter 2 and text for other details.

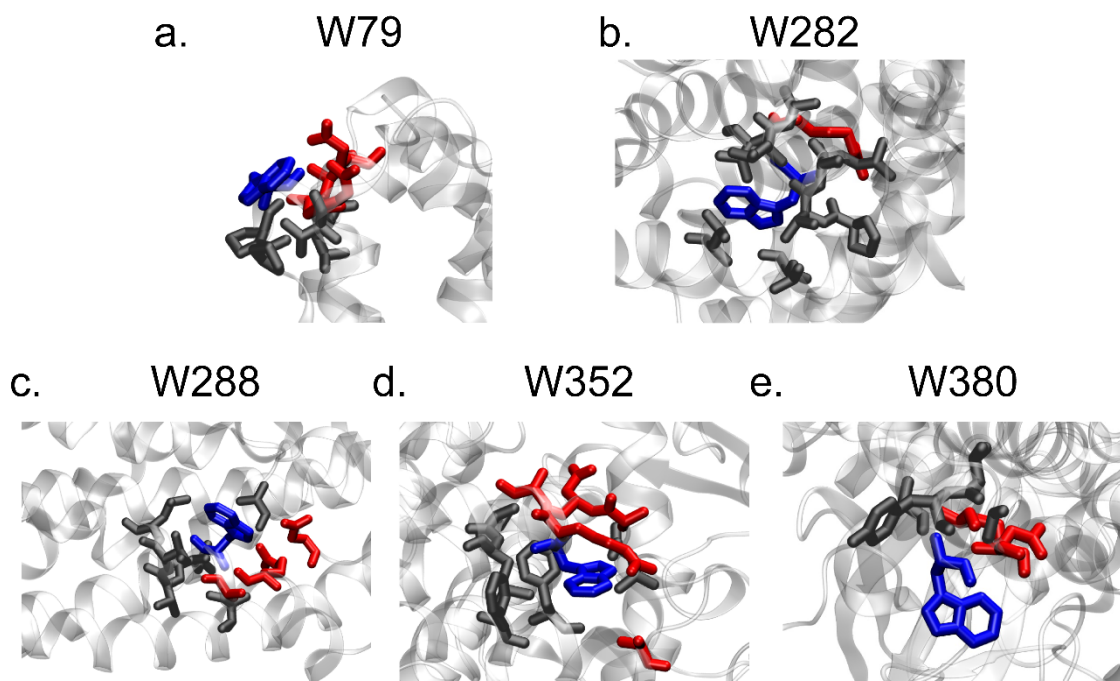


Fig. 4.5. Amino acids surrounding MgtE-Trp residues. Neighboring residues within 4 Å of (a) W79, (b) W282, (c) W288, (d) W352, and (e) W380 based on the crystal structure of MgtE (PDB: 2ZY9). The charged residues are colored red.

The well-established sensitivity of Trp fluorescence to environment factors makes an ideal choice of natural fluorophore to monitor structural dynamics and conformational changes of proteins and to characterize membrane partitioning, folding and lipid-protein interactions (Eftink, 1991b; Raghuraman and Chattopadhyay, 2004b; Rasmussen et al., 2007; Kozachkov and Padan, 2011; Ghisaidoobe and Chung, 2014; Raghuraman et al., 2019; Engelborghs, 2003; Raghuraman et al., 2005). Fig. 4.6a shows the representative emission scans of a single-Trp mutant (‘W37only’) of MgtE in micelles and membranes to highlight the difference in the

microenvironment. The fluorescence emission maximum of the Trp residues in the cytoplasmic N-domain (W37 and W79) ranges from 332 to 335 nm in micelles and membranes (Fig. 4.6b). This suggests that the microenvironment experienced by these residues are nonpolar despite the fact that they are localized at the soluble domain of MgtE. In case of Trp residues in TM-domain, the emission maximum ranges from 332 to 336 nm in micelles and 331 to 337 nm when reconstituted in membranes, indicating a preferential localization of Trp residues at the membrane interface as shown previously for channel-forming peptides and proteins in membrane-mimetic systems (Raghuraman and Chattopadhyay, 2004a,bc; Kelkar and Chattopadhyay, 2007). These results suggest that the Trp environment is similar in micelles and membranes for all single-Trp mutants (± 1 nm change) whether the Trp residue is present in soluble N-domain or TM-domain (see Fig. 4.6b). Although the emission maximum for single-Trp mutants is similar in membrane-mimetic systems, the fluorescence intensity is much higher for all the Trp mutants in micellar environment (Fig. 4.6c), suggesting that Trp residues experience a relatively hydrophobic/nonpolar environment in micelles compared to membranes. Interestingly, the Trp residues in the cytoplasmic part (N-domain) of MgtE show the maximum intensity changes (~ 2 fold) suggesting that the organization of the Trp residues in MgtE is altered in general, and the Mg^{2+} -sensing N-domain in particular in micelles and membranes.

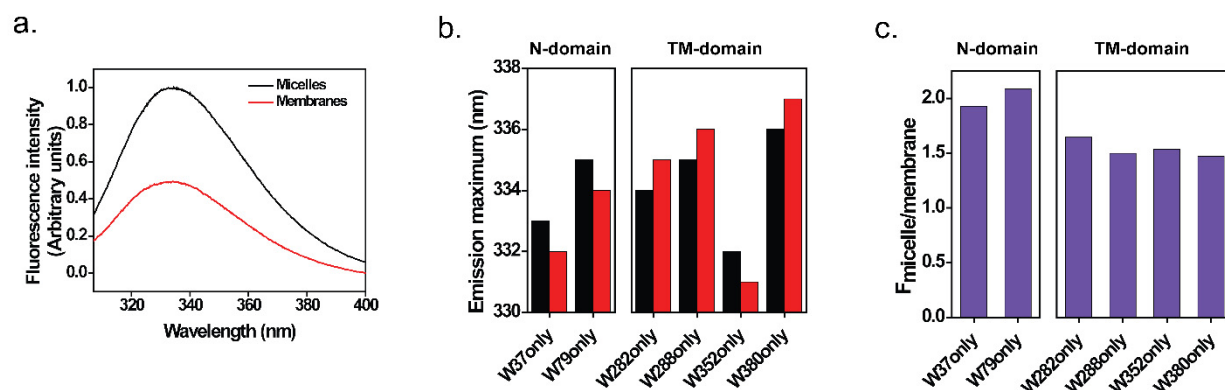


Fig. 4.6. Tryptophan fluorescence emission maximum of the MgtE single-Trp mutants in membrane-mimetic systems. (a) Representative fluorescence emission spectra of W37only in DDM micelles and POPC/POPG (3:1 mol/mol) membranes are shown. (b) Shown are the fluorescence emission maximum of MgtE-Trp mutants in the open state in micelles (black) and membranes (red) at a protein/lipid molar ratio of 1:100. (c) Changes in emission intensity of Trps ($F_{micelle}/F_{membrane}$) for single-Trp mutants observed at respective emission maximum are shown. The excitation wavelength used was 295 nm and the concentration of MgtE was 1.6 μ M in all cases. See Chapter 2 for other details.

Fluorescence emission intensity changes are not always reliable for monitoring probe localization due to its dependence on multifactorial property of emission phenomenon (Lakowicz, 2006; Raghuraman et al., 2019). In contrast, fluorescence lifetime is a faithful indicator of local environment and is an intrinsic property of the probe (Raghuraman and Chattopadhyay, 2003; Berezin and Achilefu, 2010; Raghuraman et al., 2019). Therefore, we measured Trp fluorescence lifetimes of the single-Trp mutants of MgtE in membrane-mimetic

systems (Fig. 4.7). The fluorescence lifetime of Trp has been well established to be sensitive to solvent and excited-state interactions, and can be used to directly monitor the environment of the probe especially its water accessibility due to fast deactivating processes in polar environment (Kirby and steiner, 1970; Raghuraman and Chattopadhyay, 2003; Raghuraman et al., 2019).

A typical fluorescence decay profile of ‘W37only’ with its triexponential fitting and the associated residuals are shown in Fig. 4.7a. The intensity-weighted mean fluorescence lifetimes of the single-Trp residues, $\langle\tau\rangle$, in membrane-mimetic systems are shown in Fig. 4.7b and Table 4.1. It is obvious that the mean fluorescence lifetime of single-Trp residues in micelles are higher (up to ~12%) than in membranes, which shows that the residues face a relatively hydrophobic environment in micelles than in membranes (Fig. 4.7b,c). Further, the lifetime changes in membrane-mimetic systems are more for N-domain Trp residues (‘W37only’ and ‘W79only’) compared to TM-domain with the exception of ‘W352only’. This is in agreement with the significant increase in emission intensity (see Fig. 4.6c) for Trp residues in micelles. The shortening of lifetimes for both the cytosolic as well as TM-domain Trp residues of MgtE upon membrane reconstitution could not only be due to changes in immediate polarity, but also due to cation- π interactions (Ma and Dougherty, 1997) with the neighboring positively charged residues (see Fig. 4.5). These results clearly indicate that the overall organization of MgtE is altered in physiologically-relevant membrane environment.

Table 4.1. Fluorescence lifetimes of Single-Trp mutants of MgtE in different functional states

		α_1	τ_1	α_2	τ_2	α_3	τ_3	$\langle\tau\rangle$ (ns) ^a	τ_H (ns) ^b
DDM micelles									
W37only	Open	0.51	3.45	0.17	7.32	0.32	1.26	4.60	3.59
	Closed	0.49	3.07	0.23	6.65	0.28	1.02	4.54	3.63
W79only	Open	0.37	2.89	0.45	6.25	0.18	1.22	5.10	4.28
	Closed	0.41	2.64	0.44	6.27	0.15	1.05	5.08	4.19
W282only	Open	0.19	3.01	0.72	7.08	0.09	1.33	6.56	5.79
	Closed	0.20	3.02	0.73	7.10	0.07	1.24	6.59	5.87
W288only	Open	0.64	4.51	0.22	8.45	0.14	1.54	5.86	5.76
	Closed	0.52	4.22	0.37	7.77	0.11	1.67	6.07	5.24
W352only	Open	0.63	3.76	0.21	7.28	0.16	1.44	4.93	4.24
	Closed	0.58	3.64	0.28	6.94	0.14	1.23	5.06	4.40
W380only	Open	0.53	3.40	0.35	6.58	0.12	0.87	5.08	4.44
	Closed	0.49	3.32	0.39	6.36	0.12	0.92	5.05	4.44
PC/PG membranes ^c									
W37only	Open	0.40	2.27	0.37	5.69	0.24	0.752	4.44	3.78
	Closed	0.42	1.92	0.41	5.51	0.17	0.521	4.45	3.73
W79only	Open	0.44	1.94	0.43	5.56	0.13	0.331	4.55	3.86
	Closed	0.21	7.36	0.50	3.28	0.29	1.04	4.89	3.80
W282only	Open	0.39	2.51	0.51	6.92	0.10	0.439	5.91	4.91
	Closed	0.38	2.32	0.51	6.44	0.11	0.421	5.51	4.64
W288only	Open	0.35	2.37	0.53	5.9	0.12	0.307	5.12	4.48
	Closed	0.36	2.49	0.52	6.91	0.12	0.347	5.98	5.03
W352only	Open	0.43	2.2	0.39	5.88	0.18	0.393	4.71	3.96
	Closed	0.42	1.92	0.41	5.5	0.17	0.389	4.47	3.68
W380only	Open	0.40	2.75	0.45	5.95	0.15	0.782	4.89	4.29
	Closed	0.45	3.09	0.37	6.25	0.19	0.912	4.88	4.23

The concentration of protein was 1.6 μM in all cases. The excitation wavelength was 285 nm and the emission was monitored at respective emission maximum. See Chapter 2 for other details.

^aMean fluorescence lifetime ($\langle\tau\rangle$) calculated using Eq. 7(Chapter 2); ^bCalculated using Eq. 8 (Chapter 2);

^cThe ratio of single Trp MgtE/total lipid is 1:100.

Apart from the model-dependent mean fluorescence lifetime calculation, the Trp fluorescence lifetimes from the histogram of photons counted during the time-resolved decay measurement (see Eq. 8 of Chapter 2 and Table 4.1) has also been calculated in a model-independent manner as shown previously (see Chapter 3 and ref [Fiserova and Kubala, 2012; Das et al., 2020]). Understandably, model-dependent and model-independent approaches give slightly different fluorescence lifetimes. Irrespective of the methods used to calculate Trp lifetimes, the conclusions resulting from the time-resolved experiments are consistent.

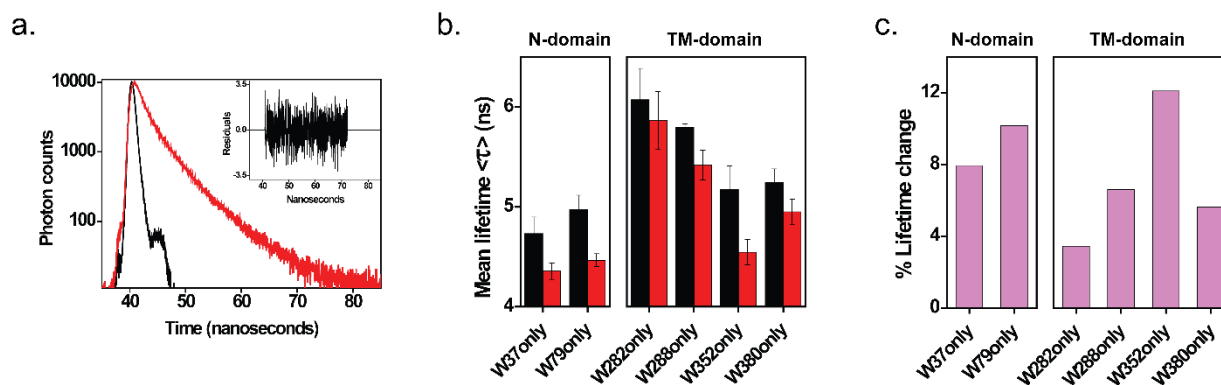


Fig. 4.7. Fluorescence lifetimes of MgtE single-Trp residues in micelles and membranes. (a) Time-resolved Trp fluorescence intensity decay of W37only in the open state (red) in DDM micelles is shown. Excitation wavelength was 285 nm, and emission was monitored at 333 nm. The sharp peak on the left (black) is the lamp profile, and the relatively broad peak on the right is the decay profile (red), fitted to a triexponential function. The plot in the inset shows the

weighted residuals of the decay fit. (b) Mean fluorescence lifetimes of Trps for single-Trp mutants in DDM micelles (black) and POPC/POPG membranes (red) in the open state are shown. Values represent mean \pm SE of three independent measurements. (c) The effect of membrane environment on the lifetimes of single-Trp mutants depicted as percent of lifetime changes is shown. All other conditions are as in Fig. 4.6. See Chapter 2 and Table 4.1 for other details.

4.2.4. Gating-related rotational dynamics of MgtE-Trp residues in micelles and membranes

It is well known that the rapidly tumbling Trp residue displays negligible polarization (Raghuraman and Chattopadhyay, 2004a) whereas its limiting anisotropy is ~ 0.16 (Eftink et al., 1990; Raghuraman et al., 2019). In this regard, the steady-state fluorescence anisotropy values of Trp residues in the open and closed states of MgtE in both DDM micelles and PC/PG membranes generally indicate a considerably restricted mobility (Fig. 4.8a,b). This is suggestive of motional restriction experienced by Trp residues in MgtE irrespective of whether the Trp residues are localized in the cytosolic or TM-domain. In the open state, for which high-resolution atomic structure is not available yet, most of the MgtE-Trp residues in DDM micelle environment display lower anisotropy (*i.e.*, increased rotational dynamics) values than PC/PG membranes. It is interesting to note that the hydrodynamic diameter of DDM micelles (Lipfert et al., 2007) and small unilamellar liposomes (Klingler et al., 2015) is ~ 7 and 40 nm, respectively. Since micelles are smaller than membranes, the curvature will be more in micelles and might have reduced order parameter due to interfacial packing defects as compared to liposomes (Lin et al., 2012).

Interestingly, the changes in rotational dynamics of Trp residues appear to be dependent on the functional state of MgtE. For instance, the anisotropy changes are modest in the closed state for MgtE in micelles and membranes (Fig. 4.8b). Interestingly, significant changes in anisotropy values are observed for Trp residues when MgtE is stabilized in the open state (Fig. 4.8a). The membrane-induced restricted dynamics (low mobility) of Trp-residues, particularly in the open state, clearly suggests the differential MgtE dynamics upon gating. The differential dynamics of MgtE in membrane-mimetic systems is reflected in difference plot (Fig. 4.8c) which shows that, although gating-related dynamic changes are observed in both micelles and membranes, the trend is quite opposite.

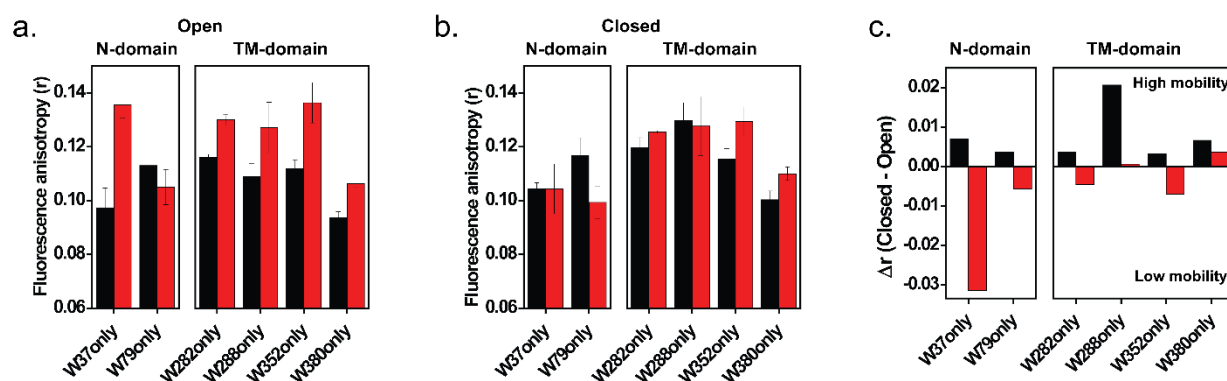


Fig. 4.8. Rotational mobility of MgtE single-Trp mutants upon gating in micelles and membranes. Steady-state anisotropy of Trp fluorescence measured for single-Trp mutants in the (a) open (absence of Mg^{2+}) and (b) closed ($20\text{ mM }Mg^{2+}$) states of MgtE in DDM micelles (black) and reconstituted in POPC/POPG (3:1 mol/mol) liposomes (red) at a protein/lipid molar ratio of 1:100. The excitation wavelength used was 295 nm; emission was monitored at their respective emission maxima in all case. Values represent mean \pm SE of three independent measurements. (c) The difference in anisotropy values (Δr) between closed and open states in

micelles (black) and membranes (red) is shown. The excitation wavelength used was 295 nm and the concentration of MgtE was 1.6 μ M in all cases. See Chapter 2 for other details.

To ensure that the anisotropy values measured for the MgtE-Trp mutants do not suffer from lifetime-induced artifacts, the apparent (average) rotational correlation times were calculated using Eq. 4 in Chapter 2. The gating-related changes in apparent rotational correlation times for MgtE-Trp residues in membranes (Fig. 4.9) and micelles (Fig. 4.10) are in excellent agreement with the anisotropy results (Fig. 4.8). Upon channel opening in the membrane environment, MgtE-Trp residues undergo decreased/restricted rotational dynamics with pronounced dynamic variability, particularly the W37, W282 and W352 residues (Fig. 4.9). Since both cytoplasmic N-domain (W37) and the TM-domain (W282 and W352) Trp residues are sensitive to gating-induced dynamic changes in membranes, this suggests that gating-related conformational dynamics might involve a ‘conformational wave’ from the Mg^{2+} -sensing cytoplasmic domain to TM-domain. However, unlike in membranes, MgtE in the micellar environment does not exhibit dynamic variability and only W288 residue shows a significantly increased dynamics upon opening (Fig. 4.10). Taken together, our data suggest that the structural dynamics of MgtE is significantly altered in physiologically-relevant membrane environment, and is supportive of the importance of side chain dynamics in channel gating (Raghuraman et al., 2012; 2014).

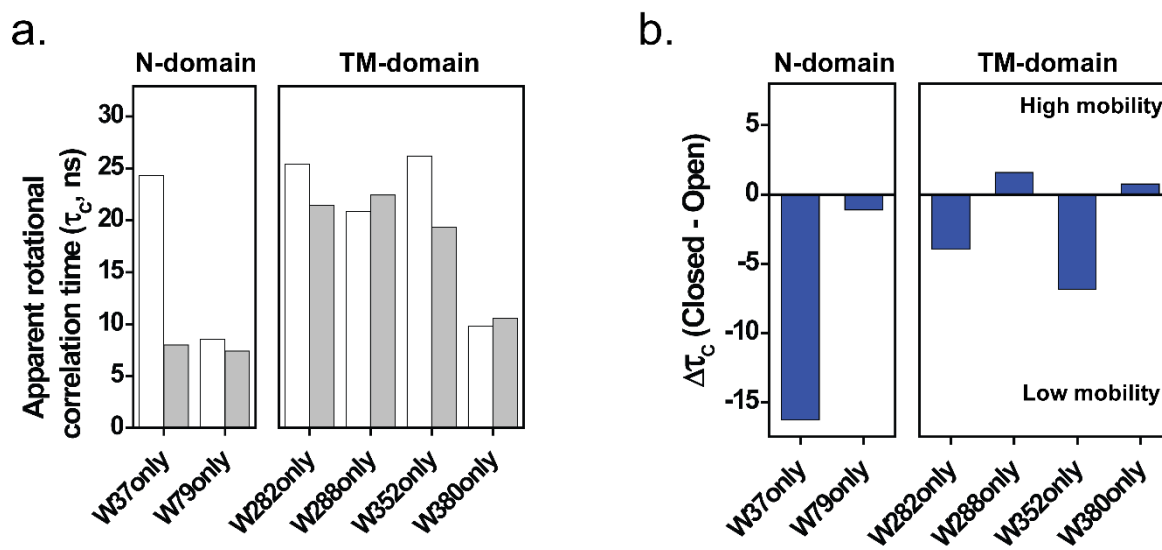


Fig. 4.9. Apparent rotational correlation times of MgtE single-Trp mutants in membranes. Shown are the (a) apparent rotational correlation times in the open (white bars) and closed (grey bars) states of MgtE-Trp mutants in membranes; and (b) difference in apparent rotational correlation times ($\Delta\tau_c$) between closed and open states. All other conditions are as in Fig. 4.8. See Chapter 2 for other details.

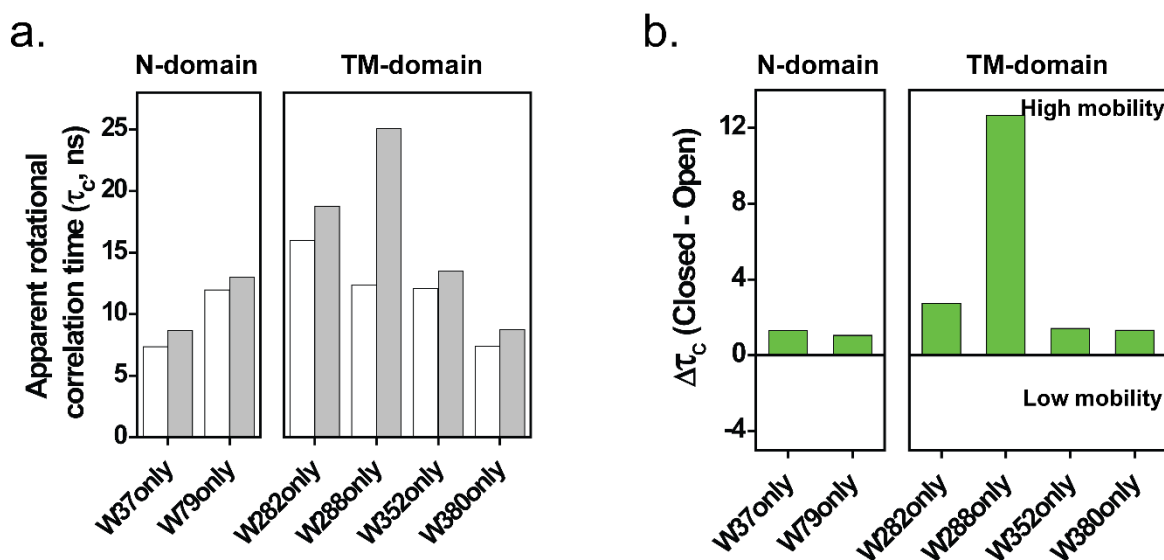


Fig. 4.10. Apparent rotational correlation times of MgtE single-Trp mutants in micelles. Shown are the (a) apparent rotational correlation times in the open (white bars) and closed (grey bars) states of MgtE-Trp mutants in DDM micelles; and (b) difference in apparent rotational correlation times ($\Delta\tau_c$) between closed and open states. All other conditions are as in Fig. 4.8. See Chapter 2 for other details.

4.2.5. Extent of water penetration for single-Trp mutants of MgtE

The above results show significant differences in the structural dynamics of MgtE in micelles and membranes. To examine the accessibility and changes in localization of the Trp residues upon gating, we probed collisional quenching of Trp fluorescence. Acrylamide is a well-known neutral aqueous quencher (Eftink 1991a), which has been widely used to study protein folding (Raghuraman and Chattopadhyay, 2006) and partitioning of membrane peptides and proteins in membrane-mimetic systems (see Chapter 3 and ref [Tory and Merrill, 1999]). Fig. 4.11a shows the representative Stern-Volmer plots for quenching of 'W380only' in the open

and closed states in PC/PG membranes by acrylamide. The Stern-Volmer quenching constant (K_{SV}) of the single-Trp MgtE mutants in membranes is shown in Fig. 4.11b. The K_{SV} values, which are related to water accessibility, of Trp residues in the TM-domain of MgtE (W282, W288, W352 and W380) are in the range of $\sim 4.5 \text{ M}^{-1}$ - 6 M^{-1} , which is consistent with the localization of Trp residues at the interface (Raghuraman and Chattopadhyay, 2004a). Considering the complete exposure of Trp residue to aqueous environment has a K_{SV} value of $\sim 18 \text{ M}^{-1}$ (Raghuraman and Chattopadhyay, 2004a; Raghuraman et al., 2019), the low K_{SV} values for the cytoplasmic Trp residues (W37 and W79) suggests that the N-domain of MgtE is significantly shielded from the aqueous phase in the open and closed states of MgtE incorporated in micelles (Fig. 4.12) and membranes (Fig. 4.11) which agrees well with our previous results (see Fig. 4.6) and the recently reported quenching results from wild-type MgtE (see Chapter 3). Since the K_{SV} values are higher in the closed state of MgtE, it appears that the water penetration accessing the Trp residues is more in the closed state than the open state of MgtE (Fig. 4.11b). Because K_{SV} values are intrinsically dependent on fluorescence lifetime (see Chapter 2, Eq. 13), we calculated the bimolecular quenching constant (k_q), which offers more precise information regarding the degree of aqueous exposure since it considers the differences in fluorescence lifetimes. Our results show that there is a significant increase in water accessibility for most of the Trp residues (W37, W79, W352 and W380) in the closed state of MgtE than open state in membranes (Fig. 4.11c) which is in excellent agreement with K_{SV} values, and supports the notion of gating-induced ‘conformational-wave’. Interestingly, the water accessibility profiles for MgtE-Trp residues in micelles (see Fig. 4.12) are almost identical to membranes except for W380 residue, which could be due to its localization in the lipid-protein interface at the upper leaflet of the membranes. Importantly, the low water accessibility for N-domain Trp residues in

the open state of MgtE also suggest that the overall structural integrity of the cytoplasmic Mg^{2+} -sensing N-domain is preserved during gating (Hattori et al., 2007).

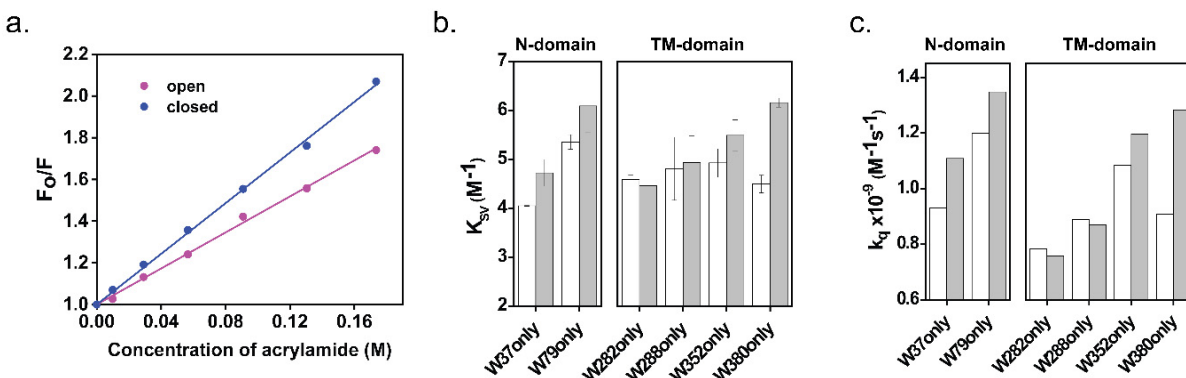


Fig. 4.11. Water accessibility probed by acrylamide quenching of Trp fluorescence in membranes. Shown are (a) Representative data for Stern-Volmer analysis of acrylamide quenching of tryptophan fluorescence of 'W380only' mutant in the open (magenta) and closed (blue) states, where F_0 is the fluorescence in the absence of quencher and F is the corrected fluorescence in the presence of quencher, (b) Stern-Volmer constants (K_{SV}) and (c) bimolecular quenching constants (k_q) for acrylamide quenching of Trp fluorescence for the single-Trp mutants in open (white bars) and closed (grey bars) states of MgtE in PC/PG membranes. The K_{SV} values represent mean \pm SE of three independent measurements. The excitation wavelength used was 295 nm, and the emission was monitored at respective emission maximum. All other conditions are as in Fig. 4.8. See Chapter 2 for other details.

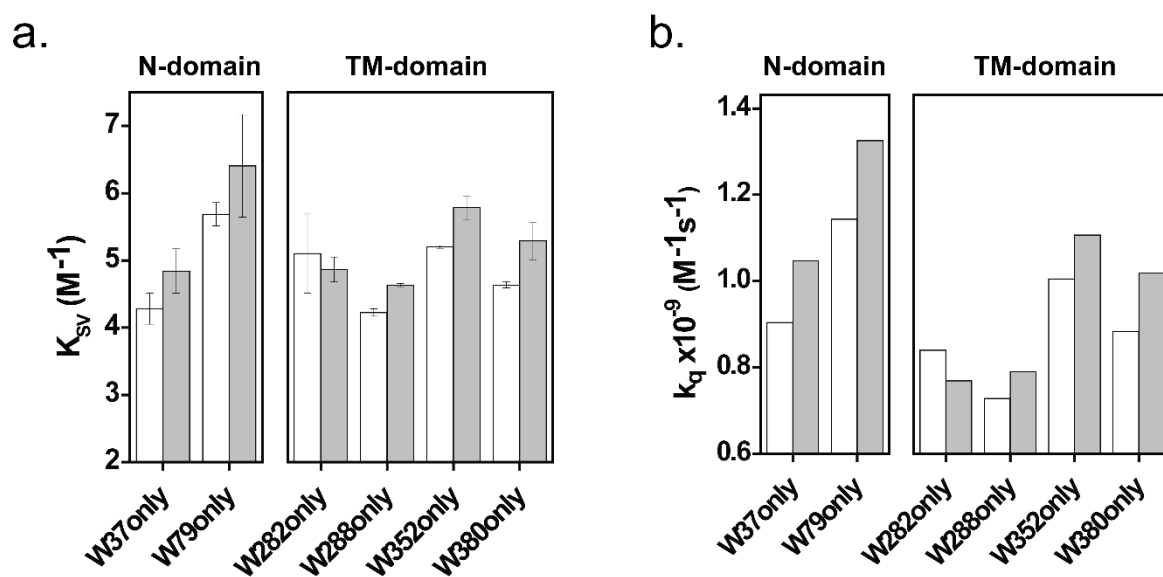


Fig. 4.12. Water accessibility probed by acrylamide quenching of Trp fluorescence in micelles. Shown are (a) Stern-Volmer constants (K_{sv}) and (b) bimolecular quenching constants (k_q) for acrylamide quenching of Trp fluorescence for the single-Trp mutants in open (white bars) and closed (grey bars) states of MgtE in DDM micelles. The K_{sv} values represent mean \pm SE of three independent measurements. The excitation wavelength used was 295 nm, and the emission was monitored at respective emission maximum. All other conditions are as in Fig. 4.8. See Chapter 2 for other details.

4.2.6. Hydration dynamics and conformational substates of MgtE-Trps as probed by REES

It is well known that that protein dynamics is intrinsically related to hydrating solvent molecules and slow solvation (Li et al., 2007). Further, hydration dynamics has been shown to play crucial roles in lipid-protein interactions (Raghuraman and Chattopadhyay, 2007), mediating ion channel functional states (Ostmeyer et al., 2013; Raghuraman et al., 2019) and ion

channel selectivity (Roux, 2017). Red edge excitation shift (REES) is a well-established fluorescence approach, which offers valuable information on the relative rates of water relaxation dynamics and is sensitive to changes in local hydration dynamics (Chattopadhyay et al., 2002; Raghuraman and Chattopadhyay, 2003). Therefore, in complex biological systems, REES is a robust tool to directly probe the environment-induced restriction and dynamics in the immediate environment of a fluorophore (for reviews see refs [Brahma and Raghuraman, 2021; Raghuraman et al., 2019; Chattopadhyay and Halder, 2014; Demchenko, 2008; Raghuraman et al., 2005]). Further, REES has been shown to be sensitive to changes in restricted motions of the surrounding protein matrix due to rearrangements in solvating polar side chains around the fluorophore (Catici et al., 2016; Mishra and Jha, 2019). In this way, REES is a powerful tool to probe the presence of restricted/bound water molecules as well as side chain rearrangements in a protein core.

REES is operationally defined as the shift in the wavelength of maximum fluorescence emission toward higher wavelengths, caused by a shift in the excitation wavelength toward the red edge of the absorption band (Raghuraman et al., 2005, Brahma and Raghuraman, 2021). The magnitude of REES, *i.e.*, the total shift in emission maximum upon changing the excitation wavelength from 295 to 305 nm, for the single-Trp mutants of the open state of MgtE in DDM micelles and PC/PG membranes is shown in the left panel of Fig. 4.13a. In general, all single-Trp mutants exhibit significant REES, which is an indication of motionally restricted environments around Trp residues in both micelles and membranes, and the presence of restricted/bound water molecules (Fig. 4.13a, left). Using REES, it has been shown that restricted or bound water molecules have substantial contribution in ion channel gating mechanism (Raghuraman et al., 2014). Interestingly, the magnitude of REES for MgtE-Trp

ranges from 4-6 nm in micelles, whereas the corresponding values are 1-3 nm in membranes. This significant reduction in the magnitude of REES for all membrane reconstituted MgtE-Trp mutants clearly suggests faster solvent (water) relaxation around the excited-state Trp residues in membranes. In other words, the dynamics of hydration is considerably increased around MgtE-Trp residues in membranes compared to micelles, which is similar to what has been recently observed for the interaction of voltage sensor loop of KvAP with membranes (Das et al., 2020). It is important to note that the changes in the hydration dynamics for MgtE-Trp residues in micelles and membrane bilayer are not only due to polarity changes in the immediate environment since emission maxima and water accessibility is similar in both membrane-mimetic systems (see Fig. 4.6b and 4.12). The differential magnitude of REES in micelles and membranes also indicates an altered organization of the side chains around the Trp residues. Interestingly, gating-induced REES changes in membranes are observed only in Trp residues in the TM-domain and not in the N-domain of MgtE (Fig. 4.13b, left). The magnitude of REES of single-Trp residues in the TM-domain of MgtE (except 'W288only') slightly increase in the closed state (Fig. 4.13b, left) suggesting a role of differential hydration dynamics during MgtE gating. Interestingly, the identical magnitude of REES for N-domain Trp residues while shuttling between open and closed states in membranes supports our earlier observation that the core packing of N-domain is not significantly altered during gating (see Fig. 4.11).

As shown above, the REES magnitude is suitable to monitor relative solvent relaxation dynamics and the corresponding changes in the bulk and restricted water molecules in a qualitative manner. Recently, a novel analysis of REES data has been demonstrated to offer unique insights on conformational changes in proteins and the equilibrium of conformational states (Catici et al., 2016), and this approach has recently been utilized to the voltage sensor of

potassium channels (Das et al., 2020). Particularly, the area extracted from fitting the REES data using Gaussian probability distribution is very useful to monitor changes in protein conformational states (Catici et al., 2016). Our REES data was fitted with Eq. 4 to extract the relative area of the distribution for MgtE-Trp residues (open state) in micelles and membranes (Fig. 4.13a, right) and upon gating in membranes (Fig. 4.13b, right). Our results show that the relative area, which is directly proportional to the number of conformational states, for membranes is significantly low (Fig. 4.13a, right), which indicates that the MgtE-Trp residues might have altered conformational states in membranes. Gating-induced changes in the obtained area is significantly different only for TM-domain Trp residues of MgtE (Fig. 4.13b, right) in which the closed state shows increased area values. Taken together, these results show that not only the dynamics of hydration is significantly different between membrane-mimetic systems, but also indicate the altered conformational states of MgtE during gating.

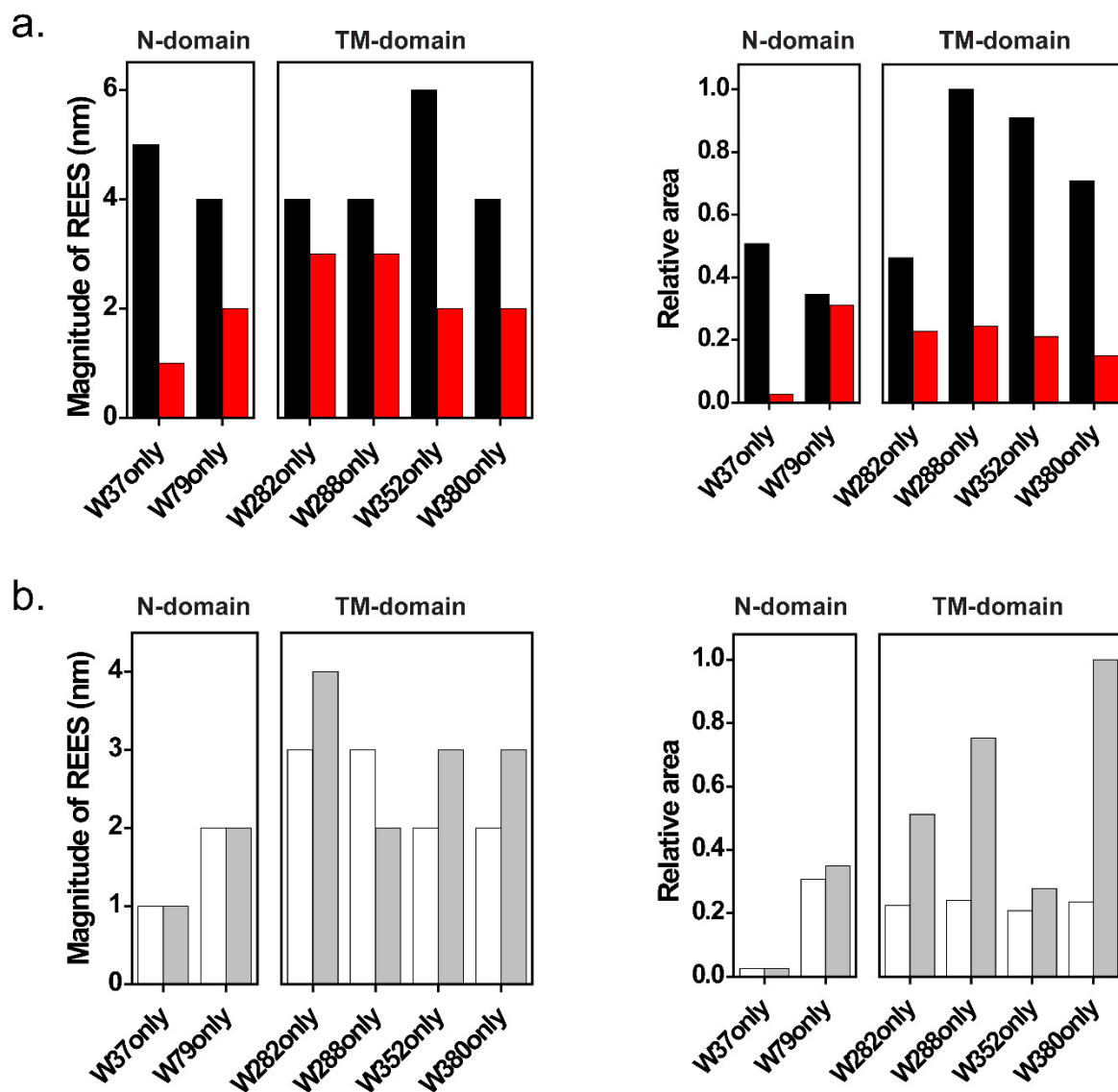


Fig. 4.13. REES of single-Trp mutants of MgtE. Comparison of the magnitude of REES (left) and the associated area (right) for (a) MgtE-Trp mutants in the open state in micelles (black) and membranes (red) and (b) during gating in membranes. The relative area was calculated by fitting the REES data using Eq. 5 (Chapter 2). All other conditions are as in Fig. 4.8. See Chapter 2 for other details.

4.2.7. Conformational heterogeneity of MgtE-Trp by Maximum Entropy Method (MEM)

As mentioned above, the REES results have indicated that gating-related changes might involve altered conformational states of MgtE. However, information on the conformational states obtained using REES approach is indirect in nature and depends on the kinetics of solvent reorientation around the fluorophore. This means that this approach cannot be reliably used for obtaining information on protein conformation if the fluorophore (Trp residue in our case) does not exhibit REES or when the magnitude of REES is very small as in the case of ‘W37only’ mutant of MgtE. In contrast, MEM-lifetime distribution is a direct read-out of structural heterogeneity irrespective of the solvent (water) relaxation dynamics around the fluorophore since fluorescence lifetime distribution gives an ultrafast snapshot of the protein population distribution (Beechem and Brand, 1985; Krishnamoorthy, 2018). MEM analysis of fluorescence decay is robust and involves resolving the lifetime components in a model-independent manner, which has been widely used to monitor unfolding transitions in soluble proteins (Swaminathan et al., 1994; Lakshmikanth et al., 2001; Jha et al., 2009; Krishnamoorthy, 2018; Sternisha et al., 2020), and membrane heterogeneity (Mukherjee et al., 2007). However, this robust MEM approach has rarely been used to decipher conformational heterogeneity of membrane proteins.

Representative MEM lifetime distributions of MgtE-Trp residues in the absence (open) and presence (closed) of magnesium ions in membranes is shown in Fig. 4.14. It should be noted that although the model-independent MEM analysis has been performed assuming the equal probability of the existence of lifetimes in the range of 0.1 to 100 ns in logscale, we have not observed any lifetime distribution beyond 10 ns. In general, irrespective of the functional state of MgtE (Fig. 4.14) and the membrane-mimetic system used (Fig. 4.15), the fluorescence

lifetime distribution profiles for all MgtE-Trp mutants contain multiple peaks and are complex. This is not surprising considering the complex nature of organized molecular assemblies such as membrane-mimetics and proteins (Mukherjee et al., 2007; Sternisha et al., 2020). Monitoring the changes in the conformational heterogeneity within various functional states of the channel is therefore not trivial. However, change in distribution profiles can offer significant insights into the nature of altered conformational substates. Most of the single Trp mutants of MgtE embedded in micelles display relatively broad peaks compared to MgtE-Trps reconstituted in membranes (Fig. 4.15), which suggests an increased conformational heterogeneity of MgtE in DDM micelles compared to PC/PG membranes. This is well supported by the observation of increased area associated with micellar environment (see Fig. 4.13a, right).

As seen from the Fig. 4.14, the cytoplasmic W37 residue has three discrete peaks in the open state. However, upon closing the channel, the discrete nature of the peaks is lost in such a way that the lifetime distribution is spread from ~1 to 8 ns, indicating an increase in conformational heterogeneity for this residue in the closed state (Fig. 4.14a). In case of cytoplasmic W79 residue, we observe a lesser number of discrete lifetime distributions in the closed state. However, the two lifetime peaks which appear in 2-6 ns region for the open state of MgtE are merged into a single broad lifetime peak in the closed state, supporting the altered sidechain conformational heterogeneity (Fig. 4.14b). The fact that the lifetime distribution profiles of W37 and W79 residues do not drastically differ between the functional states suggests that N-domain is structurally preserved during gating. Since the N-domain of MgtE has been implicated in Mg^{2+} -sensing and regulation of MgtE gating, we therefore attribute the change in conformational heterogeneity of these Trp residues to gating-related structural changes of the N-domain. In case of TM-domain Trp residues (W282 and W288), the distribution profiles are

complex in both the closed and open states of MgtE (Fig. 4.14 c,d). Interestingly, despite retaining their complicated distribution profiles, the closed state of the channel has more peaks than the open state suggesting the changes in conformational microheterogeneity during gating, which is in excellent agreement with the above-mentioned REES data (see Fig. 4.14b, right). However, the profiles of TM-domain W352 and W380 residues of MgtE do not show a significant change upon gating (Fig. 4.14e, f). Taken together, MEM-lifetime distribution analysis supports the notion of ligand-induced ‘conformational wave’ from the Mg^{2+} -sensing N-domain to TM-domain of MgtE, and the structural integrity of N-domain is preserved during the gating process.

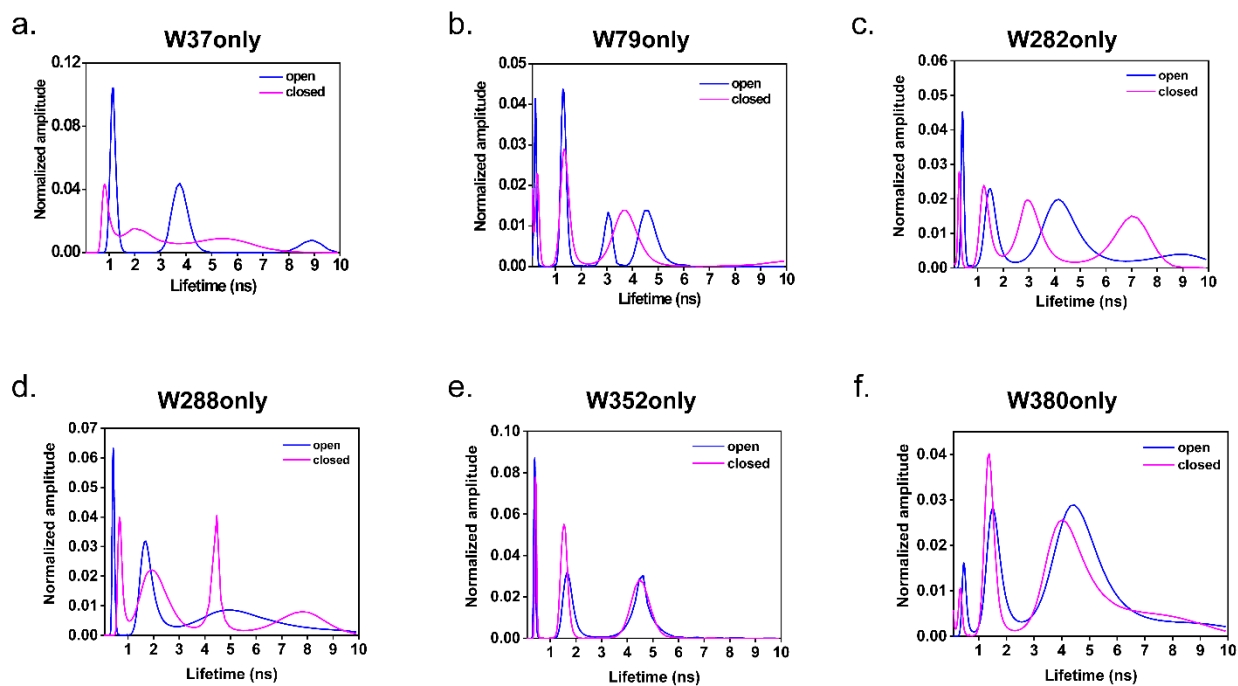


Fig. 4.14. Conformational heterogeneity of MgtE single-Trp mutants during gating in membranes. MEM tryptophan fluorescence lifetime distributions for (a) W37only, (b) W79only, (c) W282only, (d) W288only, (e) W353only and (f) W380only mutants in the open (cyan) and closed (magenta) states of MgtE in membranes are shown. The normalized probability amplitudes are plotted against their corresponding lifetime on a linear scale. All other conditions are as in Fig. 4.8. See Chapter 2 for details.

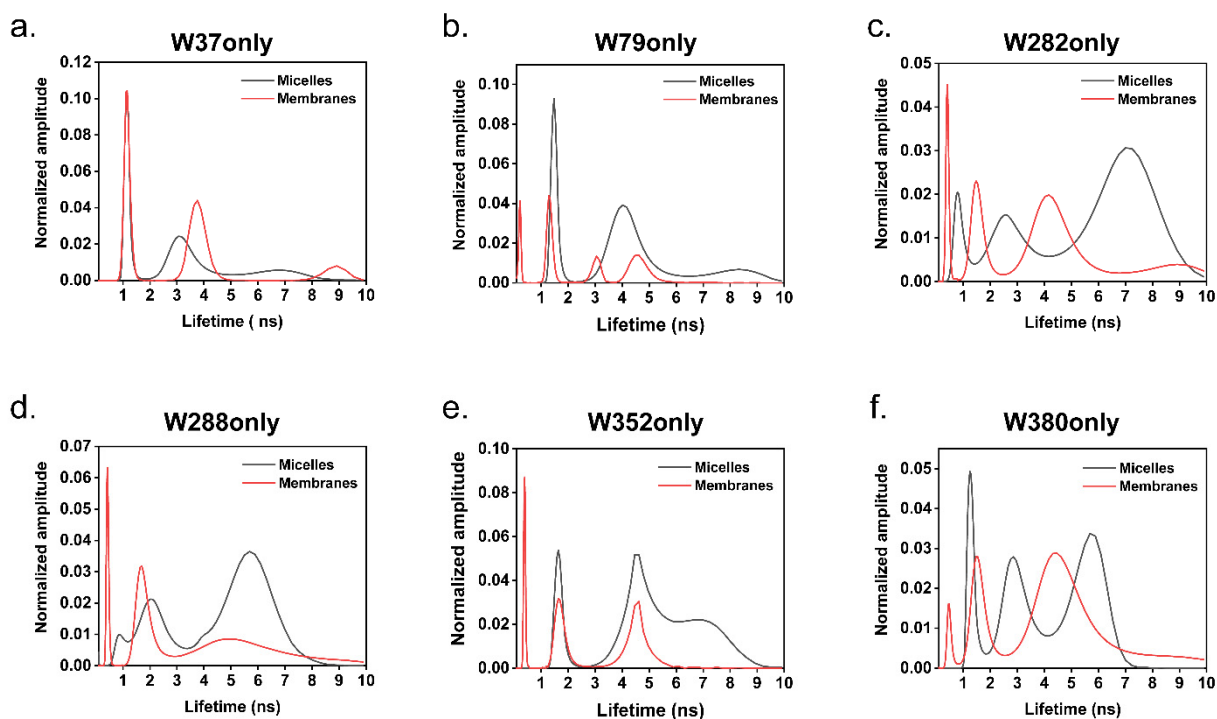


Fig. 4.15. Comparison of fluorescence lifetime distribution of MgtE single-Trp mutants in micelles and membranes. MEM tryptophan fluorescence lifetime distributions for (a) W37only, (b) W79only, (c) W282only, (d) W288only, (e) W353only and (f) W380only mutants in the open state of MgtE in DDM micelles (black) and PC/PG membranes (red) are shown. The normalized probability amplitudes are plotted against their corresponding lifetime on a linear scale. All other conditions are as in Fig. 4.7. See Chapter 2 for details.

4.3. Discussion

Biomembranes are complex assemblies of lipids and proteins, which provide a unique heterogeneous microenvironment for the optimum performance of membrane proteins and hence modulate various cellular signaling pathways (Rao and Mayor, 2014). The critical dependence of membrane proteins on lipid constituents of membranes suggests a coevolution of lipids and proteins (Lee, 2004). Further, membrane lipids have been shown to play an important role in stabilizing membrane protein structure and function, and ion channels in particular (Valiyaveetil et al., 2002; Lee, 2003; Hunte, 2005; Ramu et al., 2006; Xu et al., 2006; Jiang and Gonen, 2012). Further, local lipid composition influences the topology, structural dynamics and conformation of membrane proteins and peptides (Lee, 2003; Raghuraman and Chattopadhyay, 2004a; Hunte, 2005; Das et al., 2020), highlighting their functional dependence on lipid-protein interactions in membranes. Although the importance of lipid-protein interactions is well established, the high-resolution structures of membrane proteins is often solved in detergent micelles or amphipols using monoclonal antibodies due to technical difficulties (Moraes et al., 2014; Jin et al., 2020).

Among ion channels, magnesium ion channels are arguably the least understood despite Mg^{2+} being the most abundant divalent cation and is crucial for many cellular processes (Hartwig, 2001; Selmer et al., 2006). Despite its significance, the mechanisms governing the transport and regulation of magnesium channels are poorly understood. Our present understanding of the molecular basis of Mg^{2+} transport comes from studies on prokaryotic magnesium ion channels (CorA and MgtE) (Moomaw and Maguire, 2008; Payandeh et al., 2013). It is known that MgtE, like CorA, is the main Mg^{2+} transport system in almost half of all prokaryotes. Interestingly, unlike potassium and sodium ion channels, the subunit organization (*i.e.*, molecular architecture) of magnesium channels is not conserved as can be seen from the three-dimensional X-ray crystallographic structures of magnesium ion channels. For instance,

while CorA magnesium channel functions as a homopentamer (Moomaw and Maguire, 2008; Payandeh et al., 2013), MgtE from *Thermus thermophilus* functions as a homodimer (Hattori et al., 2009; Tomita et al., 2017). Although CorA and MgtE channels are evolutionarily distinct and have different architecture, they have conceptually similar gating mechanism. It is therefore important to understand the events associated with Mg^{2+} -dependent gating.

Interestingly, MgtE from *T. thermophilus* is distantly related to mammalian SLC41A1 transporter (Wabakken et al., 2003) and can functionally compensate TRPM7-deficiency in vertebrate B-cells (Sahni et al., 2012). Importantly, MgtE is a dual-function protein in *P. aeruginosa*, *i.e.*, it functions both as a Mg^{2+} transporter and a virulence modulator and thus playing an important role in linking magnesium availability to pathogenesis (Coffey et al., 2014), and thus a potential antibiotic target. Because the MgtE transport mechanisms across membranes at the molecular level are poorly understood due to unavailability of structural information in different functional states of full-length MgtE, the study of gating-related structural dynamics of MgtE assumes significance.

As mentioned earlier, the high-resolution closed state crystal structures of full-length MgtE has been obtained in detergent micelles (Hattori et al., 2007; 2009; Tomita et al., 2017). Further, structural and dynamic information regarding the mechanism of MgtE function has been obtained for full-length MgtE in micelles (Maruyama et al., 2018) and the isolated cytoplasmic domain in solution (Hattori et al., 2007; Imai et al., 2012) in the presence and absence of Mg^{2+} . Furthermore, the TM-domain structure of MgtE bound to Mg^{2+} have been solved using lipidic cubic phase crystallization in a monoolein lipid environment (Takeda et al., 2014). Very recently, a 3.7 Å cryo-EM structure of MgtE-Fab complex in Mg^{2+} -free conditions is available in which the cryo-EM density is only detectable for the TM-domain (Jin et al., 2021). It is obvious

from this atomic model of TM-domain structure of MgtE that the ion-conducting pore is opened on the cytoplasmic side, but closed on the periplasmic side indicating that the pore is in non-conducting configuration. This structure therefore might represent one of the partially-open ('pre-open state') conformations of MgtE under Mg^{2+} -free conditions.

To properly understand the structure-function relationship of MgtE, knowledge of changes in the structural organization and dynamics of MgtE in membrane-mimetic systems, and monitoring gating-related structural dynamic changes in membranes is therefore crucial, and this has been the focus of this work. For this purpose, we have engineered single-Trp mutants of MgtE in the functional Trp-less background as MgtE is a multi-tryptophan protein, and utilized various sophisticated fluorescence approaches to obtain site-specific information on structural dynamics. Our results utilizing the site-specific Trp fluorescence of MgtE clearly demonstrates, for the first time, the altered organization, dynamics and conformational heterogeneity of MgtE-Trp residues in physiologically-relevant PC/PG membranes compared to DDM micelles. This observation is supported by the fact that micelles, despite being widely used as membrane-mimetic systems, have been shown to drastically affect the function, dynamics, structural integrity in several membrane proteins (Encinar et al., 2005; Kofuku et al., 2014; Ge et al., 2016; Frey et al., 2017; Das et al., 2020).

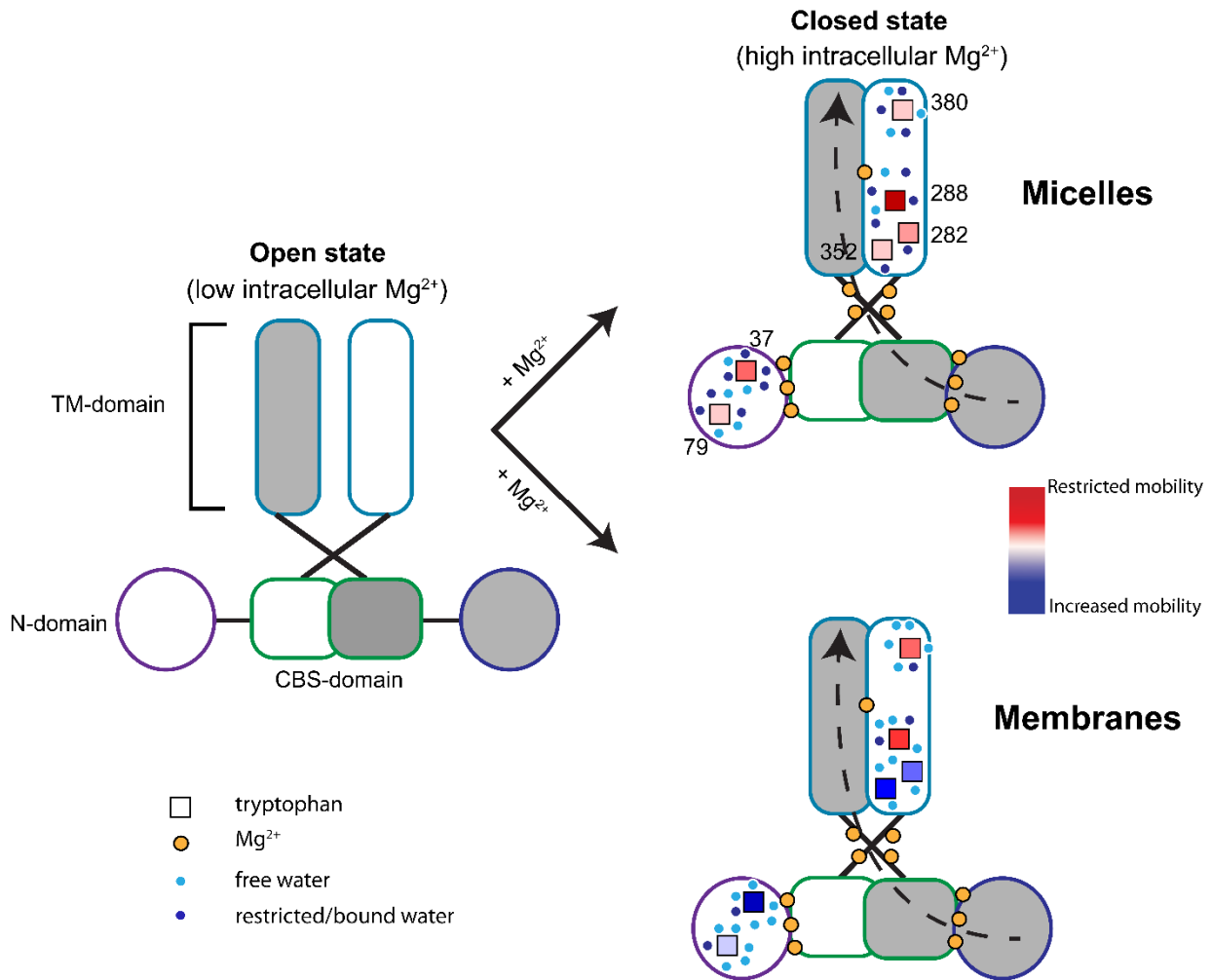


Fig. 4.16. Gating-related conformational dynamics of MgtE in micelles and membranes. Schematic representations of the events associated with Mg^{2+} -induced closing of MgtE in membrane-mimetic systems are shown. One subunit of the homodimeric MgtE is shaded grey to show the organization of the channel, and the transmembrane (TM) and cytoplasmic (N and CBS) domains are indicated. The open state representation shown is based on previous studies (Hattori et al., 2009; Tomita et al., 2017; Maruyama et al., 2018). The respective residue numbers of MgtE-Trps (denoted by squares) is shown. Gating-induced changes in motional dynamics of MgtE-Trp residues are shown with blue and red to represent increased (dynamic)

and restricted mobilities, respectively. The changes in hydration dynamics upon Mg^{2+} (yellow spheres) mediated closing is represented by the change in ratio of bulk/free (cyan spheres) vs. restricted/bound (blue spheres) water molecules. Mg^{2+} -binding induces a 'conformational wave' from N-domain to TM-domain, which is indicated by a curved broken arrow. See Discussion for details.

From our results, we propose a model that highlights significant differences in the gating-related structural dynamics of MgtE in micelles and membranes (Fig. 4.16). In the Mg^{2+} -bound (closed state) conditions, most of the MgtE-Trp residues in micelles experience decreased rotational motion (*i.e.*, relatively restricted) compared to membranes. Importantly, although MgtE is responsive to Mg^{2+} -induced gating in both micelles and membranes, the trend is quite opposite in the sense that the MgtE is not only more dynamic but also displays dynamic variability in membranes than micelles upon closing (see Fig. 4.8). This is accompanied by significant changes in environmental motional restriction (hydration dynamics and protein matrix), due to altered ratio of restricted (bound) to free (bulk) water molecules and possible polar sidechain rearrangements (see Fig. 4.14). Interestingly, the functional correlation of hydration and structural dynamics is well established in different functional states of K^+ channels (Raghuraman et al., 2014; Kratochvil et al., 2016). In this regard, the observed changes in hydration dynamics might be important for gating and permeation mechanisms of MgtE. Interestingly, our model predicts that the structural integrity of Mg^{2+} -sensing N-domain in full-length MgtE is preserved in both open and closed states of MgtE (see Fig. 4.12 and 4.14), which is in agreement with the crystal structures of the soluble cytosolic domain in the presence and absence of Mg^{2+} (Hattori et al., 2007). In other words, the N-domain does not undergo

conformational collapse in the apo/open state (*i.e.*, in the absence of Mg^{2+}). Importantly, our model also indicates the possibility of ligand-induced ‘conformational wave’ from the Mg^{2+} -sensing N-domain to TM-domain of MgtE during gating. This is supported by the recent cryo-EM structure of TM-domain of MgtE solved in Mg^{2+} -free conditions in which the side chain of Trp residues in the TM-domain have undergone significant change in orientation compared to the closed state of MgtE (see Fig. 4.17). Considering that the cryo-EM structure might represent the ‘pre-opening state’ (Jin et al., 2021), the magnitude of this structural change could be much larger in the fully open state of MgtE. Overall, our results are relevant to understand the importance of physiologically-relevant membrane environment and lipid-protein interactions in the gating mechanisms of magnesium channels in general, and MgtE in particular.

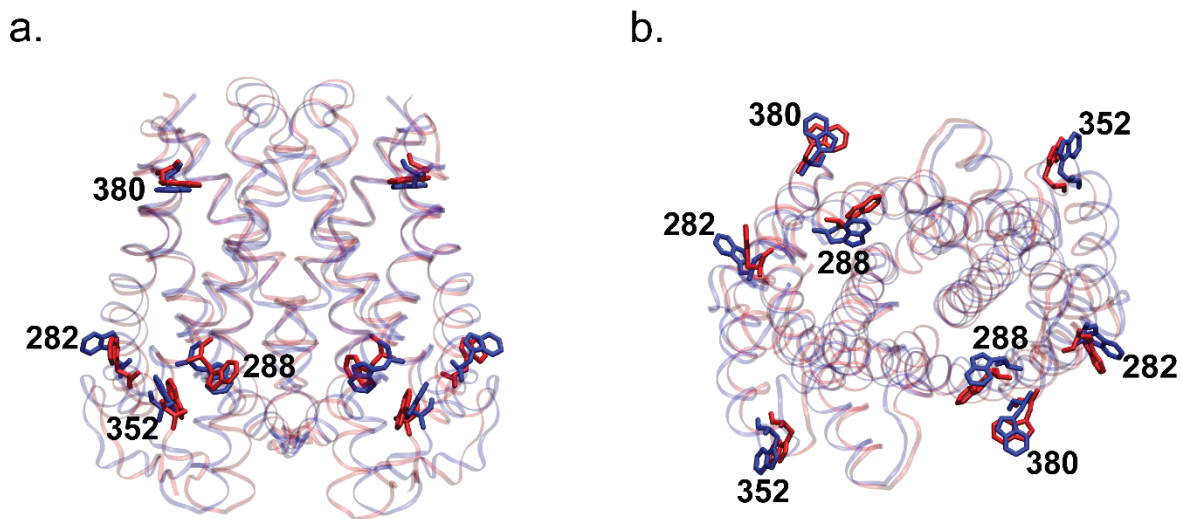


Fig. 4.17. Comparison of MgtE TM-domain structures in Mg^{2+} -free and -bound forms.

Shown are the cartoon representations of the TM-domain of MgtE in the Mg^{2+} -free (blue; PDB: 6LBH) and Mg^{2+} -bound (red; PDB: 2ZY9) forms viewed from the (a) side and (b) cytoplasm showing the possible gating-related changes in orientation of side chain of Trp residues (denoted

by respective residue numbers). The TM-domain of MgtE (residues 271-448) from the two PDB structures were aligned using VMD. The calculated RMSD of the TM-domains of the Mg^{2+} -free structure (6LBH) relative to the Mg^{2+} -bound structure of MgtE was 1.218 Å.

Chapter 5

Gating-related Structural Dynamics of the Mg²⁺ sensing N- domain of the MgtE Magnesium Channel in Membrane-Mimetics

5.1. Introduction

The cytoplasmic domain, particularly the N-domain is proposed to function primarily as a Mg^{2+} -sensor (please see Chapter 1, Section 1.6.2 for details). It is evident from the crystallographic snapshot of the closed state of full-length MgtE in DDM micelles that the cytoplasmic domain is lined with several acidic residues. Consequently, it has been proposed that electrostatic repulsion between these residues keeps the channel open in the absence of Mg^{2+} while the closed state of the channel is stabilized in the presence of high intracellular Mg^{2+} due to neutralization of these negative charges (Hattori et al., 2007, 2009). Therefore, the gating mechanism of MgtE is quite interesting, since Mg^{2+} acts as both a permeating as well as a regulatory ion.

In this work, we have monitored the gating-related structural dynamics of the residues at the interface of the N-domain and CBS-domain around the Mg^{2+} binding sites for full-length MgtE in micelles and membranes. For this purpose, we have systematically constructed single-cysteine mutants in N-domain in such a way that it is possible to probe around the Mg^{2+} binding sites between the N- and CBS-domains without perturbing the residues responsible for coordinating Mg^{2+} to MgtE. We have employed site-specific fluorescence labeling with a widely used environment-sensitive probe, 7-nitrobenz-2-oxa-1,3-diazol-4-yl (NBD) (Raghuraman et al., 2019). Coupling of cysteine scanning mutagenesis and site-directed fluorescence approach offers the advantage to selectively probe the regions of interest to appreciate the structural dynamics changes compared to the approach used in Chapter 4. Additionally, the C_{α} - C_{α} intersubunit distances of these residues are between ~ 20 to 60 Å which can be exploited for measuring gating-related changes in the intersubunit distances of the MgtE homodimer utilizing techniques

like double electron-electron resonance (DEER) spectroscopy (Jeschke, 2012; Raghuraman et al., 2014).

Our results suggest an overall decrease in mobility and variation in hydration dynamics of the N-domain residues upon gating in micelles and membranes with an overall increase in dynamic variability in membranes compared to micelles. Furthermore, MEM analysis of lifetime distribution indicates a decrease in heterogeneity upon gating in membranes. We have employed a novel quenching method, which exploits the phenomenon of tryptophan to quench the emission intensity of monobromobimane (mBBr) in a distance-dependent manner to monitor small scale conformational changes in the N-domain. This novel approach, *i.e.*, the tryptophan-induced quenching (TrIQ) has been used to map short-range distances ($\sim 5\text{-}15$ Å) in proteins (Mansoor et al., 2002; 2010; Raghuraman et al., 2019) which is otherwise not possible with Förster resonance energy transfer (FRET) technique. The lifetime distribution and TrIQ analyses of the N-domain residues suggest that the structural integrity of the N-domain is preserved during gating, which is in excellent agreement with our results using site-specific Trp fluorescence (see Chapter 4). Taken together, we demonstrate that the N-domain is structurally preserved when MgtE shuttles from the closed to the open state. Further, our results suggest that the N-domain residues assume a more restricted organization with an increase in dynamic variability in membranes upon Mg^{2+} -induced gating. Overall, our work highlights the importance of changes in structural dynamics of the Mg^{2+} -sensor N-domain in physiologically relevant membranes upon gating.

5.2. Results

5.2.1. NBD labeling does not perturb the structural integrity of MgtE

Single-cysteine mutants of the N-domain residues at the interface of the N- and CBS-domains (Fig. 5.1a) are labeled with the thiol-reactive fluorophore, NBD. The small size, visible range excitation, uncharged nature, and environment-sensitive fluorescence properties make NBD an ideal fluorophore of choice to probe the changes in structural dynamics of the N-domain residues (Raghuraman et al., 2019). The oxygen atoms and the imino group of the NBD fluorescing moiety may form hydrogen bonds with lipid carbonyls, interfacial water molecules, and the lipid headgroup. The N and O atoms impart sufficient polar character to NBD rendering it soluble in an aqueous environment making NBD an ideal reporter both in aqueous and hydrophobic environments (Shepard et al., 1998; Johnson, 2005; Raghuraman et al., 2007). To ascertain that NBD labeling of the N-domain residues does not perturb the structural integrity of MgtE, we carried out size-exclusion chromatography (SEC) of all the labeled mutants. Both NBD labeled and unlabeled analogs of MgtE (H29-NBD is shown as representative) exhibit a similar SEC profile eluting at ~10.6 ml which is also the same as that of wild-type MgtE (see Chapter 3), confirming that irrespective of NBD labeling MgtE elutes as a homodimer (Fig. 5.1b). In addition, the far-UV CD spectra (Fig. 5.1c) reveal that the labeled mutants retain their α -helical character both in micelles and membranes similar to wild-type MgtE (see Chapter 3). Taken together, our results suggest that NBD-labeling does not affect the structural integrity of MgtE and therefore can be used for monitoring the gating-related structural dynamics of the N-domain residues in micelles and membranes.

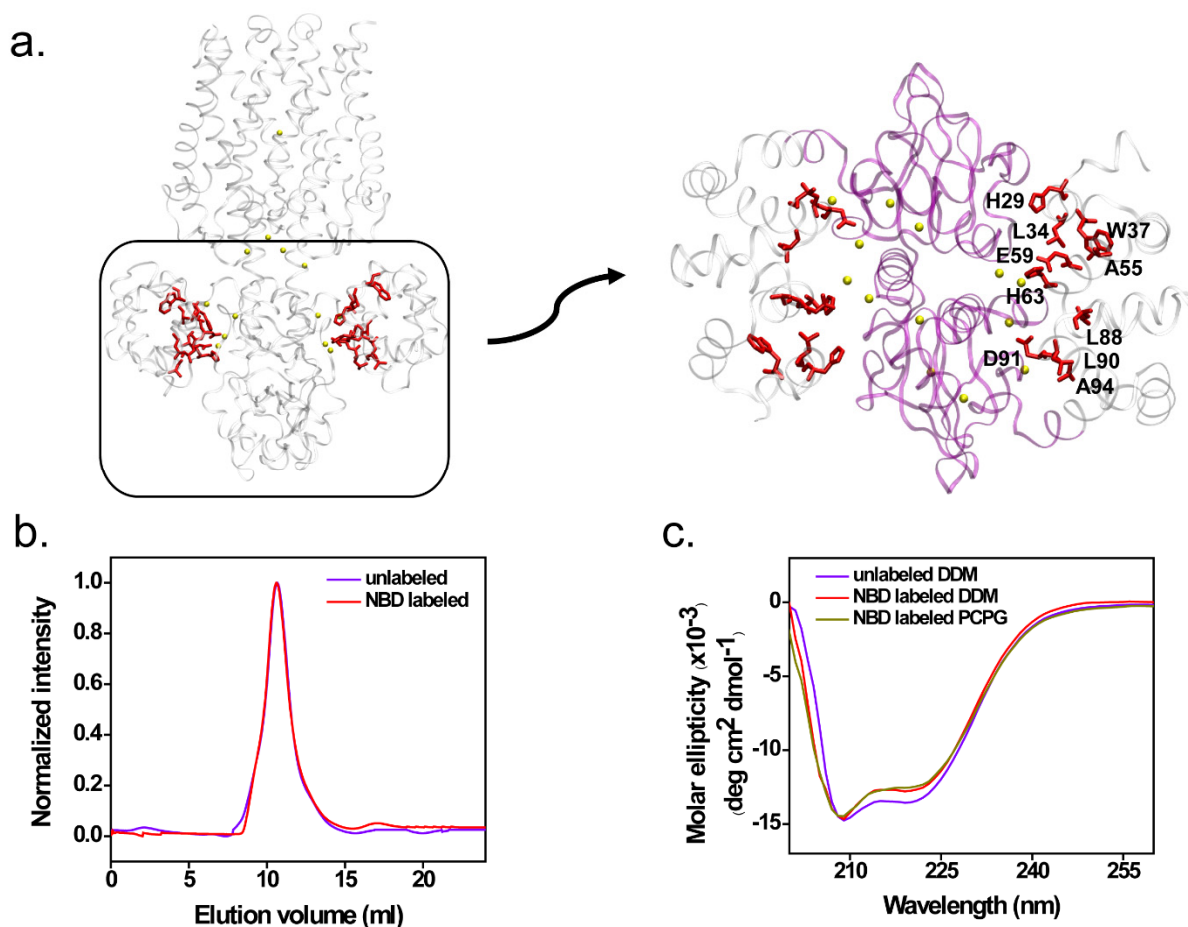


Fig. 5.1. Residues at the interface of N- and CBS-domain. (a) Shown is the cartoon representation of Mg^{2+} -bound (yellow spheres)/closed state of homodimeric MgtE (PDB: 2ZY9) showing the interfacial location of the N-domain residues (red stick representation) with the enlarged view (right) of the cytoplasmic domain. The CBS-domain is colored purple while the interfacial N-domain residues which have been selected for NBD-labeling are denoted by their respective residue numbers. (b) Size-exclusion chromatography (SEC) profiles of the unlabeled and NBD-labeled H29C mutant of MgtE N-domain are shown. (c) Representative far-UV CD

spectra of unlabeled and NBD-labeled H29C mutant in DDM micelles and PC/PG membranes. CD spectra were recorded using 2 μ M of protein in DDM micelles or reconstituted in POPC/POPG (3:1 mol/mol) membranes. See Chapter 2 and Eq. 2 for other details.

5.2.2. Microenvironment of interfacial N-domain residues upon gating

Since NBD is weakly fluorescent in water and fluoresces brightly in the visible range when transferred to a hydrophobic medium, exhibiting a high degree of environmental sensitivity (Lin and Struve, 1991; Fery-Forgues et al., 1993; Chattopadhyay et al., 2002), it has been widely used to monitor membrane dynamics (Mukherjee et al., 2004; Raghuraman et al., 2007) and structural dynamics of membrane proteins (Crowley et al., 1993; Shepard et al., 1998; Raghuraman and Chattopadhyay, 2007; Raghuraman et al., 2014; Das et al., 2020; Das and Raghuraman, 2021; for reviews see Johnson, 2005 and Raghuraman et al., 2019). Fig. 5.2a and d shows the representative emission scans of a MgtE N-domain residue in the open and closed state in micelles and PC/PG membranes, respectively. The fluorescence emission maxima of the NBD labeled MgtE N-domain residues range from 522 to 540 nm in micelles and membranes (Fig. 5.2b and e). This suggests that the microenvironment experienced by these residues is relatively nonpolar despite the cytoplasmic localization of the N-domain. This is in excellent agreement with our previous work where the native Trp residues of the N-domain also showed a hydrophobic localization (see Chapter 4). Interestingly, we observe negligible changes (± 1 nm) in fluorescence emission maxima (except for A55- and E59-NBD residues in membranes) of the N-domain residues upon gating in micelles and membranes suggesting that the microenvironment of these residues do not change significantly when MgtE shuttles from the open to the closed state. This is in excellent agreement with the notion that the structural

integrity of the N-domain is preserved during gating. Although the emission maxima for the N-domain residues is similar in micelles and membranes, the fluorescence intensity for the N-domain residues either decreases (in the case of L34 and D91) or remains constant in membranes (Fig. 5.2f) while increases in micelles (Fig. 5.2c) upon gating, suggesting an altered organization in micelles compared to membranes upon gating.

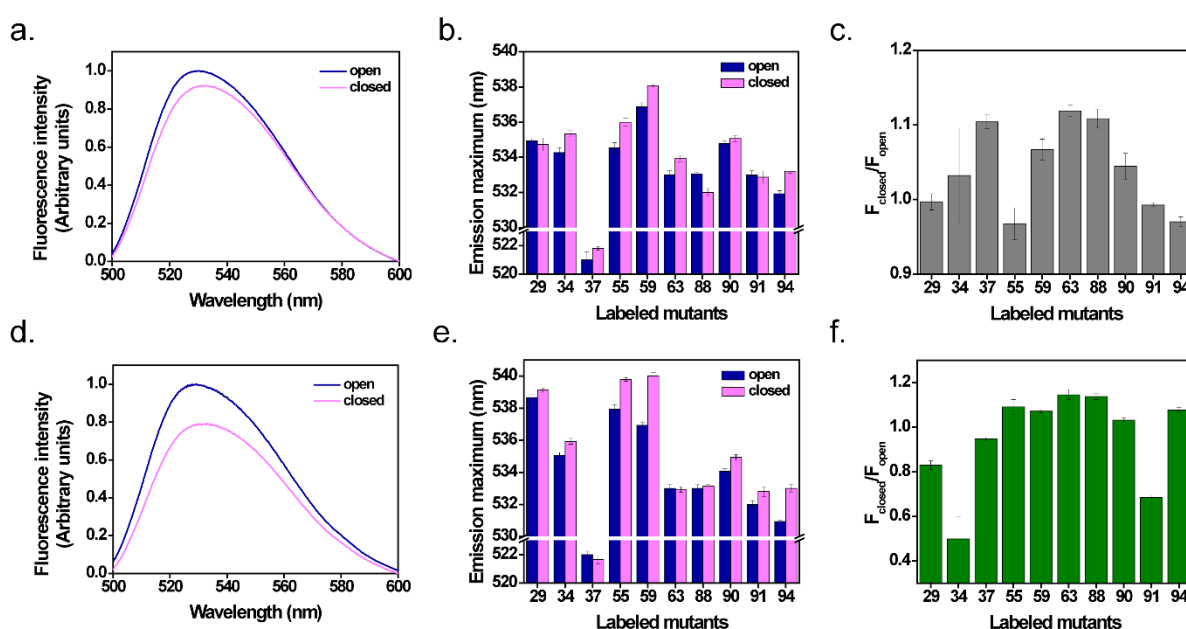


Fig. 5.2. Fluorescence emission maximum of the NBD-labeled N-domain residues in membrane-mimetic systems. Representative fluorescence emission spectra of D91-NBD in the open (absence of Mg^{2+}) and closed states (presence of 20 mM Mg^{2+}) in DDM micelles (a) and POPC/POPG (3:1 mol/mol) membranes (d) are shown. Shown are the fluorescence emission maximum of the NBD-labeled N-domain residues of MgtE in the open and closed state in micelles (b) and membranes (e) at a protein/lipid molar ratio of 1:100. Changes in emission

intensity of the N-domain residues upon gating (F_{closed}/F_{open}) observed at respective emission maximum in micelles (c) and membranes (f) are shown. The excitation wavelength used was 465 nm and the concentration of MgtE was 3.2 μ M in all cases. See Chapter 2 for other details.

Since emission intensity is a composite fluorescence property of the probe dependent on multiple factors (Lakowicz, 2006; Turconi et al., 2001), it may not always be a reliable parameter to monitor the localization of probes. Contrarily, fluorescence lifetime is an intrinsic property of the probe and is an excellent reporter of the local environment around the fluorophore (Berezin and Achilefu, 2010). Therefore, we have measured the fluorescence lifetime of NBD-labeled N-domain residues upon gating. The fluorescence lifetime of NBD is very sensitive to the local environment, ranging from $\sim 5 - 10$ ns in hydrophobic membrane interior (Mukherjee et al., 2004; Raghuraman et al., 2007) to ~ 1.5 ns when completely exposed to the aqueous environment (Lin and Struve, 1991; Crowley et al., 1993; Raghuraman and Chattopadhyay, 2007). A typical decay profile of D91-NBD in the open and closed state in micelles and membranes with its triexponential fitting and associated residuals are shown in Fig. 5.3a and c respectively. The intensity weighted mean fluorescence lifetimes of the NBD labeled N-domain residues, $\langle \tau \rangle$, in micelles and membranes, is shown in Fig. 5.3b & d respectively and in Table 5.1. Interestingly, although the N-domain residues are located in the cytoplasmic domain of MgtE, the mean fluorescence lifetime of most of the residues are >5 ns suggesting a hydrophobic localization within the protein matrix of the N-domain both in micelles and membranes which is in excellent agreement with the steady-state fluorescence emission maxima (see Fig. 5.2). Further, the changes in mean fluorescence lifetime for the N-domain residues upon gating both in micelles and membranes are modest indicating that the core structural packing of

the N-domain is not dramatically affected during gating. Taken together, our steady-state emission maxima data and lifetime data suggest a hydrophobic localization of the N-domain residues and that the overall structural integrity of the N-domain is preserved during gating in micelles and membranes.

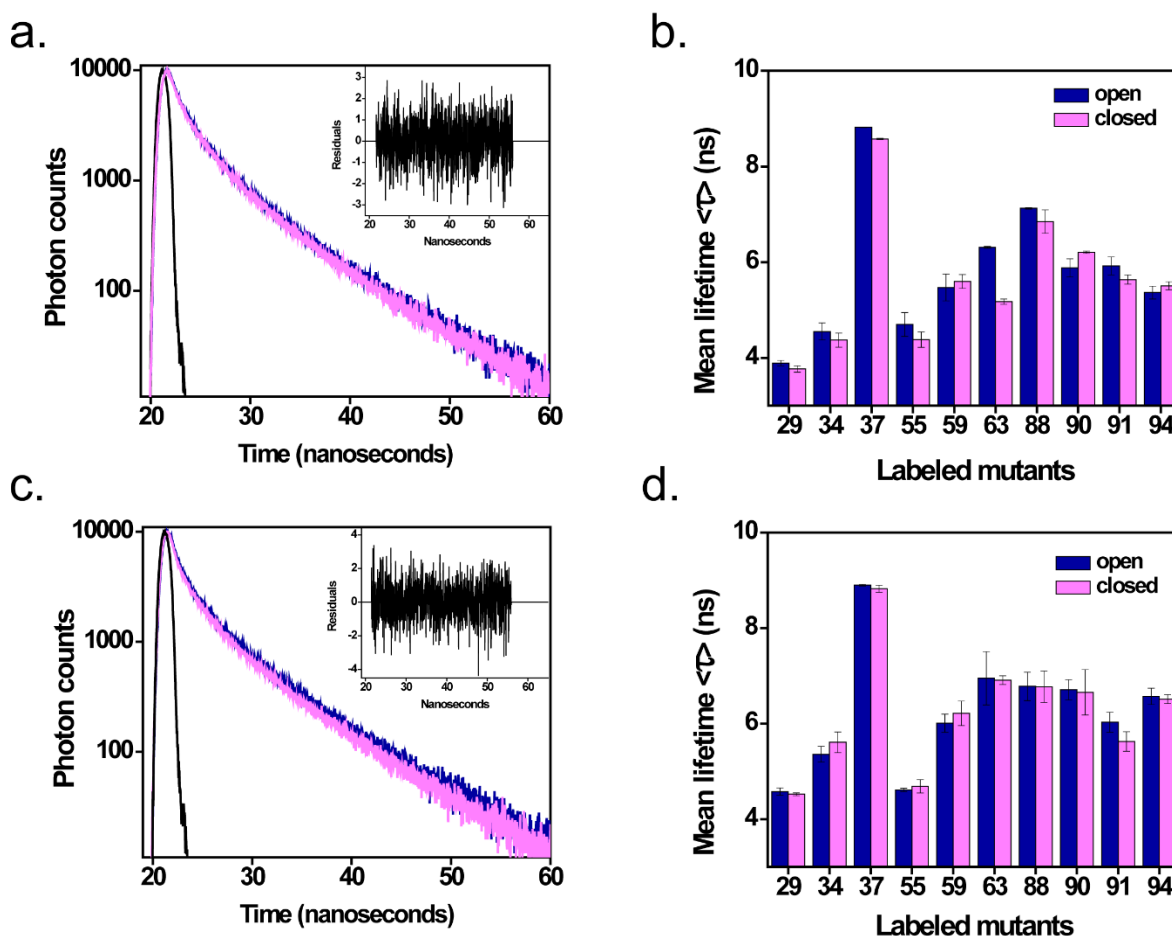


Fig. 5.3. Fluorescence lifetimes of NBD-labeled N-domain residues in micelles and membranes. Time-resolved fluorescence intensity decay of D91-NBD in the open state (blue) and closed state (magenta) in DDM micelles (a) and PC/PG membranes (c) is shown. Excitation

wavelength was 456 nm, and emission was monitored at 533 nm. The sharp peak on the left (black) is the lamp profile, and the relatively broad peak on the right is the decay profile (blue and magenta), fitted to a triexponential function. The plot in the inset shows the weighted residuals of the decay fit. Mean fluorescence lifetimes of NBD-labeled N-domain residues in the open and closed state in DDM micelles (b) and POPC/POPG membranes (d) are shown. Values represent mean \pm SE of three independent measurements. All other conditions are as in Fig. 5.2. See Chapter 2 and Table 5.1 for other details.

Table 5.1. Fluorescence lifetimes of NBD-labeled N-domain mutants of MgtE in different functional states

		α_1	τ_1	α_2	τ_2	α_3	τ_3	$\langle\tau\rangle(\text{ns})^a$
DDM micelles								
H29	Open	0.37	1.06	0.52	4.41	0.11	0.19	3.89
	Closed	0.37	1.07	0.51	4.32	0.12	0.19	3.79
L34	Open	0.40	1.36	0.47	4.96	0.13	0.31	4.22
	Closed	0.40	1.61	0.46	4.97	0.14	0.43	4.16
W37	Open	0.01	4.51	0.92	9.00	0.09	2.52	8.81
	Closed	0.08	2.87	0.88	8.80	0.03	1.17	8.59
A55	Open	0.37	2.1	0.47	6.09	0.16	0.6	5.12
	Closed	0.37	1.66	0.52	5.4	0.11	0.38	4.68
E59	Open	0.34	1.97	0.32	7.26	0.34	0.51	5.75
	Closed	0.36	1.68	0.39	6.56	0.25	0.42	5.45
H63	Open	0.40	2.57	0.37	7.91	0.23	0.64	6.33
	Closed	0.33	1.85	0.50	5.94	0.17	0.51	5.12
L88	Open	0.35	2.59	0.54	8.18	0.11	0.61	7.15
	Closed	0.34	2.57	0.55	8.29	0.10	0.61	7.30
L90	Open	0.35	1.91	0.43	6.90	0.21	4.62	5.69

	Closed	0.40	1.54	0.47	7.09	0.14	0.20	6.18
D91	Open	0.34	2.11	0.49	6.77	0.17	0.53	5.82
	Closed	0.35	1.54	0.51	6.14	0.13	0.22	5.42
A94	Open	0.37	3.02	0.41	6.52	0.22	1.09	5.23
	Closed	0.31	2.83	0.44	6.60	0.24	1.10	5.42
PC/PG membranes^b								
H29	Open	0.39	1.31	0.40	5.39	0.21	0.33	4.50
	Closed	0.40	1.33	0.39	5.42	0.21	0.29	4.50
L34	Open	0.32	1.41	0.52	5.73	0.16	0.34	5.09
	Closed	0.36	1.44	0.52	5.87	0.12	0.27	5.18
W37	Open	0.09	3.66	0.88	9.17	0.03	1.22	8.92
	Closed	0.25	5.76	0.69	9.66	0.06	1.38	8.90
A55	Open	0.36	1.35	0.46	5.29	0.18	0.28	4.56
	Closed	0.36	1.28	0.44	5.4	0.20	0.22	4.66
E59	Open	0.38	1.87	0.39	7.05	0.23	0.49	5.82
	Closed	0.34	2.32	0.35	7.46	0.31	0.66	5.96
H63	Open	0.41	1.8	0.42	7.56	0.17	0.32	6.39
	Closed	0.53	2.33	0.29	9.13	0.18	0.51	6.82
L88	Open	0.43	2.18	0.41	8.57	0.16	0.30	7.14
	Closed	0.41	1.99	0.48	7.89	0.11	0.27	6.80
L90	Open	0.43	2.06	0.41	8.30	0.16	0.35	6.92
	Closed	0.40	1.55	0.47	7.09	0.14	0.20	6.18
D91	Open	0.34	2.11	0.49	6.77	0.17	0.53	5.82
	Closed	0.35	1.54	0.51	6.14	0.13	0.22	5.42
A94	Open	0.26	1.77	0.55	7.02	0.19	0.24	6.40
	Closed	0.25	1.70	0.54	7.02	0.21	0.22	6.42

The concentration of protein was 3.2 μ M in all cases. The excitation wavelength was 456 nm and the emission was monitored at respective emission maximum. See Chapter 2 for other details.

^a*Mean fluorescence lifetime ($\langle\tau\rangle$) calculated using Eq. 7 in Chapter 2;*

^bThe ratio of NBD-labeled N-domain mutants /total lipid is 1:100.

5.2.3. Extent of water penetration for the interfacial N-domain residues

Potassium iodide (KI) is an efficient aqueous quencher of NBD fluorescence and has been widely used to monitor the topology of membrane proteins (Shepard et al., 1998; Kale et al., 2014). To explore the extent of water penetration of N-domain residues upon gating in micelles and membranes we used the aqueous quencher KI. Representative quenching results of L34-NBD upon gating in DDM micelles (Fig. 5.4a) and PC/PG membranes (Fig. 5.4d) as Stern-Volmer plots are shown. The slope (K_{SV}) obtained from such a plot is directly proportional to the extent of water accessibility of the NBD group to the aqueous phase. In other words, the higher the slope more is the degree of exposure to water assuming that there is not much difference in fluorescence lifetime. The K_{SV} values show a modest increase upon gating in micelles (Fig. 5.4b) and membranes (Fig. 5.4b). The intrinsic dependence of K_{SV} values on the fluorescence lifetime makes its interpretation complicated. Therefore, we have also calculated the bimolecular quenching constant (k_q) of the NBD-labeled N-domain residues in micelles (Fig. 5.4c) and membranes (Fig. 5.4f) upon gating which is an accurate measure of the degree of exposure since it takes into account the differences in lifetime. Our data show a modest increase in water accessibility upon gating in both micelles and membranes which is in excellent agreement with K_{SV} values supporting the fact that the N-domain is structurally preserved during gating. Considering the fact that complete aqueous exposure of NBD reports a k_q of $\sim 8 \text{ M}^{-1} \text{ ns}^{-1}$ (Crowley et al., 1993), the N-domain residues are considerably shielded from water exposure even in the open state supporting the fact that the N-domain shows a hydrophobic localization despite their cytoplasmic location. Together our quenching results support the fact that the

structural integrity of the Mg^{2+} -sensing N-domain is preserved during gating. This is in excellent agreement with our previous observation using site-specific Trp fluorescence of MgtE (see Chapter 4).

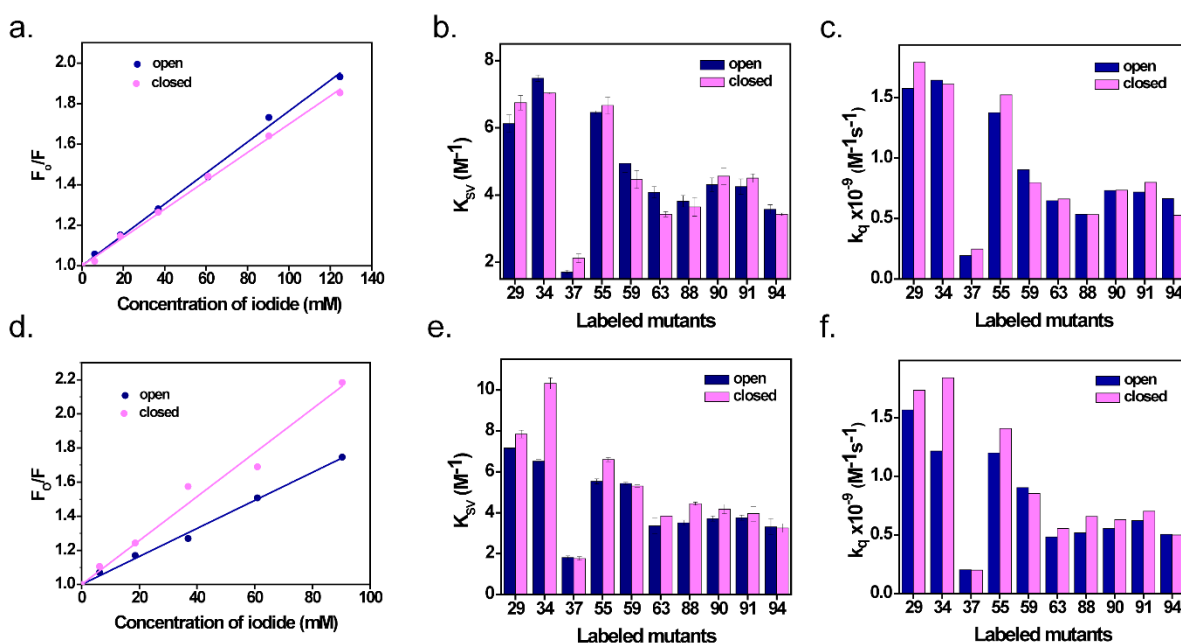


Fig. 5.4. Water accessibility probed by iodide quenching of fluorescence for NBD-labeled N-domain residues in membrane-mimetics. Shown are representative data for Stern-Volmer analysis of iodide quenching of L34-NBD in the open and closed states in micelles (a) and membranes (d), where F_0 is the fluorescence in the absence of quencher and F is the corrected fluorescence in the presence of quencher. Stern-Volmer constants (K_{SV}) in (b) micelles and (e) membranes and bimolecular quenching constants (k_q) in (c) micelles and (f) membranes for iodide quenching of NBD-labeled N-domain residues in the open and closed states of MgtE are shown, respectively. The K_{SV} values represent mean \pm SE of three independent measurements.

The excitation wavelength used was 465 nm, and the emission was monitored at the respective emission maximum. All other conditions are as in Fig. 5.2. See Chapter 2 for other details.

5.2.4. Rotational dynamics of NBD-labeled interfacial N-domain residues upon gating

Fluorescence anisotropy is a robust method to obtain information about the rotational flexibility/dynamics of a fluorophore and has been widely used to study the dynamic behavior of ion channels (Ho et al., 2013; Raghuraman et al., 2014). The fluorescence anisotropy values of the NBD-labeled N-domain interfacial residues are restricted in general in DDM micelles and PC/PG membranes (Fig. 5.5a and b, left panel). It can be easily appreciated that the changes in rotational dynamics of the N-domain residues is dependent on the functional states of MgtE both in micelles and membranes. This is not a surprise since the cytosolic domain, particularly, the N-domain acts as a Mg^{2+} -sensor and stabilizes the closed conformation of MgtE in the presence of high intracellular Mg^{2+} (Hattori et al., 2009). Interestingly, most of the N-domain residues show a restricted mobility upon gating in micelles and membranes suggesting a reduced flexibility of the N-domain residues in the presence of Mg^{2+} . Further, while most of the residues have high mobility in the open state in micelles (Fig. 5.5a, right panel), three residues (W37, H63, D91) have reduced mobility in the open state in membranes (Fig. 5.5b, right panel). This clearly suggests a differential dynamics of the N-domain residues in membranes compared to micelles and the presence of dynamic variability of the N-domain residues when MgtE is placed in a membrane environment.

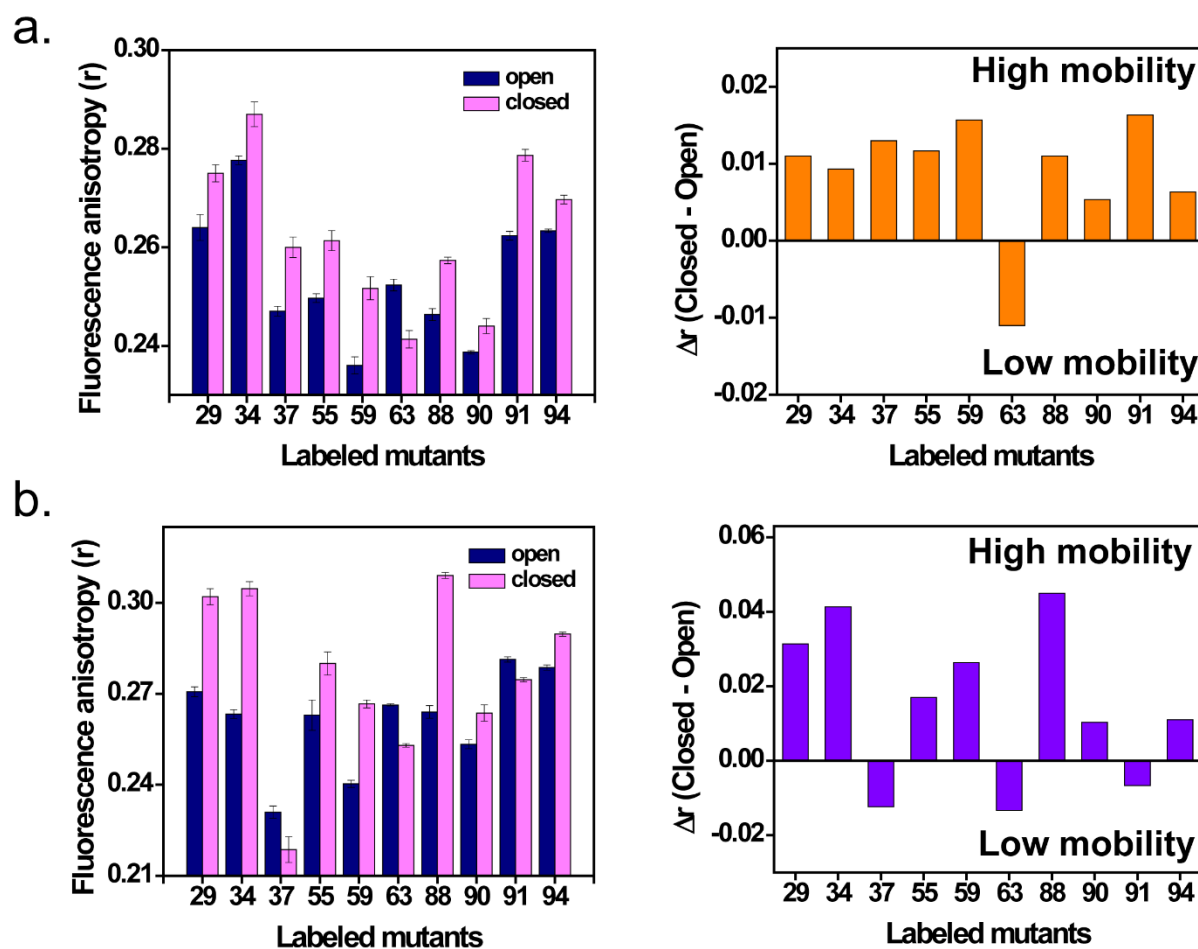


Fig. 5.5. Rotational mobility of MgtE N-domain residues upon gating in micelles and membranes. Steady-state anisotropy of NBD-labeled N-domain residues in the open (absence of Mg^{2+}) and closed (20 mM Mg^{2+}) states of MgtE in (a, left panel) DDM micelles and (b, left panel) reconstituted in POPC/POPG (3:1 mol/mol) liposomes at a protein/lipid molar ratio of 1:100. The excitation wavelength used was 465 nm; emission was monitored at their respective emission maxima in all case. Values represent mean \pm SE of three independent measurements. The difference in anisotropy values (Δr) between closed and open states in micelles (a, right panel) and membranes (b, right panel) is shown. The excitation wavelength used was 465 nm

and the concentration of MgtE was 3.2 μ M in all cases. All other conditions are as in Fig. 5.2. See Chapter 2 for other details.

To confirm that the anisotropy values of the interfacial N-domain residues do not suffer from any lifetime-induced artifacts, the apparent (average) rotational correlation times were calculated using Eq. 5 (Chapter 2). The gating-induced changes in apparent rotational correlation times for the NBD-labeled N-domain residues of MgtE in micelles (Fig. 5.6 top left) and membranes (Fig. 5.6 top right) are in excellent agreement with the anisotropy results. In the absence of Mg^{2+} , that is, upon channel opening, most of the N-domain residues undergo an increased mobility with a pronounced dynamic variability as seen by residues W37, H63, and D91, which undergo a restricted/decreased rotational dynamics in membranes (Fig. 5.6 middle right panel). On the contrary, unlike in membranes, in the micellar environment, the N-domain residues do not exhibit dynamic variability except for the NBD-labeled 37th residue which shows a restricted dynamics upon opening (Fig. 5.6 middle left panel). Mapping these differences in apparent rotation correlation times of the N-domain residues in micelles and membranes illustrates the differential dynamics of the ‘ Mg^{2+} -sensor’ N-domain of MgtE upon transition from the open to the closed state. Taken together, our data suggests an altered dynamics of the cytosolic N-domain in membranes compared to micelles and the importance of side-chain dynamics in the Mg^{2+} -induced gating mechanism of MgtE.

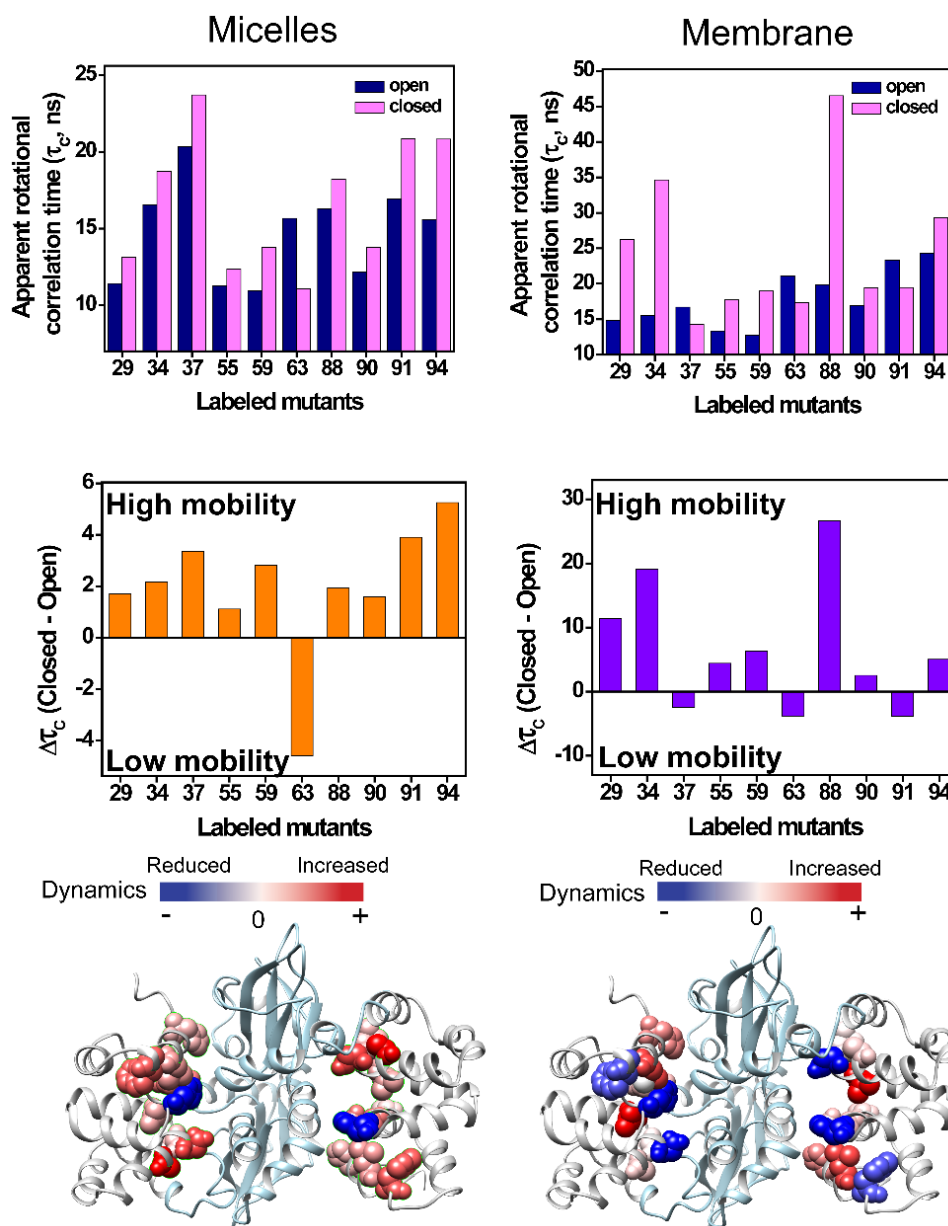


Fig. 5.6. Apparent rotational correlation times of NBD-labeled N-domain residues of MgtE in membrane-mimetics. Shown are the apparent rotational correlation times in the open and closed states of MgtE-Trp mutants in micelles (left panel) and membranes (left panel). The difference in apparent rotational correlation times ($\Delta\tau_c$) between closed and open states in micelles (middle left panel) and membranes (middle right panel) is shown. The $\Delta\tau_c$ values were

mapped on the crystal structure of MgtE (2ZY9) to highlight the changes in dynamics of the N-domain residues between the membrane-mimetics upon gating (bottom). All other conditions are as in Fig. 5.2. See Chapter 2 for other details.

5.2.5. Hydration dynamics of the NBD-labeled interfacial residues of the N-domain

As mentioned earlier (see Chapter 4, Section 4.2.6), REES is a widely used fluorescence approach to obtain important information on the relative rates of water relaxation dynamics and is sensitive to fluctuations in local hydration dynamics. The magnitude of REES, i.e., the total shift in emission maximum upon changing the excitation wavelength from 465 to 515 nm, for the NBD-labeled N-domain residues of MgtE in micelles and membranes is shown in Fig. 5.7. Interestingly, while most of the N-domain residues exhibit significant REES in micelles (Fig. 5.7a), they show low or negligible REES in membranes (Fig. 5.7b). This can be attributed to the fast solvation mechanism around and/or a rearrangement of amino acid side chains around these residues. Nevertheless, the reduced REES suggest an altered organization of the N-domain residues in membranes compared to micelles which has been shown previously for the sensor loop of KvAP (Das et al., 2020) and the TM-domain and N-domain Trp residues of MgtE (see Chapter 4). Importantly, the changes in hydration dynamics of the N-domain residues in micelles and membranes are not merely due to changes in polarity around the fluorophore as the emission maxima is similar upon gating (see Fig. 5.2b and e). Irrespective of the differences in magnitude of REES for the N-domain residues in micelles and membranes, upon gating the magnitude of REES decreases for most of the residues in micelles, particularly in membranes. This suggests a reduced hydration dynamics during Mg^{2+} -induced gating of MgtE. Taken together, our REES

data suggest a differential hydration dynamics of the N-domain residues at the interface of the N- and CBS-domain when MgtE shuttles from the open to the closed state.

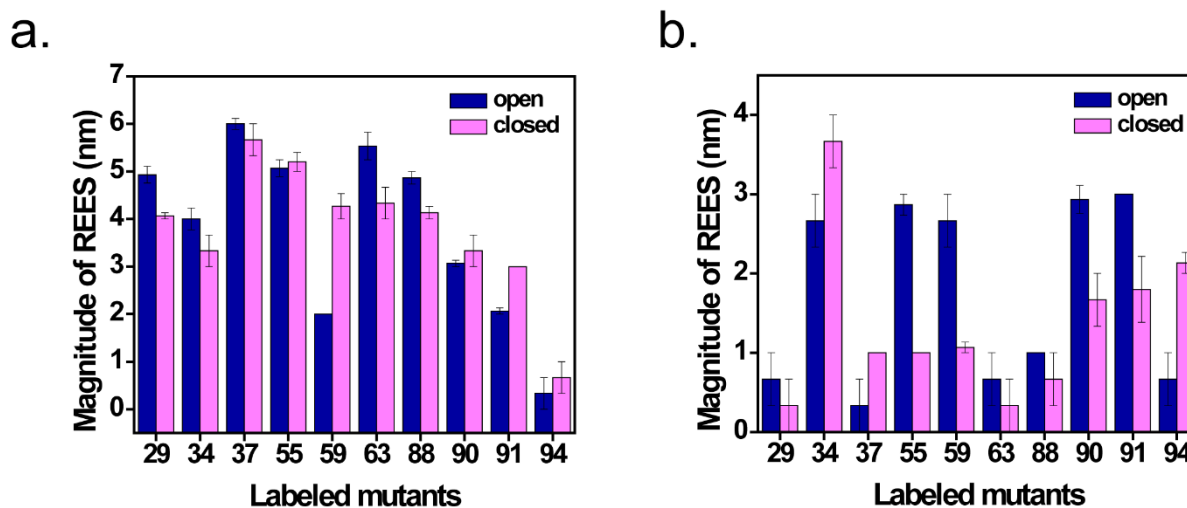


Fig. 5.7. REES of NBD-labeled N-domain residues of MgtE. The magnitude of REES of the NBD-labeled interfacial residues of the N-domain of MgtE in the open and closed state in (a) micelles and (b) membranes is shown. All other conditions are as in Fig. 5.2. See Chapter 2 for other details.

5.2.6. Gating-induced alteration of conformational heterogeneity of N-domain residues

Lifetime distribution analysis using the maximum entropy method (MEM) is a robust analysis tool to gain insights into the structural heterogeneity of a fluorophore since fluorescence lifetime distribution gives an ultrafast snapshot of the protein population distribution (Bechem and Brand, 1985; Krishnamoorthy, 2018). MEM lifetime distribution analysis is a powerful model-independent approach to resolve lifetime components and has been widely used to

monitor membrane heterogeneity (Mukherjee et al., 2007), side-chain heterogeneity in different membrane-mimetics (Das and Raghuraman, 2021; see Chapter 4) and functional states of membrane protein (see Chapter 4), and unfolding transitions in soluble proteins (Swaminathan et al., 1994; Lakshmikanth et al., 2001; Jha et al., 2009; Krishnamoorthy, 2018; Sternisha et al., 2020).

Representative MEM lifetime distributions of two NBD-labeled N-domain residues in the open and closed state in micelles (Fig. 5.8a, b) and membranes (Fig. 5.8d, e) is shown. Although, MEM analysis has been performed assuming the equal probability of the existence of lifetimes in the range of 0.1 to 100 ns logarithmically, no lifetime distributions beyond 10 ns was observed. The plots are shown in linear scale to appreciate the gating-induced change in conformational heterogeneity in different functional states. Generally, the number of peaks in the MEM profile is proportional to the number of discrete conformational states of the fluorophore while the peak areas reflect their relative populations, and the peak width is used to interpret the heterogeneity (Mukherjee et al., 2007; Krishnamoorthy, 2018). It is evident from the figure that while H29 and A55 have a broad distribution profile in micelles, they have a relatively sharp distribution in membranes upon gating, although the number of peaks essentially remains the same. In other words, upon transitioning from the open to the closed state the discrete nature of the lifetime distribution is lost in micelles while the trend is quite opposite in membranes for these two residues. Despite, altered heterogeneity, the fact that the lifetime distribution profiles do not drastically differ between the functional states, suggests that the structural integrity of the N-domain is preserved during gating.

To get more insight into the gating-induced change in conformational heterogeneity of MgtE N-domain residues in micelles and membranes, the full-width at half maximum (FWHM) of the MEM lifetime distribution has been used. We have considered the FWHM of the predominant lifetime peak of the N-domain residues in micelles and membranes in the 1-8 ns range considering the short lifetime (~ 1.5 ns) of NBD when it is fully exposed to aqueous medium (Raghuraman et al., 2019; Das and Raghuraman, 2021). Interestingly, majority of the N-domain residues show a reduced FWHM of the predominant peak lifetime distribution which is indicative of a reduced conformational heterogeneity upon gating in micelles (Fig. 5.8c) and membranes (Fig. 5.8f). This is in excellent agreement with the REES data which shows a reduced hydration dynamics and therefore reduced conformational substates upon gating (see Fig. 5.7). Overall, our MEM lifetime distribution analysis suggests altered conformational heterogeneity of the interfacial N-domain residues upon Mg^{2+} -induced gating.

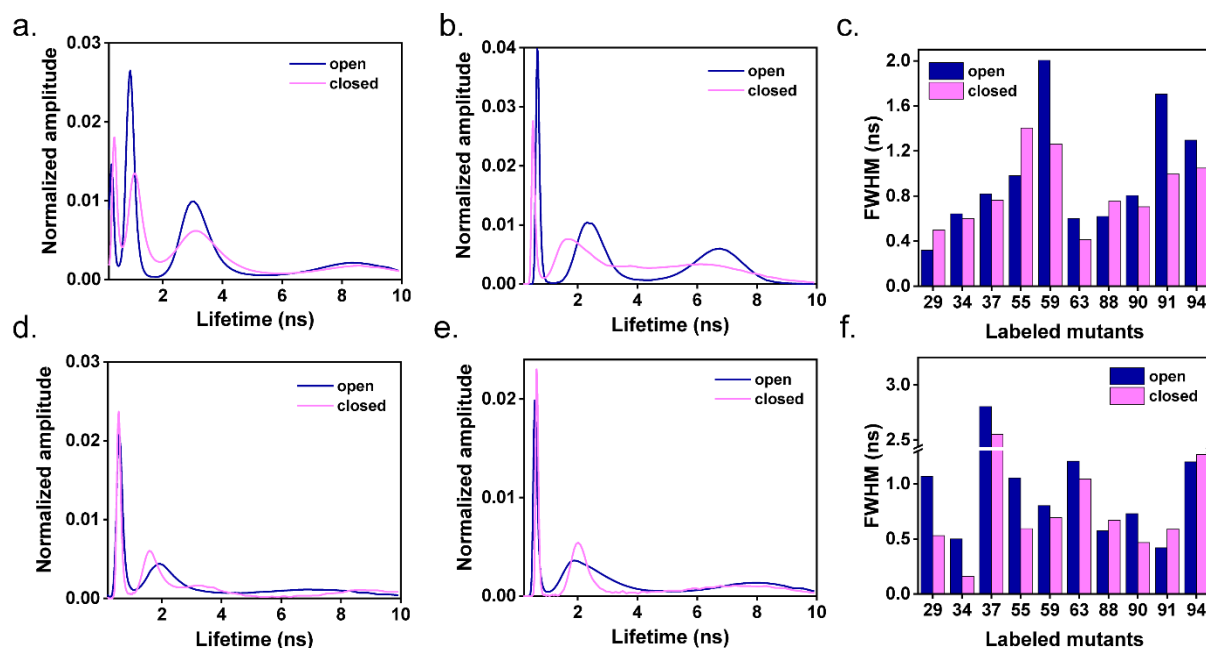


Fig. 5.8. Conformational heterogeneity of interfacial N-domain residues of MgtE during gating in micelles and membranes. MEM fluorescence lifetime distributions NBD-labeled N-domain residues, (a) H29 (b) A55 in micelles and (d) H29 and (e) A55 in membranes is shown. The normalized probability amplitudes are plotted against their corresponding lifetime on a linear scale. Full width at half maximum (FWHM) for the predominant peak of NBD lifetime distribution for the labeled N-domain residues in (c) micelles and (f) membranes were calculated from corrected lifetime amplitude of MEM distributions. All other conditions are as in Fig. 5.2. See Chapter 2 for details.

5.2.7. Probing small-scale conformational changes in N-domain residues using Tryptophan-induced quenching (TrIQ)

One of the most widely used site-directed fluorescence methods to study distance changes within protein is Förster resonance energy transfer (FRET) (Stryer, 1978; Blackman et al., 1998; Cha et al., 1999; Taraska, 2012; Raghuraman et al., 2019). However, FRET studies are not suitable for measuring small intra-subunit conformational changes since most FRET pairs are relatively large and generally require a 100% labeling efficiency. Therefore, FRET is suitable for measuring long-distance conformational changes ($\sim 20 - 100 \text{ \AA}$). Recently, Farrens lab has developed a technique, namely, Tryptophan-induced quenching (TrIQ), to measure small-scale intra-subunit conformational changes (Mansoor et al., 2002, 2010). This technique exploits the phenomenon of tryptophan to quench the emission intensity of certain fluorophores by photo-induced electron transfer (PET) (Callis, 2014). Although, both PET and FRET can report changes in fluorescence intensity depending on the presence of a quencher in a distance-dependent manner, unlike FRET, PET requires the electron donating moiety (in this case, Trp) in

van der Waal contact for efficient quenching (Doose et al., 2009). A popular acceptor probe for the TrIQ approach is bimane, which can efficiently report changes in intra-subunit distances within ~ 10 Å (Mansoor et al., 2010).

We have systematically chosen four N-domain residues (H29, L34, E59, and H63) which are from ~ 5 Å to ~ 13 Å (C_{α} - C_{α}) from the native Trp, W37 (Fig. 5.9b) and each of the cysteine substituted residues were labeled with mBBr in the presence of Trp or in the absence of Trp, that is, the respective Trp has been mutated to Phe (W37F), which served as control where no quenching would occur. Representative scans of H29 and L34 labeled with bimane in the presence or absence of W37 (W37F) in the open or closed state in micelles and membranes is shown in Fig. 5.9a. Distance-dependent quenching information can be obtained by mapping the ratio of fluorescence intensity between the fluorescence intensity of bimane in the absence of Trp (F_o) and in the presence of Trp (F_w). Interestingly, in the open state, the F_o/F_w of L34 corresponds to a C_{α} - C_{α} distances of ~ 6.5 Å from W37 in DDM micelles (Fig. 5.9c) while ~ 8.5 Å in PC/PG membranes (Fig. 5.9d) indicating an altered intra-subunit organization of the N-domain in membranes compared to micelles. Importantly, the changes in intra-subunit C_{α} - C_{α} distances upon gating is modest as observed from nominal changes in the F_o/F_w ratio and therefore conclusively prove the fact that the N-domain is structurally preserved during gating.

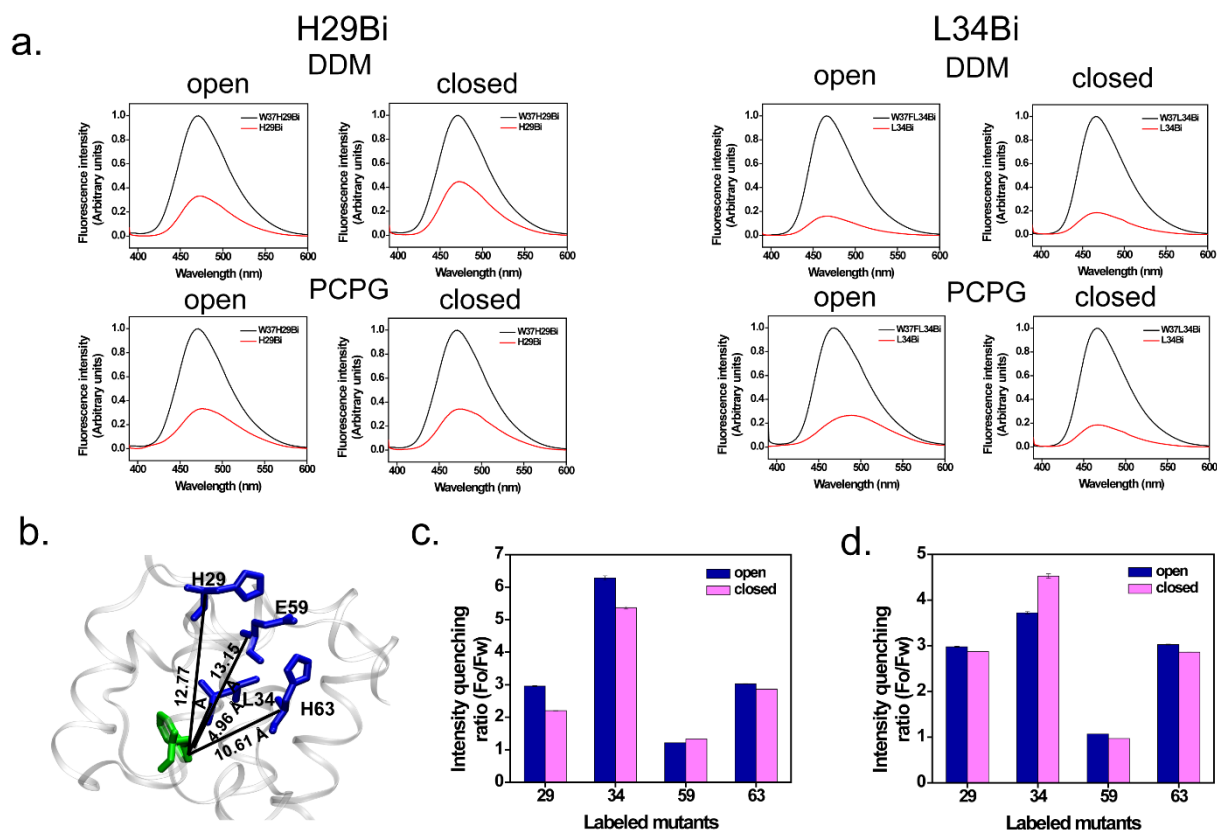


Fig. 5.9. Tryptophan-induced quenching of MgtE N-domain residues. (a) Representative fluorescence emission spectra of mBBr labeled H29 and L34 (red lines) residues with their respective Trp-less (black lines, W37 lacking mutants/W37F) mutants in the open and closed states in micelles and membranes are shown. For comparison between data, the spectra from each site/probe combination were normalized to the intensity of the Trp-less mutant. For each site/probe combination, the fluorophores' concentration was matched (for samples with and without the Trp). (b) The C_{α} - C_{α} distances between W37 and the N-domain residues is shown. Ratio of fluorescence quenching intensity in the absence (F_o) or presence (F_w) of W37 in the open and closed state for the N-domain mutants in micelles (c) and membranes (d) are shown. All other conditions are as in Fig. 5.2. See Chapter 2 for other details.

5.3. Discussion

Membrane proteins form one-third of the proteins produced by genomes of lower and higher organisms (Wallin and Heijne, 1998; Fagerberg et al., 2010) and their malfunction is associated with diseases like neurodegenerative diseases, cancer, heart disease, etc. Importantly, about two-thirds of approved drugs target membrane proteins (Terstappen and Reggiani, 2001; Yildirim et al., 2007; Bakheet and Doig, 2009; Bull and Doig, 2015) and therefore structural and functional studies of membrane proteins assumes importance. Ion channels are a special class of membrane proteins that allows electrically charged ions to pass through an otherwise hydrophobic membrane interior by providing a ‘hydrophilic tunnel’ along their electrochemical gradient. Consequently, ion channels form the fulcrum of important physiological functions like nerve impulse conduction in electrically excitable cells and maintaining osmotic balance, ion transport, etc. in non-excitable cells. While initially ion channels were thought of as passive conduits through which charged molecules (ions) can pass through without having to overcome a large energy barrier associated with crossing a hydrophobic membrane (Parsegian, 1968), later ion channels were found to have complex regulatory and gating mechanisms to have an extra layer of control to the passage of ions through them other than the selectivity filter (Gadsby, 2009). Some examples include the N-type inactivation of voltage-gated potassium channels (Kurata and Fedida, 2005), modulation of voltage-gated sodium channels by phosphorylation (Scheuer, 2011), ligand induced-gating in pentameric ligand-gated ion channels (pLGICs) (Lara et al., 2020), and Mg^{2+} -induced gating in MgtE (Hattori et al., 2009) and CorA (Payandeh and Pai, 2006). Therefore, the study of the gating-induced regulation and the associated structural dynamics of the regulatory domains of such ion channels is important.

Although magnesium is the most abundant divalent cation present in cells, being important for many cellular functions (Hartwig, 2001; Selmer et al., 2006), the transport and regulation of Mg^{2+} is not well understood. The present understanding of the Mg^{2+} transport mechanisms comes from studies on the CorA and MgtE groups of prokaryotic ion channels (Moomaw and Maguire, 2008; Payandeh et al., 2013). Interestingly, although CorA and MgtE have similar gating mechanisms, they have different architectures. In fact, unlike Na^+ or K^+ ion channels which have a conserved architecture throughout all domains of life, different families of Mg^{2+} transporters vary greatly in their regulation and subunit arrangements (Payandeh et al., 2013). Therefore, the study of the structural and functional principles governing the regulation and transport of Mg^{2+} is important. Interestingly, the mammalian SLC41A1 transporter is a distant ortholog of MgtE from *Thermus thermophilus* (Wabakken et al., 2003) and can functionally compensate Mg^{2+} transporter-deficient vertebrate B-cells (Sahni et al., 2012). Further, MgtE in *P. aeruginosa* functions not only as a Mg^{2+} transporter but also as a virulence modulator, therefore making it a potential drug target (Coffey et al., 2014). Since, Mg^{2+} transport mechanisms of MgtE across membranes is less understood due to the lack of structural data of full-length MgtE in other functional states, the study of structural dynamics of MgtE during gating assumes significance.

High-resolution structural information of MgtE combined with electrophysiology data has shown the importance of the cytoplasmic domain as a Mg^{2+} sensor and a gating modulator (Hattori et al., 2009). Importantly, deletion of the N-domain, keeping the CBS domain intact, has been shown to reduce the Mg^{2+} -dependent suppression of Mg^{2+} -influx. Therefore, the cytoplasmic CBS domain alone cannot regulate Mg^{2+} -dependent negative regulation of MgtE, conferring the N-domain to be a Mg^{2+} -sensor and regulator, stabilizing the closed state of MgtE in the presence

of high intracellular Mg^{2+} . NMR studies in detergent micelles have shown that in presence of high Mg^{2+} ($> 5mM$), both the cytoplasmic domains as well as the transmembrane TM-domain undergo Mg^{2+} -dependent changes (Maruyama et al., 2018). Interestingly, previous work from our lab, using site-specific Trp fluorescence of MgtE single-Trp mutants utilizing the fluorescence of native Trps in micelles and membranes, has shown that Mg^{2+} -dependent changes not only are restricted to the N-domain but are also translated to the TM-domain (see Chapter 4). Taking into account both these studies, it can be said that MgtE undergoes a ‘conformational wave’ from the N-domain to the TM-domain which helps in gating the channel. Hence, Mg^{2+} -sensing forms a crucial part of gating and therefore it is important to study the structural dynamics of the Mg^{2+} -sensor N-domain during Mg^{2+} -induced gating.

To understand the gating-related structural dynamics of the Mg^{2+} -sensor N-domain we have systematically constructed single-cysteine mutants of the N-domain residues around the Mg^{2+} - binding sites at the interface of the N- and the CBS domains. We have labeled these residues with the thiol-reactive environment-sensitive fluorophore NBD. We have utilized various sophisticated fluorescence approaches to obtain site-directed information on the gating-induced changes in the interfacial N-domain residues in both micelles and membranes. Our results using the NBD-labeled residues clearly show gating-related changes of the N-domain residues in both micelles and membranes. In the presence of Mg^{2+} , the rotational dynamics/motional flexibility of the interfacial N-domain residues significantly reduces (see Fig. 5.6) suggesting a more compact form of the N-domain upon gating. This is in well agreement with the crystallographic snapshots (Hattori et al., 2007) and the simulation (Ishitani et al., 2008) studies on the cytosolic domain of MgtE which becomes flexible and unlocked in the absence of Mg^{2+} while it acts like a clamp locking the CBS domains to prevent further Mg^{2+} entry in the

presence of high concentrations of Mg^{2+} . This is accompanied with a reduction in the hydration dynamics upon gating due to reduction in the ratio of restricted to bound water molecules. Importantly, the functional correlation between the hydration dynamics and channel activity is well-established in different functional states of K^+ channels (Raghuraman et al., 2014; Kratochvil et al., 2016). Therefore, these observed changes in hydration dynamics can be attributed to the gating and permeation mechanism of MgtE which was also observed in our previous work using site-specific Trp fluorescence (see Chapter 4).

Further, our MEM lifetime distribution data clearly indicates a reduced heterogeneity of the N-domain residues upon gating (Fig. 5.8) which suggest that while the N-domain fluctuates between various conformations in the absence of Mg^{2+} , the presence of Mg^{2+} stabilizes predominantly a single closed conformation of the N-domain which is well correlated with our anisotropy data which shows a reduced flexibility of the N-domain residues upon gating. This is supported by the observation that high-speed AFM imaging of MgtE shows a jagged topography of the N-domain which can be attributed to the constant fluctuations of the cytosolic domains in the absence of Mg^{2+} (Haruyama et al., 2019). Utilizing the novel TriQ method and supported by the collisional quenching data we demonstrate that the structural integrity of the N-domain is preserved during gating. Overall, our results highlight the importance of the gating-related structural changes of the Mg^{2+} -sensor, N-domain, of MgtE and is relevant to understand the transport and regulation mechanism of Mg^{2+} channels in general, MgtE in particular.

Abbreviations

ADP:	adenosine diphosphate
ATP:	adenosine triphosphate
BSA:	bovine serum albumin
CBS:	cystathione- β -synthase
CD:	circular dichroism
CMC:	critical micelle concentration
CNNM:	cyclin M
Cryo-EM:	cryo-electron microscopy
DDM:	n-dodecyl- β -D-maltopyranoside
DM:	n-decyl- β -D-maltopyranoside
DTT:	dithiothreitol
GTP:	guanosine triphosphate
HEPES:	hydroxyethylpiperazine ethane sulfonic acid
IPTG:	isopropyl β -D-1-thiogalactopyranoside
LCP:	lipidic cubic phase
MagT1:	magnesium transporter 1
MEM:	maximum entropy method
mBBr:	monobromobimane
NBD:	7 -nitrobenz-2-oxa-1,3,-diazol-4-yl
NMDG-Cl:	N-methyl-D-glucamine chloride
NMR:	nuclear magnetic resonance
NTM:	n-nonyl- β -D-thiomaltopyranoside

OG:	n-octyl- β -D-glucopyranoside
PBS:	phosphate buffered saline
PDB:	protein data bank
pLGIC:	pentameric ligand-gated ion channels
PMAL-C8:	poly (maleic anhydride-alt-1-decene) substituted with 3-(dimethylamino) propylamine
POPC:	1-palmitoyl-2-oleoyl- <i>sn</i> -glycero-3-phosphocholine
POPG:	1-palmitoyl-2-oleoyl- <i>sn</i> -glycero-3-phospho-(1'-rac-glycerol)
PRE:	paramagnetic relaxation enhancement
PVDF:	polyvinylidene difluoride
REES:	red edge excitation shift;
SDS-PAGE:	sodium dodecyl sulfate-polyacrylamide gel electrophoresis
SEC:	size exclusion chromatography
SLC:	solute carrier
STIM:	stromal interaction molecule
TCSPC:	time-correlated single photon counting
TRPM:	transient receptor potential melastatin
TrIQ:	tryptophan-induced quenching
Trp:	tryptophan
VMD	visual molecular dynamics

References

- Akashi, H., and Gojobori, T. (2002). Metabolic efficiency and amino acid composition in the proteomes of *Escherichia coli* and *Bacillus subtilis*. *Proc. Natl. Acad. Sci. U. S. A.* 99, 3695-3700.
- Alam, A., and Jiang, Y. (2009). High resolution structure of the open NaK channel. *Nat. Struct. Mol. Biol.* 16, 30-34.
- Alam, M. S., Siddiq, A. M., and Mandal, A.B. (2015). The micellization and clouding of nonionic surfactant, poly(ethylene glycol) t-octylphenyl ether (Triton X-100): Effect of halide ions of (sodium salt) electrolytes. *J. Disper. Sci. Technol.* 37, 1385-1394.
- Alberts, B., Johnson, A., Lewis, J., Roberts, K., Raff, M., and Walter, P. (2008). *Molecular biology of the cell*. 5th Ed., Garland science, New York.
- Alexander, R. T., Hoenderop, J. G., and Bindels R. J. (2008). Molecular determinants of magnesium homeostasis: insights from human disease, *J. Am. Soc. Nephrol.* 19, 1451–1458.
- Anderson, G. G., Yahr, T. L., Lovewell, R. R., and O'Toole, G. A. (2010). The *Pseudomonas aeruginosa* magnesium transporter MgtE inhibits transcription of the type III secretion system. *Infect. Immun.* 78, 1239-1249.
- Arachea, B. T., Sun, Z., Potente, N., Malik, R., Isailovic, D., and Viola, R. E. (2012). Detergent selection for enhanced extraction of membrane proteins. *Protein Exp. Purif.* 86, 12-20.
- Aron, L., Toth, C., Godfrey, H. P., and Cabello, F. C. (1996). Identification and mapping of a chromosomal gene cluster of *Borrelia burgdorferi* containing genes expressed in vivo. *FEMS Microbiol. Lett.* 145, 309-314.

- Assou, S., Cerecedo, D., Tondeur, S., Pantesco, V., Hovatta, O., Klein, B., Hamamah, S., and de Vos, J. (2009). A gene expression signature shared by human mature oocytes and embryonic stem cells. *BMC genomics* 10, 10.
- Bakheet, T. M., and Doig, A. J. (2009). Properties and identification of human protein drug targets. *Bioinformatics* 25, 451-457.
- Banerjee, P. (1999). Triton X-100 and X-114, In *The Encyclopedia of Molecular Biology*, (Creighton, T. E., Ed.), pp. 4655-4656, John Wiley, New York.
- Bayburt, T. H., and Sligar, S. G. (2010). Membrane protein assembly into nanodiscs. *FEBS Lett.* 1721-1721.
- Beechem, J. M., and Brand, L. (1985). Time-resolved fluorescence of proteins. *Annu. Rev. Biochem.* 54, 43-71.
- Bennetts, B., Rychkov, G. Y., Ng, H. -L., Morton, C. J., Stapleton, D., Parker, M. W., and Cromer, B. A. (2005). Cytoplasmic ATP-sensing domains regulate gating of skeletal muscle ClC-1 chloride channels. *J. Biol. Chem.* 280, 32452-32458.
- Berezin, M. Y., and Achilefu, S. (2010). Fluorescence lifetime measurements and biological imaging. *Chem. Rev.* 110, 2641-2684.
- Berneche, S., and Roux, B. (2003). A microscopic view of ion conduction through the K⁺ channel. *Proc. Nat. Acad. USA* 100, 8644-8648.
- Biswas, G., Ghosh, S., Raghuraman, H., and Banerjee, R. (2020). Probing conformational transitions of PIN1 from L. major during chemical and thermal denaturation. *Int. J. Biol. Macromol.* 154, 904-915.
- Blackman, S. M., Piston, D. W., and Beth, A. H. (1998). Oligomeric state of human erythrocyte band 3 measured by fluorescence resonance energy homotransfer. *Biophys. J.* 75, 1117-1130.

- Blommaert, E., Péanne, R., Cherepanova, N. A., Rymen, D., Staels, F., Jaeken, J., Race, V., Keldermans, L., Souche, E., Corveleyn A., Sparkes, R., Bhattacharya, K., Devalck, C., Schrijvers, R., Foulquier, F., Gilmore, R., and Matthijs, G. (2018). Mutations in *MAGT1* lead to a glycosylation disorder with a variable phenotype. *Proc. Natl. Acad. Sci. U.S.A* 116, 9865-9870.
- Boscardin, E., Alijevic, O., Hummler, E., Frateschi, S., and Kellenberger, S. (2016). The function and regulation of acid-sensing ion channels (ASICs) and the epithelial Na⁺ channel (ENaC): IUPHAR Review 19. *Br. J. Pharmacol.* 173, 2671-2701.
- Brahma, R., and Raghuraman, H. (2021). Novel insights in linking solvent relaxation dynamics and protein conformations utilizing red edge excitation shift approach. *Emerg. Top. Life Sc.* 5, 89-101.
- Brito, R. M. M., and Vaz, W. L. C. (1986). Determination of the critical micelle concentration of surfactants using the fluorescent probe *N*-phenyl-1-naphthylamine. *Anal. Biochem.* 152, 250-255.
- Brochon, J. C. (1994). Maximum entropy method of data analysis in time-resolved spectroscopy. *Methods Enzymol.* 240, 262-311.
- Brown, D. A., and London, E. (1998). Functions of lipid rafts in biological membranes. *Annu. Rev. Cell Dev. Biol.* 14, 111-136.
- Bui, D. M., Gregan, J., Jarosch, E., Ragnini, A., and Schweyen, R. J. (1999). The bacterial magnesium transporter CorA can functionally substitute for its putative homologue Mrs2p in the yeast inner mitochondrial membrane. *J. Biol. Chem.* 274, 20438-20443.
- Bull, S. C., and Doig, A. J. (2015). Properties of protein drug target classes. *PLoS One* 10, e0117955.

- Callis, P. R. (2014). Binding phenomena and fluorescence quenching. II: photophysics of aromatic residues and dependence of fluorescence spectra on protein conformation. *J. Mol. Struct.* 1077, 22-29.
- Carpenter, E.P., Beis, K., Cameron, A. D., and Iwata, S. (2008). Overcoming the challenges of membrane protein crystallography. *Curr. Opin. Struct. Biol.* 18, 581-586.
- Catici, D. A. M., Amos, H. E., Yang, Y., van del Elsen, J. M. H., and Pudney, C. R. (2016). The red edge excitation shift phenomenon can be used to unmask protein structural ensembles: implications for NEMO-ubiquitin interactions. *FEBS J.* 283, 2272-2284.
- Catterall, W. A. (2010). Ion channel voltage sensors: structure, function, and pathophysiology. *Neuron* 67, 915-928.
- Catterall, W. A. (2000). Structure and regulation of voltage-gated Ca²⁺ channels. *Annu. Rev. Cell Dev. Biol.* 16, 521-555.
- Cha, A., Snyder, G. E., Selvin, P. R., and Bezanilla, F. (1999). Atomic scale movement of the voltage-sensing region in a potassium channel measured via spectroscopy. *Nature* 402, 809-813.
- Chakrapani, S., Cordero-Morales, J.F., and Perozo, E. (2007). A quantitative description of KcsA gating II: Single-channel currents. *J. Gen. Physiol.* 130: 479-496.
- Chattopadhyay, A., and Haldar, S. (2014). Dynamic insight into protein structure utilizing red edge excitation shift. *Acc. Chem. Res.* 47, 12-19.
- Chattopadhyay, A., and Raghuraman, H. (2004). Application of fluorescence spectroscopy to membrane protein structure and dynamics. *Curr. Sci.* 87, 175-180.
- Chattopadhyay, A., Mukherjee, S., and Raghuraman, H. (2002). Reverse micellar organization and dynamics: A wavelength-selective fluorescence approach. *J. Phys. Chem. B* 106, 13002-13009.

- Cho, H., Stanzione, F., Oak, A., Kim, G. H., Yerneni, S., Qi, L., Sum, A. K., and Chan, C. (2019). Intrinsic structural features of the human IRE1a transmembrane domain sense membrane lipid saturation. *Cell Rep.* 27, 307-320.
- Chothia, C. (1976). The nature of the accessible and buried surfaces in proteins. *J. Mol. Biol.* 105, 1-12.
- Clapham, D. E. (2003). TRP channels as cellular sensors. *Nature* 426, 517-524.
- Coffey, B. M., Akhand, S. S., and Anderson, G. G. (2014). MgtE is a dual-function protein in *Pseudomonas aeruginosa*. *Microbiology* 160, 1200-1213.
- Coste, B., Mathur, J., Schmidt, M., Earley, T.J., Ranade, S., Petrus, M.J., Dubin, A.E., and Patapoutian, A. (2010). Piezo1 and Piezo2 are essential components of distinct mechanically activated cation channels. *Science* 330, 55-60.
- Craven, K. B., and Zagotta, W. N. (2006). CNG and HCN channels: two peas, one pod. *Annu. Rev. Physiol.* 68, 375-401.
- Cromie, M. J., Shi, Y., Latifi, T., and Groisman, E. A. (2006). An RNA sensor for intracellular Mg^{2+} . *Cell* 125, 71-84.
- Crowley, K. S., Reinhart, G. D., and Johnson, A. E. (1993). The signal sequence moves through a ribosomal tunnel into a noncytoplasmic aqueous environment at the ER membrane early in translocation. *Cell* 73, 1101-1115.
- Cuello, L. G., Cortes, D. M., Jogini, V., Sompornpisut, A., and Perozo, E. (2010). A molecular mechanism for proton-dependent gating in KcsA. *FEBS Lett.* 584, 1126-1132.
- Cuello, L. G., Jogini, V., Cortes, D. M., and Peorzo, E. (2010). Structural mechanism of C-type inactivation in K^+ channels. *Nature* 466, 203-208.

- Dalmas, O., Sompornpisut, P., Bezanilla, F., and Perozo, E. (2014). Molecular mechanisms of Mg^{2+} -dependent gating in CorA. *Nat. Commun.* 5, 3590.
- Dann, C. E., Wakeman, C. A., Sieling, C. L., Baker, S. C., Irnov, I., and Winkler, W. C. (2007). Structure and mechanism of a metal-sensing regulatory RNA. *Cell* 130, 878-892.
- Das, A., and Raghuraman., H. (2021). Conformational heterogeneity of the voltage sensor loop of KvAP in micelles and membranes: A fluorescence approach. *Biochim. Biophys. Acta – Biomembranes* 1863, 183568.
- Das, A., Chatterjee, S., and Raghuraman, H. (2020). Structural dynamics of the paddle motif loop in the activated conformation of KvAP voltage sensor. *Biophys. J.* 118, 873-884.
- de Baaij, J. H. F., Hoenderop, J. G. J., and Bindels, R. J. M. (2015). Magnesium in man: implications for health and disease. *Physiol. Rev.* 95, 1-46.
- de Baaij, J. H., Groot Koerkamp, M. J., Lavrijsen, M., van Zeeland, F., Meijer, H., Holstege, F. C., Bindels, R. J., and Hoenderop, J. G. (2013). Elucidation of the distal convoluted tubule transcriptome identifies new candidate genes involved in renal magnesium handling. *Am. J. Physiol. Renal Physiol.* 305, F1563-F1573.
- de Jesus, A. J., and Allen, T. W. (2013). The determinants of hydrophobic mismatch for transmembrane helices. *Biochim. Biophys. Acta* 1828, 851-863.
- de Rouffignac, C., and Quamme, G. (1994). Renal magnesium handling and its hormonal control. *Physiol. Rev.* 74, 305-322.
- Demchenko, A. P. (2008). Site-selective red-edge effects. *Methods Enzymol.* 450, 59-78.
- Demmers, J. A. A., van Duijn, E., Haverkamp, J., Greathouse, D. V., Koeppe, R. E. I. I., Heck, A. J. R., and Killian, J. A. (2001). Interfacial positioning and stability of transmembrane peptides

- in lipid bilayers studied by combining hydrogen/deuterium exchange and mass spectrometry. *J Biol. Chem.* 276, 34501-34508.
- Dieckmann, R., Pavela-Vrancic, M., Von Dohren, H., and Kleinkauf, H. (1999). Probing the domain structure and ligand-induced conformational changes by limited proteolysis of tyrocidine synthetase 1. *J. Mol. Biol.* 288, 129-140.
- Doose, S., Neuweiler, H., and Sauer, M. (2009). Fluorescence quenching by photoinduced electron transfer: a reporter for conformational dynamics of macromolecules. *Chem. Phys. Chem.* 10, 1389-1398.
- Doyle, D. A., Morais-Cabral, J., Pfuetzner, R. A., Kuo, A., Gulbis, J. M., Cohen, S. L., Chait, B. T., and MacKinnon, R. (1998). The structure of the potassium channel: molecular basis of K⁺ conduction and selectivity. *Science* 280, 69-77.
- Eftink, M. R. (1991a) Topics in Fluorescence Spectroscopy, (Lakowicz J. R., Ed.), pp. 53-126, Plenum Press, New York.
- Eftink, M. R. (1991b). Fluorescence techniques for studying protein structure. *Methods Biochem. Anal.* 35, 127-205.
- Eftink, M. R., Selvidge, L. A., Callis, P. R., and Rehms, A. A. (1990). Photophysics of indole derivatives: experimental resolution of La and Lb transitions and comparison with theory. *J. Phys. Chem.* 94, 3469-3479.
- Eilers, M., Patel, A. B., Liu, W., and Smith, S.O. (2002). Comparison of helix interactions in membrane and soluble α -bundle proteins. *Biophys. J.* 82, 2720-2736.
- Elberon, B.W., Whisenant, T.E., Cortes, D.M., and Cuello, L.G. (2017). A cost-effective protocol for the over-expression and purification of fully-functional and more stable *Erwinia chrysanthemi* ligand-gated ion channel. *Protein Exp. Purif.* 133, 177-186.

- Encinar, J. A., Molina, M. L., Poveda, J. A., Barrera, F. N., Renart, M. L., Fernandez, A. M., and Gonzalez-Ros, J. M. (2005). The influence of a membrane environment on the structure and stability of a prokaryotic potassium channel, KcsA. *FEBS Lett.* 579, 5199-5204.
- Engelborghs, Y. (2003). Correlating protein structure and protein fluorescence. *J. Fluoresc.* 13, 9-16.
- Eshaghi, S., Niegowski, D., Kohl, A., Martinez, M., Lesley, S. A., and Nordlund, P. (2006). Crystal structure of a divalent metal ion transporter CorA at 2.9 angstrom resolution. *Science* 313, 354-357.
- Fagerberg, L., Jonasson, K., Von Heijne, G., Uhlen, M., and Berglund, L. (2010). Prediction of the human membrane proteome. *Proteomics* 10, 1141-1149.
- Feroz, H., Kwon, H., Peng, J., Oh, H., Ferlez, B., Bakes, C.S., Golbeck, J. H., Bazan, G. C., Zydney, A. L., and Kumar, M. (2018). Improving the extraction and post-purification concentration of membrane proteins. *Analyst* 143, 1378-1386.
- Fery-Forgues, S., Fayet, J. -P., and Lopez, A. J. (1993). Drastic changes in the fluorescence properties of NBD probes with the polarity of the medium: involvement of a TICT state? *J. Photochem. Photobiol. A* 70, 229-243.
- Fiserova, E., and Kubala, M. (2012). Mean fluorescence lifetime and its error. *J. Lumin.* 132, 2059-2064.
- Fontana, A., De Laureto, P. P., Spolaore, B., Frare, E., Picotti, P., and Zambonin, M. (2004). Probing protein structure by limited proteolysis. *Acta Biochim. Pol.* 51, 299-321.
- Frey, L., Lakomek, N. -A., Riek, R., and Bibow, S. (2017). Micelles, bicelles and nanodiscs: Comparing the impact of membrane mimetics on membrane protein backbone dynamics. *Angew. Chem. Int. Ed.* 56, 380-383.

- Fu, D., Libson, A., Miercke, L. J., Weitzman, C., Nollert, P., Krucinski, J., and Stroud, R. M. (2000). Structure of a glycerol-conducting channel and the basis for its selectivity. *Science* 290, 481-486.
- Funato, Y., and Miki, H. (2019). Molecular function and biological importance of CNNM family of Mg²⁺ transporters. *J. Biochem.* 165, 219-225.
- Gadsby, D. C. (2009). Ion channels versus ion pumps: the principal difference, in principle. *Nat. Rev. Mol. Cell Biol.* 10, 344-352.
- Garavito, R. M., and Ferguson-Miller, S. (2001). Detergents as tools in membrane biochemistry. *J. Biol. Chem.* 276, 32403-32406.
- Ge, L., Villinger, S., Mari, S. A., Giller, K., Griesinger, C., Becker, S., Muller, D. J., and Zweckstetter, M. (2016). Molecular plasticity of the human voltage-dependent anion channel embedded into a membrane. *Structure* 24, 585-594.
- Ghisaidoobe, A. B. T., and Chung, S. J. (2014). Intrinsic tryptophan fluorescence in the detection and analysis of proteins: A focus on Forster resonance energy transfer techniques. *Int. J. Mol. Sci.* 15, 22518-22538.
- Goldschen-Ohm, M., and Chanda, B. (2017). Snapshot: Channel gating mechanisms. *Cell*, 170, 594.
- Graschopf, A., Stadler, J. A., Hoellerer, M. K., Eder, S., Sieghardt, M., Kohlwein, S. D., and Schweyen, R. J. (2001). The yeast plasma membrane protein Alr1 controls Mg²⁺ homeostasis and is subject to Mg²⁺-dependent control of its synthesis and degradation. *J. Biol. Chem.* 276, 16216-16222.
- Groisman, E. A., Hollands, K., Kriner, M. A., Lee, E. -J., Park, S. -Y., and Pontes, M. H. (2013). Bacterial Mg²⁺ homeostasis, transport, and virulence. *Annu. Rev. Genet.* 47, 625-646.

- Guskov, A., Nordin, N., Reynaud, A., Engman, H., Lundbäck, A.K., Jong, A.J., Cornvik, T., Phua, T., and Eshaghi, S. (2012). Structural insights into the mechanisms of Mg^{2+} uptake, transport, and gating by CorA. *Proc. Natl. Acad. Sci. U. S. A.* 109, 18459-18464
- Hardy, S., Uetani, N., Wong, N., Kostantin, E., Labbe, D. P., Begin, L. R., Mes-Masson, A., Miranda-Saavedra, D., and Tremblay, M. L. (2015). The protein tyrosine phosphatase PRL-2 interacts with the magnesium transporter CNNM3 to promote oncogenesis. *Oncogene* 34, 986-995.
- Hartwig, A. (2001). Role of magnesium in genomic stability. *Mutat. Res.* 475, 113-121.
- Haruyama, T., Sugano, Y., Kodera, N., Uchihashi, T., Ando, T., Tanaka, Y., Konno, H., and Tsukazaki, T. (2019). Single-unit imaging of membrane protein-embedded nanodiscs from two oriented sides by high-speed atomic force microscopy. *Structure* 27, 152-160.
- Hattori, M., Iwase, N., Furuya, N., Tanaka, Y., Tsukazaki, T., Ishitani, R., Maguire, M.E., Ito, K., Maturana, A., and Nureki O. (2009) Mg^{2+} -dependent gating of bacterial MgtE channel underlies Mg^{2+} homeostasis. *EMBO J.* 28, 3602-3612.
- Hattori, M., Tanaka, Y., Fukai, S., Ishitani, R., and Nureki, O. (2007). Crystal structure of the MgtE Mg^{2+} transporter. *Nature* 448, 1072-1075.
- Heginbotham, L., Lu, Z., Abramson, T., and Mackinnon, R. (1994). Mutations in the K^+ channel signature sequence. *Biophys. J.* 66, 1061-1067.
- Helenius, A., and Simons, K. (1975). Solubilization of membranes by detergents. *Biochim. Biophys. Acta* 415, 29-79.
- Hille, B. (2001). Ion channels of excitable membranes. 3rd Ed., Sinauer associates, Inc., Massachusetts.

- Hmiel, S. P., Snavely, M. D., Florer, J.B., Maguire, M. E., and Miller, C. G. (1989). Magnesium transport in *Salmonella typhimurium*: genetic characterization and cloning of three magnesium transport loci. *J. Bacteriol.* 171, 4742–4751.
- Ho, D., Lugo, M. R., and Merrill, A. R. (2013). Harmonic analysis of the fluorescence response of bimane adducts of colicin E1 at helices 6,7, and 10. *J. Biol. Chem.* 288, 5136-5148.
- Houston, M. (2011). The role of magnesium in hypertension and cardiovascular disease. *J. Clin. Hypertens. (Greenwich)* 13, 843-847.
- Hubbard, S.J. (1998). The structural aspects of limited proteolysis of native proteins. *Biochim. Biophys. Acta* 1382, 191-206.
- Hunte, C. (2005). Specific protein-lipid interactions in membrane proteins. *Biochem. Soc. Trans.* 33, 938-942.
- Ignoul, S., and Eggermont, J. (2005). CBS domains: structure, function, and pathology in human proteins. *Am. J. Physiol. Cell Physiol.* 289, C1369–C1378.
- Imai, S., Maruyama, T., Osawa, M., Hattori, M., Ishitani, R., Nureki, O., and Shimada, I. (2012). Spatial distribution of cytoplasmic domains of the Mg^{2+} -transporter MgtE, in a solution lacking Mg^{2+} , revealed by paramagnetic relaxation enhancement. *Biochem. Biophys. Acta* 1824, 1129-1135.
- Ishitani, R., Sugita, Y., Dohmae, N., Furuya, N., Hattori, M., and Nureki, O. (2008). Mg^{2+} -sensing mechanism of Mg^{2+} transporter MgtE probed by molecular dynamics study. *Proc. Natl. Acad. USA* 105, 5393-15398.
- Jacobson, K., Mouritsen, O. G., and Anderson, R. G. W. (2007). Lipid rafts: at crossroad between cell biology and physics. *Nat. Cell Biol.* 9, 7-14.

- Jalilehvand, F., Spangberg, D., Lindqvist-Reis, P., Hermansson, K., Persson, I., and Sandström, M. (2001). Hydration of the calcium ion. An EXAFS, large-angle X-ray scattering, and molecular dynamics simulation study. *J. Am. Chem. Soc.* 123, 431-441.
- Jeschke, G. (2012). DEER distance measurements on proteins. *Annu Rev Phys Chem* 63, 419-446.
- Jha, S. K., Dhar, D., Krishnamoorthy, G., and Udgaonkar, J. B. (2009). Continuous dissolution of structure during the unfolding of a small protein. *Proc. Natl. Acad. Sci. USA* 106, 11113-11118.
- Jiang, Q. -X., and Gonen, T. (2012) The influence of lipids on voltage-gated ion channels. *Curr. Opin. Struct. Biol.* 22, 529-536.
- Jiang, Y., Lee, A., Chen, J., Ruta, V., Cadene, M., Chait, B. T., and MacKinnon, R. (2003). X-ray structure of a voltage-dependent K⁺ channel. *Nature* 423, 33-41.
- Jin, F., Sun, M., Fujii, T., Yamada, Y., Wang, J., Maturana, A. D., Wada, M., Su, S., Ma, J., Takeda, H., Kusakizako, T., Tomita, A., Nakada-Nakura, Y., Liu, K., Uemura, T., Nomura, Y., Nomura, N., Ito, K., Nureki, O., Namba, K., Iwata, S., Yu, Y., and Hattori, M. (2021). The structure of MgtE in the absence of magnesium provides new insights into channel gating. *PLoS Biol.* 19, e3001231.
- Johnson, A. E. (2005). Fluorescence approaches for determining protein conformations, interactions and mechanisms at membranes. *Traffic* 6, 1078-1092.
- Kale, J., Chi, X., Leber, B., and Andrews, D. (2014). Examining the molecular mechanism of Bcl-2 family proteins at membranes by fluorescence spectroscopy. *Meth. Enzymol.* 544, 1-23.
- Katz, A. K., Glusker, J. P., Beebe, S. A., and Bock, C. W. (1996). Calcium ion coordination: a comparison with that of beryllium, magnesium, and zinc. *J. Am. Chem. Soc.* 118, 5752-5763.

- Kelkar, D.A., and Chattopadhyay, A. (2007). Modulation of gramicidin channel conformation and organization by hydrophobic mismatch in saturated phosphatidylcholine bilayers. *Biochim. Biophys. Acta* 1768, 1103-1113.
- Killian, J. A., and von Heijne, G. (2000). How proteins adapt to a membrane-water interface. *Trends Biochem. Sci.* 25, 429-434.
- Kim, A., and Cross, T. A. (2002). Uniformity, ideality, and hydrogen bonds in transmembrane α -helices. *Biophys. J.* 83, 2084-2095.
- Kim, D. M., and Nimigean, C. M. (2016). Voltage-gated potassium channels: a structural examination of selectivity and gating. *Cold Spring Harb. Perspect. Biol.* 8, a029231.
- Klein, D.J., Moore, P.B., and Steitz, T.A. (2004). The contribution of metal ions to the structural stability of the large ribosomal subunit. *RNA* 10, 1366-1379.
- Klingler, J., Vargas, C., Fiedler, S., and Keller, S. (2015). Preparation of ready-to-use small unilamellar phospholipid vesicles by ultrasonication with a beaker resonator. *Anal. Biochem.* 477, 10-12.
- Knoop, V., Groth-Malonek, M., Gebert, M., Eifler, K., and Weyand, K. (2005). Transport of magnesium and other divalent cations: evolution of the 2-TM-GxN proteins in the MIT superfamily. *Mol. Genet. Genomics* 274, 205-216.
- Kofuku, Y., Ueda, T., Okude, J., Shiraishi, Y., Kondo, K., Mizumura, T., Suzuki, S., and Shimada, I. (2014). Functional dynamics of deuterated β_2 -adrenergic receptor in lipid bilayers revealed by NMR spectroscopy. *Angew. Chem. Int. Ed.* 53, 13376-13379.
- Kolisek, M., Launay, P., Beck, A., Sponder, G., Serafini, G., Brenkus, M., Froschauer, E. M., Martens, H., Fleig, A., and Schweigel, M. (2008). SLC41A1 is a novel mammalian Mg^{2+} carrier, *J. Biol. Chem.* 283, 16235-16247.

- Kolisek, M., Nestler, A., Vormann, J., and Schweigel-Röntgen, M. (2012). Human gene SLC41A1 encodes for the Na⁺/Mg²⁺ exchanger. *Am. J. Physiol. Cell Physiol.* 302, C318–C326.
- Kolisek, M., Sponder, G., Mastrototaro, L., Smorodchenko, A., Launay, P., Vormann, J., and Schweigel-Röntgen, M. (2013). Substitution p.A350V in Na⁺/Mg²⁺ exchanger SLC41A1, potentially associated with Parkinson's disease, is a gain-of-function mutation. *PLoS ONE* 8, e71096.
- Kolisek, M., Zsurka, G., Samaj, J., Weghuber, J., Schweyen, R. J., and Schweigel, M. (2003). Mrs2p is an essential component of the major electrophoretic Mg²⁺ influx system in mitochondria. *EMBO J.* 22, 1235-1244.
- Kowal, P., Gurtan, A. M., Stuckert, P., D'Andrea, A. D., and Ellenberger, T. (2007). Structural determinants of human FANCF protein that function in the assembly of a DNA damage signaling complex. *J. Biol. Chem.* 282, 2047-2055.
- Kozachkov, L., and Padan, E. (2011). Site-directed tryptophan fluorescence reveals two essential conformational changes in the Na⁺/H⁺ antiporter NhaA. *Proc. Natl. Acad. Sci. USA* 108, 15769-15774.
- Kratochvil, H. T., Carr, J. K., Matulef, K., Anne, A. W., Li, H., Maj, M., Ostmeier, J., Serrano, A. L., Raghuraman, H., Moran, S. D., Skinner, J. L., Perozo, E., Roux, B., Valiyaveetil, F. I., and Zanni, M. T. (2016). Instantaneous ion configurations in the K⁺ ion channel selectivity filter revealed by 2D IR spectroscopy. *Science* 353, 1040-1044.
- Krepkiy, D., Mihailescu, M., Freitas, J. A., Schow, E. V., Worcester, D. L., Gawrisch, K., Tobias, D. J., and White, S. H. (2009). Structure and hydration of membranes embedded with voltage-sensing domains. *Nature* 462, 473-479.

- Krishnamoorthy, G. (2018). Fluorescence lifetime distribution brings out mechanisms involving biomolecules while quantifying population heterogeneity, In *Reviews in Fluorescence* (Geddes, C. D. ed.), pp. 75-98, Springer Nature, Switzerland AG.
- Kuo, A., Gulbis, J. M., Antcliff, J. F., Rahman, T., Lowe, E. D., Zimmer, J., Cuthbertson, J., Ashcroft, F. M., Ezaki, T., and Doyle, D. A. (2003). Crystal structure of the potassium channel KirBac1.1 in the closed state. *Science* 300, 1922-1926.
- Kurata, H. T., and Fedida, D. (2006). A structural interpretation of voltage-gated potassium channel inactivation. *Prog. Biophys. Mol.* 92, 185-208.
- Lakowicz, J. R. (2006). *Principles of Fluorescence spectroscopy*. 3rd Ed., Springer, New York.
- Lakshmikanth, G. S., Sridevi, K., Krishnamoorthy, G., and Udgaonkar, J. B. (2001). Structure is lost incrementally during the unfolding of barstar. *Nat. Struct. Biol.* 8, 799-804.
- Lara, C. O., Burgos, C. F., Moraga-Cid, G., Carrasco, M. A., and Yevenes, G. E. (2020). Pentameric ligand-gated ion channels as pharmacological targets against chronic pain. *Front. Pharmacol.* 11, 167.
- Le Maire, M., Champeil, P., and Moller, J. V. (2000). Interaction of membrane proteins and lipids with solubilizing detergents. *Biochim. Biophys. Acta* 1508, 86-111.
- Lee, A. G. (2003). Lipid-protein interactions in biological membranes: a structural perspective. *Biochim. Biophys. Acta* 1612, 1-40.
- Lee, A. G. (2004). How lipids affect the activities of integral membrane proteins. *Biochim. Biophys. Acta* 1666, 62-87.
- Li, Q., Wanderling, S., Paduch, M., Medovoy, D., Singharoy, A., McGreevy, R., Villalba-Galea, C. A., Hulse, R. E., Roux, B., Schulten, K., Kossiakoff, A., and Perozo, E. (2014). Structural mechanism of voltage-dependent gating in an isolated voltage-sensing domain. *Nat. Struct. Mol.*

Biol. 21, 244-252.

Li, T., Hassanali, A. A., Kao, Y. T., Zhong, D., and Singer, S. J. (2007). Hydration dynamics and time scales of coupled water-protein fluctuations. *J. Am. Chem. Soc.* 129, 3376-3382.

Lim, B., Sim, S. H., Sim, M., Kim, K. Jeon, C. O., Lee, Y., Ha, N. C., and Lee, K. (2012). RNase III controls the degradation of corA mRNA in *Escherichia coli*. *J. Bacteriol.* 194, 2214-2220.

Lin, C. M., Li, C. S., Sheng, Y. J., Wu, D. T., and Tsao, H. K. (2012). Size-dependent properties of small unilamellar vesicles formed by model lipids. *Langmuir* 28, 689-700.

Lin, S., and Struve, W. S. (1991). Time-resolved fluorescence of nitrobenzoxadiazol-aminohexanoic acid: effect of intermolecular hydrogen bonding on non-radiative decay. *Photochem. Photobiol.* 54, 361-365.

Lin, Y., Cheng, F., Chien, L., Lin, J., Jiang, R., and Liu, S. (2015). Expression of magnesium transporter in head and neck cancer patients underwent neoadjuvant cisplatin-based chemotherapy. *Eur. Arch. Otorhinolaryngol.* 272, 3051-3057.

Lipfert, J., Columbus, J., Chu, V. B., Lesley, S. A., and Doniach, S. (2007). Size and shape of detergent micelles determined by small-angle X-ray scattering. *J. Phys. Chem. B* 111, 12427-12438.

Liu, G. J., Martin, D. K., Gardner, R. C., and Ryan, P. R. (2002). Large Mg²⁺-dependent currents are associated with the increased expression of ALR1 in *Saccharomyces cerevisiae*. *FEMS Microbiol. Lett.* 213, 231-237.

Lomize, M. A., Pogozheva, I. D., Joo, H., Mosberg, H. I., and Lomize, A. L. (2012). OPM database and PPM web server: resources for positioning of proteins in membranes. *Nucleic Acids Res.* 40, D370-D376.

- Luckey, M. (2008). Membrane structural biology: with biochemical and biophysical foundations. 1st Ed., Cambridge university press, New York.
- Lunin, V. V., Dobrovetsky, E., Khutoreskaya, G., Zhang, R., Joachimiak, A., Doyle, D. A., Bochkarev, A., Maguire, M. E., Edwards, A. M., and Koth, C. M. (2006). Crystal structure of the CorA Mg²⁺ transporter. *Nature* 440, 833-837.
- Ma, J. C., and Dougherty, D. A. (1997). The cation- π interaction. *Chem. Rev.* 97, 1303-1324.
- MacKinnon, R. (2003). Potassium channels. *FEBS Lett.* 555, 62-65.
- Maguire, M. E., and Cowan, J. A. (2002). Magnesium chemistry and biochemistry. *Biometals* 15, 203–210.
- Mandt, T., Song, Y., Scharenberg, A.M., and Sahni, J. (2011). SLC41A1 Mg²⁺ transport is regulated via Mg²⁺-dependent endosomal recycling through its N-terminal cytoplasmic domain. *Biochem. J.* 439, 129–139.
- Mansoor, S. E., DeWitt, M. A., and Farrens, D. L. (2010). Distance mapping in proteins using fluorescence spectroscopy: The tryptophan-induced quenching (TriQ) method. *Biochemistry* 49, 9722-9731.
- Mansoor, S. E., McHaourab, H. S., and Farrens, D. L. (2002). Mapping proximity within proteins using fluorescence spectroscopy. A study of T4 lysozyme showing that tryptophan residues quench bimane fluorescence. *Biochemistry* 41, 2475–2484.
- Maruyama, T., Imai, S., Kusakizako, T., Hattori, M., Ishitani, R., Nureki, O., Ito, K., Maturana, A. D., Shimada, I., and Osawa, M. (2018). Functional roles of Mg²⁺ binding sites in ion-dependent gating of a Mg²⁺ channel, MgtE, revealed by solution NMR. *eLife* 7, e31596.

- Matthies, D., Dalmas, O., Borgnia, M. J., Dominik, P. K., Merk, A., Rao, P., Reddy, B. G., Islam, S., Bartesaghi, A., Perozo, E., and Subramaniam, S. (2016). Cryo-EM structures of the magnesium channel CorA reveal symmetry break upon gating. *Cell* 164, 747-756.
- Merino, S., Gavin, R., Altarriba, M., Izquirdo, L., Maguire, M. E., and Tomas, J. M. (2001). The MgtE Mg²⁺ transport protein is involved in *Aeromonas hydrophila* adherence. *FEMS Microbiol. Lett.* 198, 189-195.
- Meyer, S., Savaresi, S., Forster, I. C., and Dutzler, R. (2007). Nucleotide recognition by the cytoplasmic domain of the human chloride transporter ClC-5. *Nat. Struct. Mol. Biol.* 14, 60-67.
- Mishra, P., and Jha, S. K. (2019). Slow motion protein dance visualized using red-edge excitation shift of a buried fluorophore. *J. Phys. Chem. B* 123, 1256-1264.
- Moomaw, A. S., and Maguire, M. E. (2008). The unique nature of Mg²⁺ channels. *Physiology (Bethesda)* 23, 275-285.
- Moraes, I., Evans, G., Sanchez-Weatherby, J., Newstead, S., and Stewart, P. D. S. (2014). Membrane protein structure determination - The next generation. *Biochim. Biophys. Acta* 1838, 78-87.
- Morais-Cabral, J. H., Zhou, Y., and Mackinnon, R. (2001). Energetic optimization of ion conduction rate by the K⁺ selectivity filter. *Nature* 414, 37-42.
- Mukherjee, S., Kombrabail, M., Krishnamoorthy, G., and Chattopadhyay, A. (2007). Dynamics and heterogeneity of bovine hippocampal membranes: Role of cholesterol and proteins. *Biochim. Biophys. Acta* 1768, 2130-2144.
- Mukherjee, S., Raghuraman, H., Dasgupta, S., and Chattopadhyay, A. (2004). Organization and dynamics of *N*-(7-nitrobenz-2-oxa-1,3-diazol-4-yl)-labeled lipids: a fluorescence approach. *Chem. Phys. Lipids* 127, 91-101.

- Murata, Y., Iwasaki, H., Sasaki, M., Inaba, K., and Ikamura, Y. (2005). Phosphoinositide phosphatase activity coupled to an intrinsic voltage sensor. *Nature* 435, 1239-1243.
- Nadler, J. L., and Rude, R. K. (1995). Disorders of magnesium metabolism. *Endocrinol. Metab. Clin. North Am.* 24, 623-641.
- Nadler, M. J., Hermosura, M. C., Inabe, K., Perraud, A. L., Zhu, Q, Stokes, A. J., Kurosaki, T, Kinet, J. P., Penner, R, Scharenberg, A. M., and Fleig A. (2001). LTRPC7 is a Mg.ATP-regulated divalent cation channel required for cell viability. *Nature* 411, 590-595.
- Nelson, D. L., and Kennedy, E. P. (1971). Magnesium transport in *Escherichia coli*. Inhibition by cobaltous ion *J. Biol. Chem.* 246, 3042-3049.
- Niegowski, D., and Eshaghi, S. (2007). The CorA family: structure and function revisited. *Cell. Mol. Life Sci.* 64, 2564-2574.
- Ostmeyer, J., Chakrapani, S., Pan, A. C., Perozo, E., and Roux, B. (2013). Recovery from slow inactivation in K^+ channels is controlled by water molecules. *Nature* 501, 121-124.
- Palombo, I., Daley, D. O., and Rapp, M. (2013). Why is the GMN motif conserved in the CorA/Mrs2/Alr1 superfamily of magnesium transport proteins? *Biochemistry* 52, 4842-4847.
- Papp-Wallace, K. M., Nartea, M., Kehres, D. G., Porwollik, S., McClelland, M., Libby, S. J., Fang, F. C., and Maguire, M. E. (2008). The CorA Mg^{2+} channel is required for the virulence of *Salmonella enterica* serovar typhimurium. *J. Bacteriol.* 190, 6517-6523.
- Park, M. H., Wong, B. B., and Lusk, J. E. (1976). Mutants in three genes affecting transport of magnesium in *Escherichia coli*: genetics and physiology *J. Bacteriol.* 126, 1096-1103.
- Parsegian, A. (1969). Energy of an ion crossing a low dielectric membrane: solutions to four relevant electrostatic problems. *Nature* 221, 844-846.

- Pavlov, M., Siegbahn, P. E. M., and Sandström, M. (1998). Hydration of beryllium, magnesium, calcium, and zinc ions using density functional theory. *J. Phys. Chem. A* 102, 219-228.
- Payandeh, J., and Pai, E. F. (2006). A structural basis for Mg^{2+} homeostasis and the CorA translocation cycle. *EMBO J.* 25, 3762-3773.
- Payandeh, J., Li, C., Ramjeesingh, M., Poduch, E., Bear, C. E., and Pai, E. F. (2008). Probing structure-function relationships and gating mechanisms in the CorA Mg^{2+} transport system. *J. Biol. Chem.* 283, 11721-11733.
- Payandeh, J., Pfoh, R., and Pai, E. F. (2013). The structure and regulation of magnesium selective ion channels. *Biochim. Biophys. Acta* 1828, 2778-2792.
- Pisat, N. P., Pandey, A., and Macdiarmid, C. W. (2009). MNR2 regulates intracellular magnesium storage in *Saccharomyces cerevisiae*. *Genetics* 183, 873-884.
- Piskacek, M., Zotova, L., Zsurka, G., and Schweyen, R. J. (2009). Conditional knockdown of hMRS2 results in loss of mitochondrial Mg^{2+} uptake and cell death. *J. Cell. Mol. Med.* 13, 693-700.
- Pitt, G. S. (2016). Ion channels in health and disease. 1st Ed., Academic press, Cambridge
- Plested, A. J. (2016). Structural mechanisms of activation and desensitization in neurotransmitter-gated ion channels. *Nat. Struct. Mol. Biol.* 23, 494-502.
- Prendergast, F. G. (1991). Time-resolved fluorescence techniques: methods and applications in biology. *Curr. Opin. Struct. Biol.* 1, 1054-1059.
- Prive, G. (2007). Detergents for the stabilization and crystallization of membrane proteins. *Methods* 41, 388-397.
- Quamme, G. A. (2010). Molecular identification of ancient and modern mammalian magnesium transporters. *Am. J. Physiol. Cell. Physiol.* 298, C407-C429.

- Raghuraman, H., and Chattopadhyay, A. (2003). Organization and dynamics of melittin in environments of graded hydration. *Langmuir* 19, 10332-10341.
- Raghuraman, H., and Chattopadhyay, A. (2004a). Effect of micellar charge on the conformation and dynamics of melittin. *Eur. Biophys. J.* 33, 611-622.
- Raghuraman, H., and Chattopadhyay, A. (2004b). Interaction of melittin with membrane cholesterol: a fluorescence approach. *Biophys. J.* 87, 2419-2432.
- Raghuraman, H., and Chattopadhyay, A. (2004c). Influence of lipid chain unsaturation on membrane-bound melittin: a fluorescence approach. *Biochim. Biophys. Acta* 1665, 29-39.
- Raghuraman, H., and Chattopadhyay, A. (2007). Orientation and dynamics of melittin in membranes of varying composition utilizing NBD fluorescence. *Biophys. J.* 92, 1271-1283.
- Raghuraman, H., Chatterjee, S., and Das, A. (2019). Site-directed fluorescence approaches for dynamic structural biology of membrane peptides and proteins. *Front. Mol. Biosci.* 6, 96.
- Raghuraman, H., Coredero-Morales, J. F., Jogini, V., Pan, A. C., Kollwe, A., Roux, B., and Perozo, E. (2012). Mechanism of Cd^{2+} coordination during slow inactivation in potassium channels. *Structure* 20, 1332-1342.
- Raghuraman, H., Islam, S. M., Mukherjee, S., Roux, B., and Perozo, E. (2014). Dynamics transitions at the outer vestibule of the KcsA potassium channel during gating. *Proc. Natl. Acad. Sci. USA* 111, 1831-1836.
- Raghuraman, H., Kelkar, D. A., and Chattopadhyay, A. (2005). Novel insights into protein structure and dynamics utilizing red edge excitation shift approach, *Reviews in Fluorescence* (Geddes, C.D., Lakowicz, J.R. Eds.), pp. 199-214, Springer, New York.
- Raghuraman, H., Pradhan, S. K., and Chattopadhyay, A. (2004). Effect of urea on the organization and dynamics of Triton X-100 micelles: A fluorescence approach. *J. Phys. Chem. B*

108, 2489-2496.

Raghuraman, H., Shrivastava, S., and Chattopadhyay, A. (2007). Monitoring the looping up of acyl chain labeled NBD lipids in membranes as a function of membrane phase state. *Biochim. Biophys. Acta* 1768, 1258-1267.

Ramu, Y., Xu, Y., and Lu, Z. (2006). Enzymatic activation of voltage-gated potassium channels. *Nature* 442, 696-699.

Rangl, M., Schmandt, N., Perozo, E., and Scheuring, S. (2019). Real time dynamics of gating-related conformational changes in CorA. *eLife* 8, e47322.

Rao, M., and Mayor, S. (2014). Active organization of membrane constituents in living cells. *Curr. Opin. Cell Biol.* 29, 126-132.

Rasmussen, A., Rasmussen, T., Edwards, M.D., Schauer, D., Schumann, U., Miller, S., and Booth, I. R. (2007). The role of tryptophan residues in the function and stability of the mechanosensitive channel MscS from *Escherichia coli*. *Biochemistry* 46, 10899-10908.

Romani, A. M. (2011). Cellular magnesium homeostasis. *Arch. Biochem. Biophys.* 512, 1-23.

Romani, A., and Scarpa, A. (1992). Regulation of cell magnesium. *Arch. Biochem. Biophys.* 298, 1-12.

Ross, A. J. B., Laws, W. R., Rousslang, K. W., and Wyssbrod, H. R. (1992). Tyrosine fluorescence and phosphorescence from proteins and polypeptides. In *Topics in Fluorescence Spectroscopy, Biochemical Applications* (Lakowicz, J. R. ed.), pp. 1-63, Plenum Press, New York.

Roux, B. (2017). Ion channels and ion selectivity. *Essays Biochem.* 61, 201-209.

Rubin, H. (2005). Central roles of Mg^{2+} and $MgATP^{2-}$ in the regulation of protein synthesis and cell proliferation: significance of neoplastic transformation. *Adv. Cancer Res.* 93, 1-58.

- Sahni, J., and Scharenberg, A. M. (2013). The SLC41 family of MgtE-like magnesium transporters. *Mol. Aspects Med.* 34, 620-628.
- Sahni, J., Song, Y., and Scharenberg, A. M. (2012). The *B. subtilis* MgtE Magnesium transporter can functionally compensate TRPM7-deficiency in vertebrate B-cells. *PLoS ONE* 7, e44452.
- Scheuer, T. (2011). Regulation of sodium channel activity by phosphorylation. *Semin. Cell Dev. Biol.* 22, 160-165.
- Schiffer, M., Chang, C. H., and Stevens, F. J. (1992). The functions of tryptophan residues in membrane proteins. *Protein Eng.* 5, 213-214.
- Schirmer, T., Keller, T. A., Wang, Y. F., and Rosenbusch, J. P. (1995). Structural basis for sugar translocation through maltoporin channels at 3.1-angstrom resolution. *Science* 267, 512-514.
- Schmitz, C, Perraud, A. L., Johnson, C. O., Inabe, K., Smith, M. K., Penner, R., Kurosaki, T., Fleig, A., and Scharenberg, A. M. (2003). Regulation of vertebrate cellular Mg²⁺ homeostasis by TRPM7. *Cell* 114, 191-200.
- Seddon, A.M., Curnow, P., and Booth, P.J. (2004). Membrane proteins, lipids and detergents: not just a soap opera. *Biochim. Biophys. Acta* 1666, 105-117.
- Selmer, M., Dunham, C. M., Murphy, F. V. 4th, Weixlbaumer, A., Petry, S., Kelley, A. C., Weir, J. R., and Ramakrishnan, V (2006). Structure of the 70S ribosome complexed with mRNA and tRNA. *Science* 313, 1935-1942.
- Shai, Y. (2001). Molecular recognition within the membrane milieu: implications for the structure and function proteins. *J Membr. Biol.* 182, 91-104.
- Shepard, L. A., Heuck, A. P., Hamman, B. D., Rossjohn, J., Parker, M. W., Ryan, K. R., Johnson, A. E., and Tweten, R. K. (1998). Identification of a membrane-spanning domain of the

- thiol-activated pore-forming toxin *Clostridium perfringens* perfringolysin O: An α -helical to β -sheet transition identified by fluorescence spectroscopy. *Biochemistry* 37, 14563-14574.
- Simons, K., and Ikonen, E. (1997). Functional rafts in cell membranes. *Nature* 387, 569-572.
- Singer, S. J., and Nicolson, G. L. (1972). The fluid mosaic model of the structure of cell membranes. *Science* 175, 720-731.
- Smith, D. A., McKenzie, G. A., Jones, C., and Smith, T. A. (2017). Analysis of TCSPC data: a comparative evaluation of deterministic and probabilistic approaches. *Methods Appl. Fluoresc.* 5, 042001.
- Smith, R. L., Thompson, L. J., and Maguire, M. E. (1995). Cloning and characterization of MgtE, a putative new class of Mg^{2+} transporter from *Bacillus firmus* OF4. *J. Bacteriol.* 177, 1233-1238.
- Sponder, G., Abdulhanan, N., Frohlich, N., Mastrototaro, L., Aschenbach, J. R., Rontgen, M., Pilchova, I., Cibulka, M., Racay, P., and Kolisek, M. (2018). Overexpression of Na^+/Mg^{2+} exchanger SLC41A1 attenuates pro-survival signaling. *Oncotarget* 9, 5084-5104.
- Stauffer, K. A., Kumar, N. M., Gilula, N. B., and Unwin, N. (1991). Isolation and purification of gap junction channels isolation of gap junctions from insect cells. *J. Cell Biol.* 115, 141-150.
- Sternisha, S. M., Whittington, A. C., Fiesco, J. A. M., Porter, C., McCray, M. M., Logan, T., Olivieri, C., Veglia, G., Stienbach, P. J., and Miller, B. G. (2020). Nanosecond-timescale dynamics and conformational heterogeneity in human GCK regulation and disease. *Biophys. J.* 118, 1109-1118.
- Stetsenko, A., and Guskov, A. (2017). An overview of the top ten detergents used for membrane protein crystallization. *Crystals* 7, 197.

- Stetsenko, A., and Guskov, A. (2020). Cation permeability in CorA family of proteins. *Sci. Rep.* 10, 840.
- Street, T. O., Bolen, W. D., and Rose, G. D. (2006). A molecular mechanism for osmolyte-induced protein stability. *Proc. Natl. Acad. Sci. USA* 103, 13997-14002.
- Stryer, L. (1978). Fluorescence energy transfer as a spectroscopic ruler. *Annu. Rev. Biochem.* 47, 819-846.
- Swaminathan, R. (2003). Magnesium metabolism and its disorders. *Clin. Biochem. Rev.* 24, 47-66.
- Swaminathan, R., and Periasamy, N. (1996). Analysis of fluorescence decay by maximum entropy method: Influence of noise and analysis parameters on the width of the distribution of lifetimes. *Proc. Indian Acad. Sci. (Chem. Sci.)* 108, 39-49.
- Swaminathan, R., Krishnamoorthy, G., and Periasamy, N. (1994). Similarity of fluorescence lifetime distributions for single tryptophan proteins in the random coil state. *Biophys. J.* 67, 2013-2023.
- Swartz, D., Singh, A., Sok, N., Thomas, J. N., Weber, J., and Urbatsch, I. L. (2020). Replacing the eleven native tryptophans by directed evolution produces an active P-glycoprotein with site-specific, non-conservative substitutions. *Sci. Rep.* 10, 3224.
- Tai, S. K., Wu, G., Yuan, S., and Li, K. C. (2010) Genome-wide expression links the electron transfer pathway of *Shewanella oneidensis* to chemotaxis. *BMC Genomics* 11, 319.
- Takeda, H., Hattori, M., Nishizawa, T., Yamashita, K, Shah, S. T. A., Caffrey, M, Maturana, A. D., Ishitani, R., and Nureki, O. (2014). Structural basis for ion selectivity revealed by high-resolution crystal structure of Mg²⁺ channel MgtE. *Nat. Commun.* 5, 5374.

- Takezawa, R., Schmitz, C., Demeuse, P., Scharenberg, A. M., Penner, R., and Fleig, A. (2004). Receptor-mediated regulation of the TRPM7 channel through its endogenous protein kinase domain. *Proc Natl Acad Sci U.S.A.* 101, 6009-6014.
- Tai, S. -K., Wu, G., Yuan, S., and Li, K. -C. (2010). Genome-wide expression links to electron transfer pathway of *Shewanella oneidensis* to chemotaxis. *BMC Genomics* 11, 319.
- Tao, T., Grulich, P. F., Kucharski, L. M., Smith, R. L., and Maguire, M. E. (1998). Magnesium transport in *Salmonella typhimurium*: biphasic magnesium and time dependence of the transcription of the *mgtA* and *mgtCB* loci. *Microbiology* 144(Pt. 3), 655-664.
- Taraska, J. (2012). Mapping membrane protein structure with fluorescence. *Curr. Opin. Struct. Biol.* 22, 507-513.
- Terstappen, G. C., and Reggiani, A. (2001). *In silico* research in drug discovery. *Trends Pharmacol. Sci.* 22, 23-26.
- Tilegenova, C., Vemulapally, S., Cortes, D. M., and Cuello, L. G. (2016). An improved method for the cost-effective expression and purification of large quantities of KcsA. *Protein Exp. Purif.* 127, 53-60.
- Tomita, A., Zhang, M., Jin, F., Zhuang, W., Takeda, H., Maruyama, T., Osawa, M., Hashimoto, K., Kawasaki, H., Ito, K., Dohmae, N., Ishitani, R., Shimada, I., Yan, Z., Hattori, M., and Nureki, O. (2017). ATP-dependent modulation of MgtE in Mg²⁺ homeostasis. *Nat. Commun.* 8, 148.
- Tory, M. C., and Merrill, A. R. (1999). Adventures in membrane protein topology: a study of the membrane-bound state of colicin E1. *J. Biol. Chem.* 274, 24539-24549.

- Townsend, D. E., Esenwine, A. J., George 3rd, J., Bross, D., Maguire, M. E., and Smith, R. L. (1995). Cloning of the *mgtE* Mg²⁺ transporter from *Providencia stuartii* and the distribution of *mgtE* in gram-negative and gram-positive bacteria. *J. Bacteriol.* 177, 5350-5354.
- Turconi, S., Bingham, R. P., Haupts, U., and Pope, A. J. (2001). Developments in fluorescence lifetime-based analysis for ultra-HTS. *Drug Discov. Today* 6, S27-S39.
- Ulmschneider, M. B., and Sansom, M. S. P. (2001). Amino acid distributions in integral membrane protein structures. *Biochim. Biophys. Acta* 1512, 1–14.
- Valiyaveetil, F. I., Zhou, Y., and Mackinnon, R. (2002). Lipids in the structure, folding, and function of the KcsA K⁺ channel. *Biochemistry* 41, 10771-10777.
- Vivian, J. T., and Callis, P. R. (2001). Mechanisms of tryptophan fluorescence shifts in proteins. *Biophys. J.* 80, 2093-2109.
- Volkov, V (2015). Quantitative description of ion transport via plasma membrane of yeast and small cells. *Front. Plant Sci.* 6, 425.
- Wabakken, T., Rian, E, Kveine, M.,and Aasheim, H. -C. (2003). The human solute carrier SLC41A1 belongs to a novel eukaryotic subfamily with homology to prokaryotic MgtE Mg²⁺ transporters. *Biochem. Biophys. Res. Commun.* 306, 718-724.
- Wachek, M., Aichinger, M.C., Stadler, J.A., Schweyen, R.J.,and Graschopf, A. (2006). Oligomerization of the Mg²⁺-transport proteins Alr1p and Alr2p in yeast plasma membrane. *FEBS J.* 273, 4236-4249.
- Wallace, B. A., and Janes, R. W. (1999). Tryptophans in membrane proteins, In Tryptophan, Serotonin, and Melatonin: Basic Aspects and Applications; Advances in Experimental Medicine and Biology, Vol.467, (Huether, G., Kochen, W., Simat, T. J., and Steinhart, H., Eds.) pp. 789-799, Springer (Science+Business Media), New York.

- Wallin, E., and Heijne, G.V. (1998). Genome-wide analysis of integral membrane proteins from eubacterial, archaean, and eukaryotic organisms. *Protein Sci.* 7, 1029-1038.
- Weitzman, C., Consler, T. G., and Kaback, R. (1995). Fluorescence of native single-Trp mutants in the lactose permease from *Escherichia coli*: structural properties and evidence for a substrate-induced conformational change. *Protein Sci.* 4, 2310-2318.
- Welch, W.J., and Brown, C.R. (1996). Influence of molecular and chemical chaperones on protein folding. *Cell Stress Chaperones* 1, 109-115.
- White, S. H., and Wimley, W. C. (1994). Peptides in lipid bilayers: structural and thermodynamic basis for partitioning and folding. *Curr. Opin. Struct. Biol.* 4, 79-86.
- Wolf, F. I., and Trapani, V. (2012). Magnesium and its transporters in cancer: a novel paradigm in tumour development. *Clin. Sci.* 123, 417-427.
- Xu, Y., Ramu, Y., and Lu, Z. (2008). Removal of phospho-head groups of membrane lipids immobilizes voltage sensors of K⁺ channels. *Nature* 451, 826-829.
- Yang, W., Lee, J. Y., and Nowotny, M. (2006). Making and breaking nucleic acids: two-Mg²⁺-ion catalysis and substrate specificity, *Mol. Cell* 22, 5-13.
- Yau, W.-M., Wimley, W. C., Gawrisch, K., and White, S. H. (1998). The preference of tryptophan for membrane interfaces. *Biochemistry* 37, 14713-14718.
- Ye, S., Li, Y., and Jiang, Y. (2010). Novel insights into K⁺ selectivity from high resolution structures of an open K⁺ channel pore. *Nat. Struct. Mol. Biol.* 17, 1019-1023.
- Yellen, G. (2002). The voltage-gated potassium channels and their relatives. *Nature* 419, 35-42.
- Yildirim, M. A., Goh, K. -I., Cusick, M. E., Barabsai, A. -L., and Vidal, M. (2007). Drug-target network. *Nat. Biotechnol.* 25, 1119-1126.

Zhou, H.-X., and Cross, T. A. (2013). Influences of membrane mimetic environments on membrane protein structures. *Annu. Rev. Biophys.* 42, 361-392.

Zhou, Y., Morais-Cabral, J. H., Kaufman, A., and MacKinnon, R. (2001). Chemistry of ion coordination and hydration revealed by a K⁺ channel Fab complex at 2.0 Å resolution. *Nature* 414, 43-48.

Zhu, Y., Davis, A., Smith, B.J., Curtis, J., and Handman, E. (2009). Leishmania major CorA-like magnesium transporters play a critical role in parasite development and virulence. *Int. J. Parasitol.* 39, 713-723.

Thesis Highlight

Name of the student: Satyaki Chatterjee

Name of the CI/OCC: Saha Institute of Nuclear Physics

Enrolment No.: LIFE05201604001

Thesis title: Gating-Induced Structural and Functional Dynamics of Magnesium Channels in Membranes

Discipline: Life Sciences

Sub-Area of Discipline: Membrane protein biophysics

Magnesium is the most abundant divalent cation present in the cell, and abnormal Mg^{2+} homeostasis is associated with several diseases in humans. However, among ion channels, the mechanisms of intracellular regulation and transport of Mg^{2+} are poorly understood. MgtE is a homodimeric Mg^{2+} -selective channel and is negatively regulated by high intracellular Mg^{2+} concentration where the cytoplasmic domain of MgtE acts as a Mg^{2+} sensor. To date, the purification and structure determination of MgtE from *Thermus thermophilus* has been carried out using the widely used nonionic detergent, n-dodecyl- β -D-maltopyranoside (DDM). However, DDM is an expensive detergent and alternative methods to produce high-quality proteins in a stable and functional form will be practically advantageous to carry out structural studies in a cost-effective manner. We have developed a 'dual-detergent strategy' to successfully purify MgtE channel in a stable and functional form by employing relatively inexpensive detergents (like Triton X-100) for membrane solubilization. Further, we monitored the changes in gating-related structural dynamics, hydration dynamics, and conformational heterogeneity of MgtE in membrane-mimetics using the site-directed intrinsic Trp fluorescence. For this purpose, we have engineered six single-Trp mutants in the functional Trp-less background of MgtE to obtain site-specific information on the gating-related structural dynamics of MgtE in membrane-mimetic systems. Our results indicate that Mg^{2+} -induced gating might involve the possibility of a 'conformational wave' from the cytosolic N-domain to the transmembrane domain of MgtE. Although MgtE is responsive to Mg^{2+} -induced gating in both micelles and membranes, its structural dynamics is substantially altered in physiologically important membranes compared to micelles. Importantly, the cytoplasmic region of MgtE, particularly the N-domain, is known to function as a ' Mg^{2+} -sensor' and a gating-modulator. However, the structural-dynamics changes of the N-domain residues in response to Mg^{2+} -dependent gating is not well understood. For this purpose, we have used sophisticated fluorescence approaches utilizing 7-nitrobenz-2-oxa-1,3-diazol-4-yl (NBD) and bimane fluorescence to study the gating-induced changes in mobility, hydration dynamics, and conformational heterogeneity of N-domain residues around the Mg^{2+} -binding sites at the interface of the CBS- and N-domain. Our results suggest an overall decrease in the mobility and conformational heterogeneity and variation in hydration dynamics of the N-domain residues without compromising the structural integrity of the N-domain upon gating in membrane-mimetics. Overall, the work presented in this thesis highlights the importance of membrane environment and lipid-protein interactions in the gating mechanisms of ion channels in general, and the MgtE Mg^{2+} channel in particular.

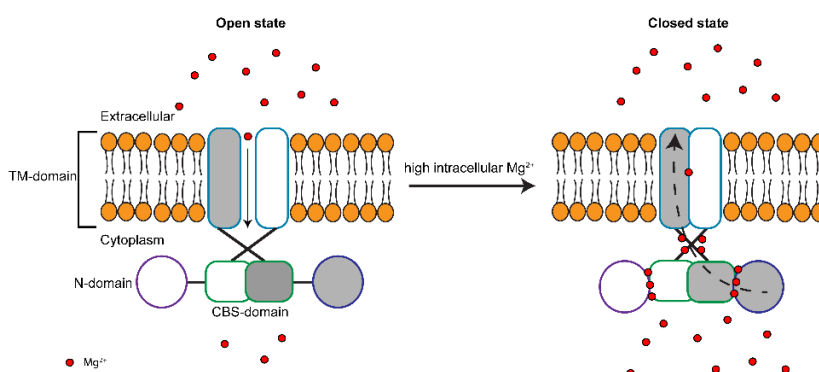


Fig.1. The cytoplasmic N-domain of MgtE functions as a Mg^{2+} -sensor and high intracellular Mg^{2+} concentration induces a 'conformational wave' from the cytoplasmic N-domain to the transmembrane (TM) domain when MgtE transitions from the open to the closed state in membranes.